CHALMERS

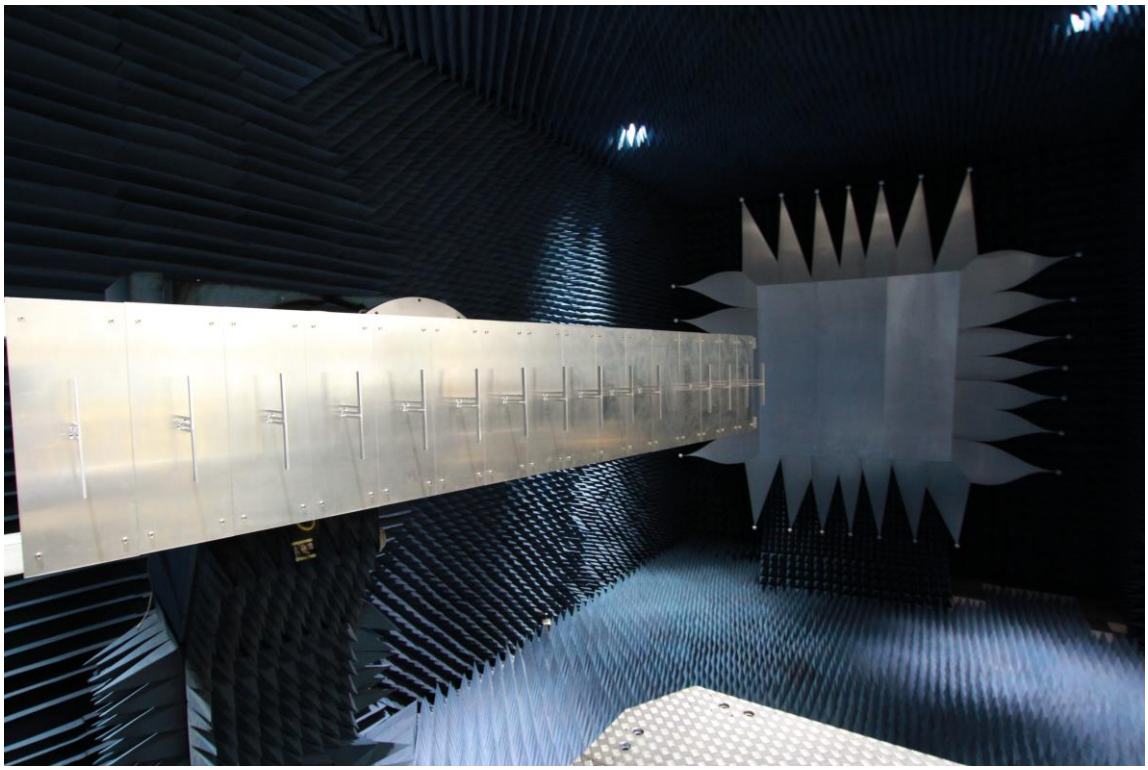

Active electronically controlled IFF-antenna for L-band

Master's thesis in Wireless, Photonics and Space Engineering

ALBIN NILSSON, DAVID SCHULTZE

Department of Microtechnology and Nanoscience
CHALMERS UNIVERSITY OF TECHNOLOGY
Gothenburg, Sweden 2018

Active electronically controlled IFF-antenna for L-band

ALBIN NILSSON
DAVID SCHULTZE

Department of Microtechnology and Nanoscience
Microwave Electronics Laboratory
Chalmers University of Technology
Gothenburg, Sweden 2018

Active electronically controlled IFF-antenna for L-band
ALBIN NILSSON, DAVID SCHULTZE

Supervisor: Bengt Svensson, Hans-Olof Vickes, Klas Axelsson, Saab Surveillance
Examiner: Christian Fager, Chalmers University of Technology, Microtechnology and Nanoscience

Department of Microtechnology and Nanoscience
Microwave Electronics Laboratory
Chalmers University of Technology
SE-412 96 Gothenburg
Telephone +46 31 772 1000

Gothenburg, Sweden 2018

ABSTRACT

The projects purpose is to design, build and measure a transmitter and receiver module (TRM) and antenna prototype for an IFF/SSR system using Active Electronically Scanned Array (AESA) technique, which is unique in these systems.

The project concludes the design, build and measurement of a TRM split in its basic blocks in the form of test circuits. An antenna array with 10+4 active elements are designed, build and measured in an anechoic chamber. The project successfully resulted in a theoretical power to each element of 953W at 1dB compression. The 2^{nd} and 3^{rd} harmonic generated from the system could be kept within the IFF standard limit with the manufactured filter in this project. The antenna constructed using dipoles has an active reflection factor of around 10 dB for the worst element at 0 steering angle, and at 60 steering angle it was 5dB for the worst element and edge frequency. The complete TRM was only in the design stage in this master thesis, the size of the design resulted in the dimensions 250x117mm.

In conclusion, the power requirement for 700W per module was met and the power in 1 dB compression were 953W with losses after the power amplifier accounted for. The linear power from the amplifier yielded a power of 800W, also meeting the power requirements. The antenna did not meet the requirement of 10 dB return loss, however, the antenna design in itself resulted in a small and light antenna array which was desirable attributes in this project. The requirement for the size of the complete TRM was 250 mm x 120 mm and this requirement was met in the design stage for this project. There were two different phase shifters in this project and the conclusion was to go for the phase shifter designed with transmission lines instead of the IC circuit. This decision was made because the designed phase shifter had a lower and more even insertion loss. It also had a more predicable phase shift for 180°.

Keywords: Active Electronically Scanned Array (AESA), Active reflection coefficient, Embedded element pattern, Integrated Circuit (IC), Power Amplifier (PA), Transmitter-Receiver Module (TRM), Identification, Friend or Foe (IFF), secondary surveillance radar (SSR), Low Noise Amplifier (LNA), Balun, Hybrid, High power amplifier.

Abstract

Rapporten syfte är att designa, bygga och utföra mätningen av sändare/mottagare modul och antennen ämnad för IFF/SSR system med aktiv elektriskt styrbar gruppantennteknik, vilket är unikt bland dessa system.

Projektet inkluderar design, bygg och mätning av sändare/mottagare modulen uppdelad i dess grundläggande delar. En gruppantenn bestående av 10+4 aktiva antenn-element är designad, byggd och uppmätt i en ekofri kammare. Projektet resulterade i en teoretisk effekt levererad till varje element på 953W vid 1dB kompression. Harmonierna från systemet i.e. andra och tredje övertonerna höll sig inom IFF standarden med det tillverkade filtret som användes i projektet. Antennen som är konstruerad med hjälp av dipoler har en reflektion på 10 dB för en utstyrning av 0°, vid 60° utstyrning för det värsta elementet och kantfrekvensen är reflektionen 5dB. Den slutgiltiga TRM blev bara designad i detta mastersarbete, dimensionerna för denna design blev 250x117mm.

När det kommer till effekt kravet för TRM, så var det på 700W och den uppnådda effekten vid 1 dB kompression var 953W. Vilket betyder att kravet blev uppfyllt och den linjära effektförstärkningen låg på 800W så även detta uppfyller effekt kravet. Antennen som konstruerades i mastersarbetet uppnådde inte kravet på en aktiv reflektionsfaktor på 10 dB, däremot så resulterade arbetet i en kompakt och liten antenn vilket var önskvärt för projektet. De framställda kraven för vilka dimensioner som den slutgiltiga TRM skulle ha var 250x120 mm, detta krav blev uppfyllt i den design som gjordes. Det togs fram två stycken fasvridare i detta projekt och en slutsats av dessa två var att man borde använda sig av den fasvridare med transmissionsledningar. Detta beslut baserades på att denna fasvridaren mot den integrerade kretsen hade lägre och jämnare förluster. Den har även en mer förutsägbar fasvridning vid 180°.

Preface

In this thesis a prototype for an IFF system has been simulated, designed and manufactured in the form of test circuits. Furthermore, a linear antenna array was simulated, designed and manufactured, however, the antenna was tested separately from the test circuits.

The thesis project was carried out at Saab AB Surveillance, the supervisor at Saab were Bengt Svensson, Hans-Olof Vickes and Klas Axelsson. The examiner at Chalmers for the thesis project was Christian Fager. The thesis work took place at Saab AB from January 2018 to August 2018.

Firstly, we would to thank our supervisors from Saab AB Bengt Svensson, Hans-Olof Vickes and Klas Axelsson for their good guidance from the very start to the end of this project. Secondly, we would like to thank our examiner Christian Fager for the valuable insights during this thesis project. We would further also want to thank Maria Köhler and Ninva Shamoun at Saab AB for making this thesis project possible.

Lastly, we would also like to thank a lot of other helpful people at Saab AB such as Andreas Frid, Andreas Wikström, Henrik Voos, Johan Bodin, Niklas Eriksson, Olle Grundén, Per Agesund, Sigrid Hammarqvist, Theofilos Markopoulos and other colleagues at Saab AB.

David Schultze Albin Nilsson, Gothenburg, August 2018

Table of Contents

1. Introduction

Modern radar systems utilize the AESA technology to scan the airspace. The main advantage is you don't need a mechanical rotating platform to scan the surroundings. Furthermore, this AESA technology will lead to more flexibility, being able to sustain multiple main lobes in different directions in rapid successions. The AESA will also give better redundancy since the system will work even when a failure for one or more TRM modules occur. In a traditional combined system with radar and Identification, Friend or Foe (IFF) a mechanical platform is needed to rotate the antennas since the IFF systems today has a fixed main lobe. It is therefore of interest to develop an IFF system with AESA technology in order for the systems to work coherent. As a result, you can have the system in a fixed position and scan a wanted sector of the airspace with both the IFF and radar, simultaneously or separate. This report builds upon a similar master's thesis done in 2009 with the same objective but with different specifications.

1.1 Aim of the project

Development and prototyping of an IFF system containing a transceiver and a linear 15-dipole array antenna. For the transceiver, focus will be to avoid distortion of the pulse train from the interrogator and harmonics while sustaining a high output power. The focus for the antenna will be to develop an active electronically scanned array antenna within the specifications and framework provided by SAAB.

1.2 Limitations

Voltages

The voltages are supplied from multiple lab power supplies, not limiting us to use standard voltage rails.

TRM modules

The project is not intended to lead to a fully working prototype, but merely a proof of concept for the AESA IFF system. This can be done with just one TRM module or test circuits, as the others are to be identical in design.

Limited to commercial amplifier blocks and components

The decision to only use commercial available amplifier blocks will enable us to design and build the test circuit for the TRM on the given timeframe. As for other components it is to our advantage to use as many common components as possible to simplify the design stage.

Antenna design

The antenna will be regulated in the design aspect, that is, the number of elements as well as element spacing is set as well, see APPENDIX A. Basic HFSS design has been set up for us by SAAB of antenna elements and we are to work from those designs, constructing a functional antenna for the intended frequency band.

The pulses will not contain a message and only a certain pulse width will be tested

The test pulses generated to test the TRM will only be one of the IFF pulses standard used in a specific mode. This specific pulse has a width of 0.25μs and a pulse period of 12.5μs.

We will only amplify the received signals, not encode them or sample them

The signal received is only to be amplified. The TRM we are building is not to include any form of decoding, modulation or pre-distortion, merely amplifying and phase shifting it.

2. Theory

2.1 Identification, friend or foe

The Identification, friend or foe (IFF) system is a well-established standard and was developed during World War Two to identify airborne friend or foe out on the battlefield via radio communication. It consists of two parts, the interrogator and the transponder, where the interrogator is the asking part located at 1030MHz and the transponder in the answering part at 1090MHz centre frequency. The IFF system can only identify a "friend" and can indirect detect a foe based on if no answer is received from the transponder. Today the identification system is used for both military aircrafts and civilian aircrafts. The interrogator is often a ground based station and the transponder is often located in the aircraft. [1] As a reference for power, ICAO annex 10 states has set a peak effective isotropic radiated power (EIRP) of max 52.5dBW [2].

There are several different modes for the IFF system and some of them are strictly military. The different interrogation modes can be seen below:

- **Mode 1 (Military)**
  The non-secure method used to track aircrafts where the code is set by the pilot but is first assigned by the Air Traffic Control.
- **Mode 2 (Military)**
  This is strictly for identification i.e. the tail number of the aircraft.
- **Mode 3/A (Military and civilian)**
  The standard system used by the military and civilians to relay their position to the ground controls throughout the world.
- **Mode C (Military and civilian)**
  Altitude information from the aircraft.
- **Mode 4 (Military)**
  The secure encrypted IFF system used by the military.
- **Mode S**
  Aircraft can be addressed uniquely using its 24-bit ICAO address or to address all. Military aircrafts can change its ICAO code, but not during flight. [3] [4]

The military and civilian transponders respond differently i.e. they don't respond to the same interrogation modes. The military transponders reply to modes 1, 2, 3/A, mode S and possibly mode C. The civilian transponder doesn't respond to mode 1 and mode 2. However, they must respond to modes 3/A mode S and C. [1]

2.1.1 Mode S

There are 24 different formats for the interrogation and response and categorised as short, 56-bit, or long, 112-bit. The interrogator uses several pulses called P1-P5 to set up and specify the mode, format and sync the phase. The data contained in P6 sent from the interrogator are modulated using differential phase shift keying (DFSK) of 0 and 180°. The transponder uses pulse modulation and binary pulse position modulation, (BPPM) to answer. [3]

Examples of different formats can be the mode S format 11, which is an all call format where all transponders are requested to answer. The transponders then answer with its communication capabilities as well as its ICAO 24-bit address and the interrogators identity code. Mode S can also be used as a data link as for Format 20, 21 and 24 where Format 20 and 21 also includes surveillance functions. [3]

The standard contains a lot of specifications required from the interrogator; not all have come in consideration for this project or stated in this report. For Mode S the rise time of all the pulses P1 to P6 shall be between 0.05 and 0.1μs and a fall time between 0.05 and 0.2μs. [3] [1] There are also criteria defined in the frequency spectra consisting of a tapered window in which the frequency spectra must fit and the amplitude of the harmonics in reference to the carrier, seen in Figure 2.1 and Table 3.5. [2] [3]

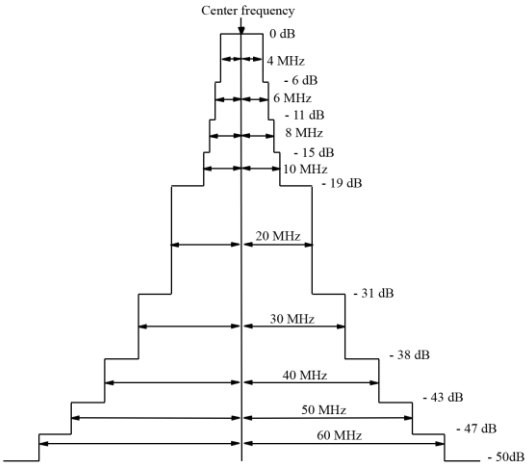

Figure 2.1 Interrogator bandwidth specification around the centre frequency to fulfil the STANAG 4193 criteria [3].

2.2 Transmit receive module

A Transmit receive module (TRM), is a device that in a common housing can both transmit and receive signals. In a broad aspect this can mean that the device also houses the signal processing side of generating and decoding the signal. However, in this paper the TRM refers to a device containing the transmitter and receiver together with all the other component necessary in the signal path to create a phase shift and attenuation control. A diagram of the design is presented in Figure 2.2.

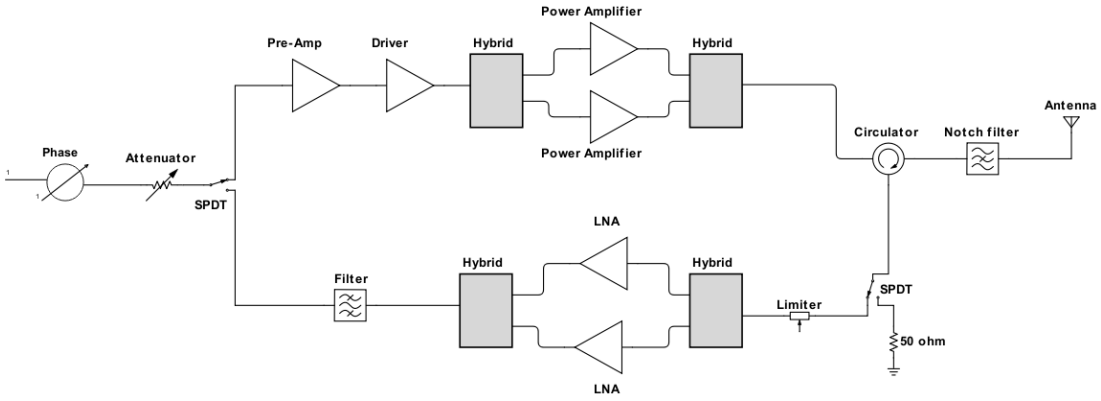

Figure 2.2 The general view of the TRM block diagram where you can see the main parts needed for a TRM circuit.

2.2.1 Phase Shifter

In the design, the phase shifting for each element are to be in the TRM's common path at the input. This is due to both the signal transmitted and received are in the same azimuth angle and therefore almost the same phase shift is needed for both transmit and received after each other. The switching time needs to be fast as the time difference between a transmit mode and receive mode needs to be short for a high preforming product.

Phase shifting a signal is equivalent to creating a time delay. This can be done in different ways but an easy way is using transmission lines with different length to create a longer path for the delayed signal. The length of the transmission line (TL) is dependent on the speed of the wave in that material, dependent on the effective dielectric constant, or the dielectric constant ε_r for a TL substrate. [5]

2.2.2 Attenuator

The attenuators purpose is to attenuate a signal in an accurate way to a fixed value or between predefined levels. The attenuation should not distort the signal in anyway when the signals propagates through the attenuator. Some characteristics important for the attenuator is the accuracy of the attenuator and that the frequency band should have a flat response. Furthermore, the reflection i.e. the SWR should be low so you have a high transmittance. The purpose of the attenuator in the TRM module is to be able to perform tapering for the antenna array, shaping the beam. [6]

2.2.3 Pre-amplification

The signal received from a signal generator is often very weak, the gain of the power amplifier, PA, is only in the order of 15dB, so in order to reach 60dBm from a source of couple of dBm, pre-amplification is needed. These systems are merely to boost the system in a linear manner, not going into compression to early. Ideally, only the final stage is going into compression while the pre-amplifiers (pre-amps) are linear. In this system, the pre-amps are divided into two parts, the pre-amp and the driver. The driver task is to provide the PA with enough input power, as these demands a lot of power to operate. The pre-amp is used to boost the signal level so no high power signal needs to go through the phase shifter and attenuator as this can cause compression and distortion.

2.2.4 Power amplifier

The power amplifier is the last stage in an amplification chain, the power amplifier often operates in the non-linear domain which means that the small-signal S-parameters is not enough when designing them. The power amplifier can be designed to be a class A, AB, B or C by setting the bias point for the amplifier. [7]

The power amplifier in the following project is a class AB power amplifier, thus this class will be described in more detail. The class AB amplifier is defined by the conduction angle being somewhere between 180° and 360° for each transistor pair, combining them to ensure 100 % conduction for the two transistors when you have small signals incident on the PA. This yields a higher efficiency than a classical class A amplifier. [8]

The push-pull configuration can be done by using a 180° transformer to let the two amplifiers work with a 180° difference and then combine the power at the output with another transformer. This means that one of the transistors will amplify the signal and the other one a 180° phase shifted part. The positive and negative parts of the signal will come together with a second transformer as stated before. [9]

The Balanced amplifier can make use of a hybrid coupler to double the output power if the

coupler is considered ideal in phase and amplitude. The hybrid would cancel out the mismatch signals from the amplifier since the reflection from the two transistors will be 180° out of phase. This is only true if the transistors are identical. Other reflection in the circuit will end up in the terminated port. However, this is also only true if the coupler is considered ideal in its self. [9]

The power amplifier will in the non-linear region generate harmonics. They will appear in the following manner (n=0, 1, 2, 3…) where you have odd and even harmonics. The harmonics are all generated from the fundamental tone. This will lead to signal distortion of the fundamental tone and is unwanted in a power amplifier. There are several solutions to this problem where e.g. you can use the fact that the even order harmonics always have a positive phase out from the amplifier, this means that you can cancel them with a 180° transformer at the output. There is also a possibility to use a quarter wave stub connected to ground to direct the even order harmonics to ground. [9] [10]

2.2.5 **Circulator**

The circulator is a three-port device which is a non-reciprocal device. The scattering matrix for an ideal circulator can be seen in Equation 1.

$$\begin{bmatrix} 0 & 0 & 1 \\ 1 & 0 & 0 \\ 0 & 1 & 0 \end{bmatrix} \qquad 1$$

From this you can see that the signal only can propagate from port 1 to port 2, port2 to port 3 and port 3 to port 1. The device will have isolation in the reverse direction. The circulator can be used as a switch before the antenna and switch between Rx and Tx mode using the three ports without any control signals. The circulator can also act as an isolator if the circuit design has a 50 ohm resistor at port 3 for the circulator. This will lead to isolation between port 1 and 2 in the reverse direction i.e. isolate the amplifier from reflections. [11]

2.2.6 **Switch**

In the design there are two switches which directs the signal depending if the system is in a transmit or receive state. There are also a total of seven switches in the phase shifter. The switches used in this project are the single pole double throw and double pole double throw, shorten SPDT and DPDT. The SPDT has a single line that switches between two states of output. The DPDT switch used in this project has two inputs and two outputs. It operates by either connecting the outputs straight or in the switched position by crossing the outputs. This means that the two signals on each input pin, both can be directed at the same time to each output pin, unlike if two SPDT would be connected back to back. [12]

2.2.7 **Limiter**

The limiters purpose in a receiver design is to protect the low power components such as the LNA from high power signals. The limiter should have low loss to be able to receive small signals at low power level. Furthermore, the limiter needs to be sufficiently fast, so that the spike leakage doesn't damage the front end of the receiver. The switch between low loss and highly reflective mode of the limiter needs to be swift since the receiver is blind during the limiters "blocking mode". The basic concept of a limiter circuit can be seen in Figure 2.3. When a high power RF signal lays over the diode, it starts to conduct. The impedance gets low and starts to reflect most of the incoming RF-power since you get a large impedance mismatch. This protects the receiver circuit and the limiter itself doesn't need to withstand much power in itself. The purpose of the inductor is to generate a DC path to ground when the diode gets self-biased by the high incoming RF power. This lets the DC current flow through the diode and the inductor. The inductors second purpose is to be a RF choke when the limiter is in the low loss mode. [13]

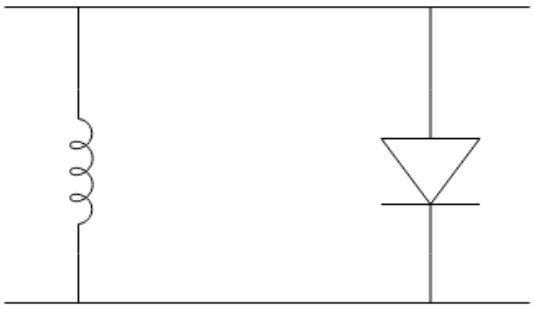

Figure 2.3 Basic limiter circuit consisting of an inductor in the left and a diode on the left.

When there is high power incoming on the limiter there will first be a spike leakage passing through the limiter, this spike leakage needs to be sufficiently small to not damage the receiver. The diodes that are to be used in this project should be able to reflect enough power to not exceed the critical power limit of the receiver circuit. The threshold of a limiter is defined as when the diode used is 1 dB into compression i.e. when the insertion loss is 1 dB higher than the insertion loss when you have a small signal incident upon the diode. The threshold level is mostly decided by the thickness of the I-layer between the P- and N-layers. They are so to say proportional to each other. Another characteristic of the I-layer is the minority carrier life time which is the mean time for a free charge carrier to exist before you get a recombination of the free charge carrier. The I-layers volume and resistivity are directly proportional to the minority carrier life time. The minority carrier life time should be kept short because the limiter will reflect the RF signal faster and thus better protect the receiver with short minority carrier life time. The drawback with short minority carrier life time is a thinner I-layer and you can't handle as a high input power as with a diode with thicker I-layer. [14]

The limiter design seen in Figure 3.25 is a design that has a quarter length of transmission line between the diode with the thinner I-layer and one with the thicker I-layer. The first one is called coarse diode that has a thicker I-layer and the second one with the thinner I-layer is called a clean-up diode. When you have an incoming large RF-signal upon the limiter, the diode with the thinner I-layer will change its impedance first as it has a shorter minority carrier life time. The reflection creates a standing wave with voltage maxima at the diode with the thicker I-layers which will force this diode into conduction earlier. This means that the design will be able to be fast and still protect the circuit from high RF-power since you have the diode with the thicker I-layer as a first stage. [15]

2.2.8 LNA

The low noise amplifier's (LNA) main purpose is to have a low noise figure as the name suggests. The LNA is often used in receivers since the noise floor is closer to the signal peak, this means that if the noise figure isn't low enough for the amplifier the signal to noise ratio (SNR) become too low to detect the signal. To achieve minimum noise, one must compromise and accept a lower gain by matching the input closer to Γ_{opt}. In this project the LNA is used in the receiver part of the TRM. [11]

2.3 Stability

Instability in a circuit is when it has the potential to oscillate. The reason for this phenomenon is often due to the port impedance of the circuit has a real part less than zero resulting in a $|\Gamma_{in}| > 1$ or $|\Gamma_{out}| > 1$. This oscillation can also occur at other frequencies than those your designs are made for. [11]

Measuring the stability, one can use Rollet's condition. The test is defined so that if k>1 and $|\Delta| < 1$ are satisfied, the circuit are unconditionally stable. The definitions for k and Δ can be seen in Equation 2 and 3. [11]

$$\boldsymbol{k = \frac{1 - |s_{11}|^2 - |s_{22}|^2 + |\Delta|^2}{2|s_{12}s_{21}|} > 1} \quad (2)$$

$$\boldsymbol{|\Delta| = |s_{11}s_{22} - s_{12}s_{21}| < 1} \quad (3)$$

Where s_{xx} are the scattering parameters of your devise.

2.4 Antenna

The antenna in the following thesis will be a linear array antenna and therefore this type of antenna will be described here in more detail. Then two of the important characteristics and measurements that are to be done for this type of antenna, this will be discussed in the chapters 2.4.1 and 2.4.2.

An array antenna always consists of several antennas and differs from a classical single antenna. There are some advantages to use an array rather than a single antenna, where one of the advantages is that you can steer the antenna beam by phase shifting every antenna element. For the best result when it comes to shaping and steering the antenna beam you should be able to change both the phase and amplitude of each antenna element in the array. Another advantage is that you can keep the size down for the array i.e. have a slimmer design if you compare it to a reflector antenna. However, one disadvantage is that it is more expensive to design an array and manufacture it. The array can be designed to have a so called full scan and that means $\pm$ 60°, this is the intended goal in this master thesis project. [16]

2.4.1 Embedded element pattern

The embedded element pattern is the radiation pattern for one element while the other elements are terminated. Superposition of the embedded element patterns represents the radiation pattern of the full antenna with an ideal feed network [17]. By measuring the embedded element patterns of each element different beams can be generated in post simulations. In these post simulations, the full system can be simulated, and the phase and amplitude of each antenna element's electric field can be modulated to see the effect in the far field.

2.4.2 Active reflection coefficients

The active reflection coefficient for an antenna element is the reflection seen when all elements are excited at the same time, i.e. including mutual coupling. Typical unit cell simulations, in e.g. HFSS, assumes uniform excitation with same amplitude for all elements in an infinite array and a progressive phase shift for a particular scan angle. If the full S-matrix is measured or simulated for a finite array the active reflection coefficient for each element can be computed by applying the desired amplitude and phase excitations at each port, [18]

3. Design of TRM

Manufacturing of the test boards are done in order to classify the components and make necessary changes to optimize the circuits individually. Post improvements and classifications for future work are also easier if there are test circuits of the components used. The most important components are the phase shifter, LNA, power amplifier and filter. They are crucial in order to make the system reach the specifications and regulations set by SAAB and the IFF standards. For future work, things as isolation and filters may be of interest for a second evaluation if the power demand increases or substitutions are to be made of some components.

The designs used in the test boards were taken from the suggested circuit from the data sheet, if included. It was applied on our substrate and tuned for this project needs using ADS. As for the amplifier without a large signal model the goal was to sustain the suggested impedance on the source and load. For amplifiers without an optimal source and load suggestion, s-parameter matching was made. For the large signal models, the design was optimized to reach a good compromise between linearity, high 1 dB compression point and suppressing the harmonics.

3.1 TRM block diagram

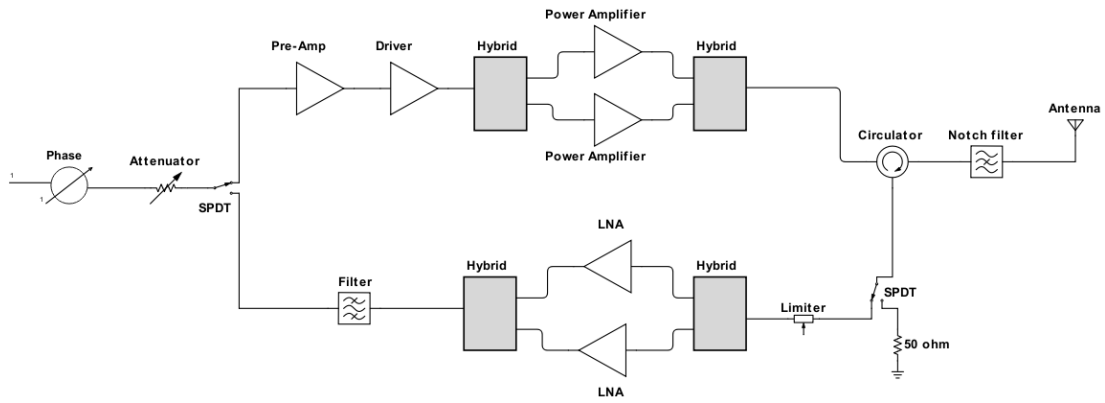

Figure 3.1 The general view of the TRM block diagram where you can see the main parts needed for a TRM circuit. The different parts/components will be discussed in this chapter.

3.2 Substrate

Substrates are important depending on the applications. In the 1GHz area, most substrates are sufficient as for higher frequencies there can be problems to have a stable dielectric constant for a wide frequency band. Referring to the project back in 2009 they used Rogers 4350B for their project [19]. This substrate is a well-established and known substrate capable of handling high frequencies. This substrate was also stated on the PCB-manufactures website to always be on hand, leading to fast turnaround on the manufacturing. The substrate used to design the TRM in this project is Rogers 4350B. The properties concerning a power amplifier design for the substrate can be found in Table 3.1

Table 3.1 Properties of the substrate ROG4350B

Properties	Typical Values	Test Condition
Dielectric Constant, $[\varepsilon_r]$	3.66 $\pm$1,5 %	8-40 GHz
Dissipation Factor, tan$[\delta]$	0.0031	2.5 GHz
Thermal Coefficient of ε_r	50 [ppm/°C]	-50 °C to 150°C
Thermal Conductivity	0.69 [W/m/°K]	80 °C

The loss tangent has a high impact on the loss of the circuit and should be as low as possible for the substrate. The importance of a low variation of the dielectric constant, ε_r, is related to the impedance match of the power amplifier which in turn will affect both gain and power. According to J. Coonrod [20] you should have a tolerance of 1.5 % or better which is the case for the chosen substrate ε_r. Thermal coefficient (TCD_k) illustrates how much the dielectric constant changes with temperature. Since a power amplifier will generate its own heat variation it's especially important to have a low TCD_k. The property thermal conductivity is a key figure that illustrates how good the substrate will transfer heat. The thermal conductivity as a rule of thumb should be 0.5 W/m/°K or higher when using the substrate for a power amplifier [20]. This can be seen in Table 3.1 that the value is 0.69 W/m/°K. The material properties of Rog4350B are therefore well suited for a power amplifier mounted on it.

3.3 Phase shifter

Difficulty in finding a phase shifter in stock for the IFF frequency band led to two different phase shifters to be designed for this project. One IC bought and one we designed. The bought one is a MAPS-011007 and is rated for 1.2 to 1.4 GHz, however the .s2p file available spans from 200MHz to 2.4 GHz enabling an evaluation of the product.

Due to the MAPS-011007 was not intended for use outside of the 1.2 to 1.4GHz band, a design was made for the IFF band as well. The two could then be compared to each other and the best design could be picked for the task.

The phase shifter design is built using the time delay between two TL of different lengths, calculated using LineCalc for the lower centre frequency 1030MHz. This was made due to the specification of 6 bits resolution and both 1030MHZ and 1090MHz need to be able to phase shift 360°. The wavelength of 1090MHz is shorter than 1030MHz and is there for phase shifted 380.968°, for filling the specification.

The design is built on DPDT switches of model MASWSS0129 connecting a TL of length ε and one of length $LSB \cdot 2^n + \varepsilon$ where LSB is the least significant bit length. N is an integer from 0 to 5 and ε is the minimum TL needed in order to construct the circuit due to dc block capacitors needed between the switches and clearance. The general typology used can be seen in Figure 3.2.

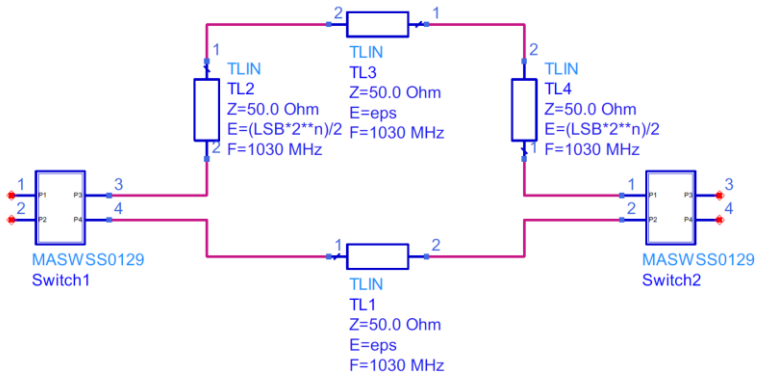

Figure 3.2 The design typology used for the phase shifter.

Each bit was EM simulated at the ends of the TL and tuned for close approximation to the ideal phase shift. The data for each bit is included in Table 3.2

Table 3.2 The EM simulated phase shift for each bit in the phase shifter

Ideal Phase Shift for the 6 Bits	EM Simulated Phase Shift	
	1030 MHz	1090 MHz
5.625°	5.628°	5.955°
11.25°	11.246°	11.899°
22.5°	22.494°	23.801°
45°	44.998°	47.612°
90°	90.264°	95.513°
180°	180.025°	190.483°

This design was implemented in cascade coupled design with a SPDT at each end of the phase shifter. The SPDF switch used was MASWSS0157 from Macom rated from DC to 2.5GHz. The layout was made compact and capacitors were added. The control signals for the switches were added. The final design can be seen in Figure 3.3.

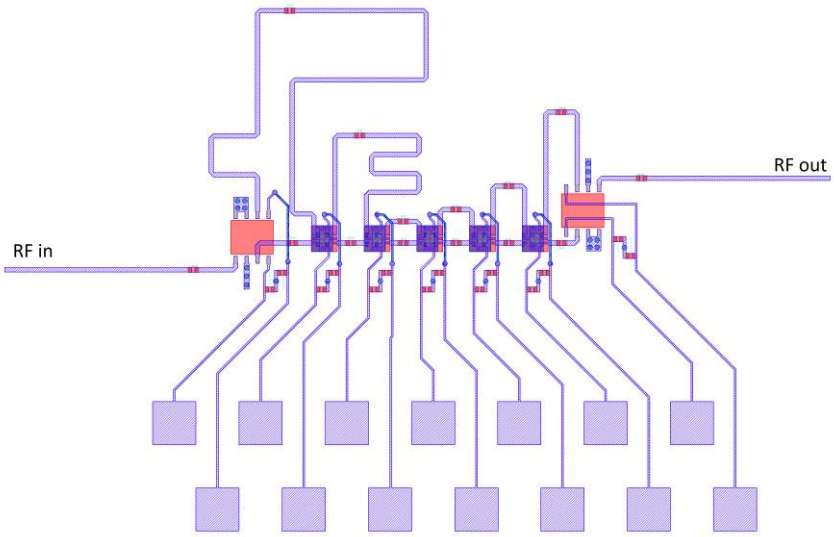

Figure 3.3 Layout of the phase shift test circuit. From left to right is the 180°, 90°, 5.625°, 11.25°, 22.5° and 45° phase shift TL. On the bottom is the control bus connected to pads for easy soldering, added to the bus are a potential pull down resistor if wanted.

3.4 Attenuator

The attenuator has the function within the TRM to perform tapering of the antenna beam forming and attenuate the signal. The attenuator is placed after the phase shifter in the common signal path of the Rx and Tx. The chip selected were HMC624a from Analog Devices. The chip has a 31.5dB max attenuation with a resolution of 0.5dB controllable using 6 bits. This is enough for us to have the 1dB resolution for 0 to 10dB attenuation.

The attenuator insertion loss is at its highest 1.35 dB, this is a low insertion loss, and insertion loss in this part of the circuit is not critical since the attenuator is located in the low power part of the TRM. The insertion loss can be seen in Figure 3.4 below. The simulated insertion loss is simulated by the help of the manufactures S-parameters. In Table 3.3 you can observe the different attenuation levels from 1 dB up to 10 dB for the transmitter and receiver frequency.

Table 3.3 The ideal attenuation compared with the simulated one using S-parameters for the frequencies 1030MHz and 1090MHz. The simulated attenuation in is reference to the insertion loss of 1.35dB.

Ideal attenuation	Simulated [1030 MHz]	Simulated [1090 MHz]
1 dB	1.02	1.02
2 dB	2.02	2.02
3 dB	3.04	3.04
4 dB	4.00	4.00
5 dB	5.01	5.01
6 dB	6.02	6.02
7 dB	7.03	7.03
8 dB	7.94	7.94
9 dB	8.96	8.96
10 dB	9.97	9.97

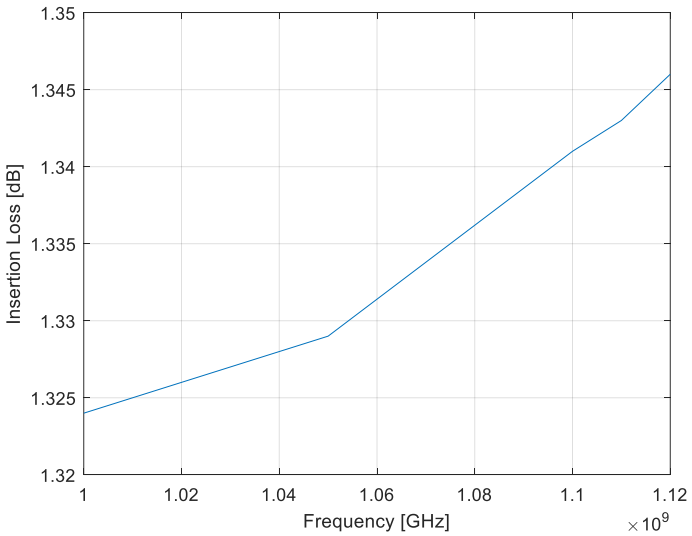

Figure 3.4 The insertion loss for the attenuator when zero attenuation is set.

The test circuit for the attenuator can be seen in Figure 3.5. Different combination of bits can be set by applying positive voltage to the 6 pads connected to top part of the IC circuit.

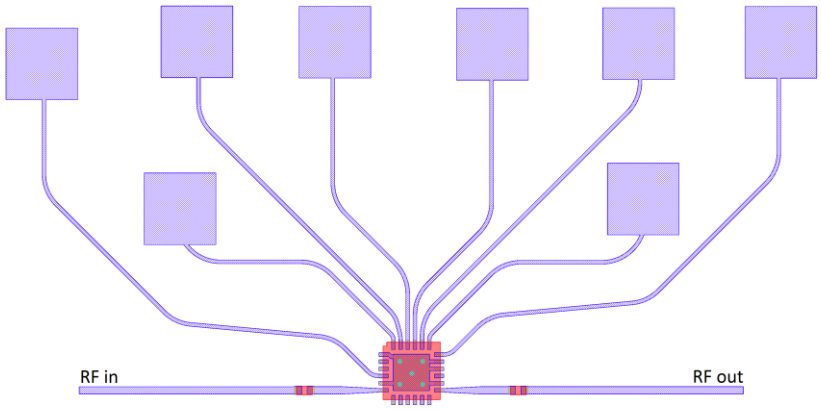

Figure 3.5 The layout of the attenuator. RF in and out is located at the bottom of the circuit. On top of the circuit are pads for setting the bits and bias voltage. The pad farthest to the left is the bit to set full attenuation or to be controlled by the parallel bits.

3.5 Power amplifier

The power amplifier is essential to reach the power levels needed in this project. The specification for the project states a minimum of 700 watts to each antenna element. We selected two 700W amplifiers from NXP called AFV10700 as our amplifiers to accommodate losses and not reaching full power of the amplifiers. This gave us plenty of margin as these two would be able to deliver 1400W in theory. This amplifier is intended for use in IFF systems and second surveillance radars, making them ideal for this project. Each amplifier is constructed by two identical 350W amplifiers in the same capsule working in a class AB configuration. This gives the user the ability to drive the amplifiers in different configurations. A common way is to drive them in a 180° phase difference giving a push pull configuration, seen in many data sheets for other amplifiers from NXP. For AFV10700, included in the data sheet, is a matching network for driving the amplifier in phase, resulting in a small and compact design if desired.

3.5.1 Matching of PA

Included in the data sheet are two different evaluation boards, one driving the two internal amplifiers in phase for 1030MHz to 1090MHz and one driving it in a push-pull configuration for 1030MHz narrow band.

Due to troubles stabilizing the amplifier design driving them in phase, a test was done, switching to a push-pull configuration intended for another amplifier by NXP, the MMRF1317H, which uses a balun for the 180° phase shift between the two amplifiers. The reason for selecting another amplifiers's push-pull matching network instead of the intended one is the intended one uses coaxial cables in the layout to realise the balun, making it hard to realize and manufacture. The Balun used for the MMRF1317H also has s-parameters and is therefore easy to simulate.

Using a balun at the output combining the signals helps with the even harmonics. This is due to the balun is phase shifting the signal n*180°, where n is the harmonic order. This combined the even harmonic 180° out of phase from each other, resulting in destructive interference. [10] [9]

The layout was done with MMRF1317H's matching network in mind. There are included recommended source and load matching impedance for the AFV10700, but when tried, the results were modest, and the circuit became hard to stabilize. To get a good result, the circuit was optimized for a stable circuit, high output power and stable gain for large range of power, making it more linear. Simulations were tried with changing the capacitor connecting the outputs of the amplifiers seen in Figure 3.6. This was done to see if this value can be tuned for a stable circuit, which worked.

3.5.2 Layout

Due to the matching primarily was done using SMD components, the layout manages to become quite compact, minimizing the TL's length and the space is largely occupied by the baluns. Due to these having an impedance of 12.5+j Ohm, they are part of the matching impedance up to 50 Ohm. A lot of space is also taken up by the electrolytic capacitors as well, needed at the drain. These have a diameter of 13mm each and are put in the layout were they would take up as little horizontal space as possible, seen in Figure 3.6. This is due to the final design being constructed of two power amplifiers, the design will be mirrored and added in parallel. This adds up in width and the design coming close to the limit of 120mm.

In order to minimize coupling from the output to input resulting in possible instability due to increased S_{12}, seen in Equation 2, ground planes are added around the amplifier. The slot for the capsule also acts as isolation between the input and output, isolating it further. This slot was extended to the neighbouring amplifier, also leaving a gap between them for the antenna contact to go through. Minimize the coupling between the amplifiers was done with a strip of grounded line located between them. This can be seen on top of the layout in Figure 3.6 as well as in the middle of the double amplifier in Figure 3.7. To minimize the even harmonics, a stub to ground at the output was made possible to be tuned for a quarter wavelength, reflecting the harmonics. Via holes on either side are for grounding tape located over the TL, decreasing the length of the stub in tuning.

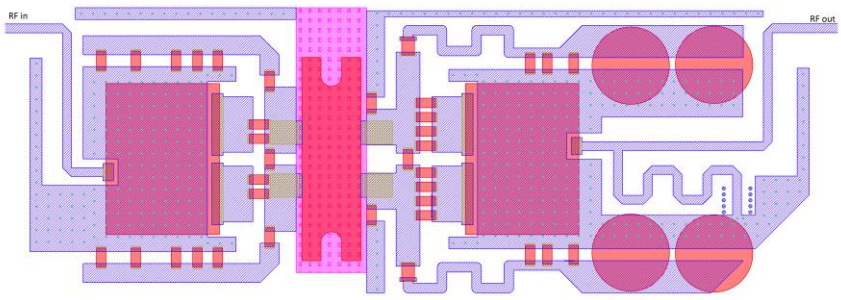

Figure 3.6 The layout of a single PA. Input on the left and output on the right hand side. On ether end of the TL for input and output are the baluns represented as two large red blocks. In the centre is a large pink cut out for the amplifier-chip, in red, to make contact with ground.

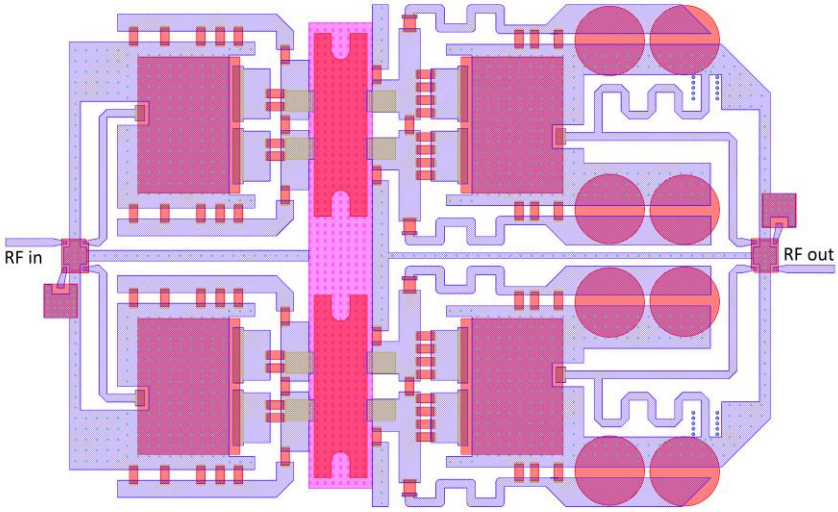

Figure 3.7 The layout of two amplifiers as seen in Figure 3.6, connected using a hybrid and a high power terminating resistor for the isolated port on each side

.

3.5.3 PA performance

The PA, due to having a non-linear model, compression points and large signal gain can be simulated using ADS. Of interest are the power output and gain of the double amplifier configuration. To compare the simulations with the test circuit, simulation of the single amplifier is included, seen in Figure 3.8.

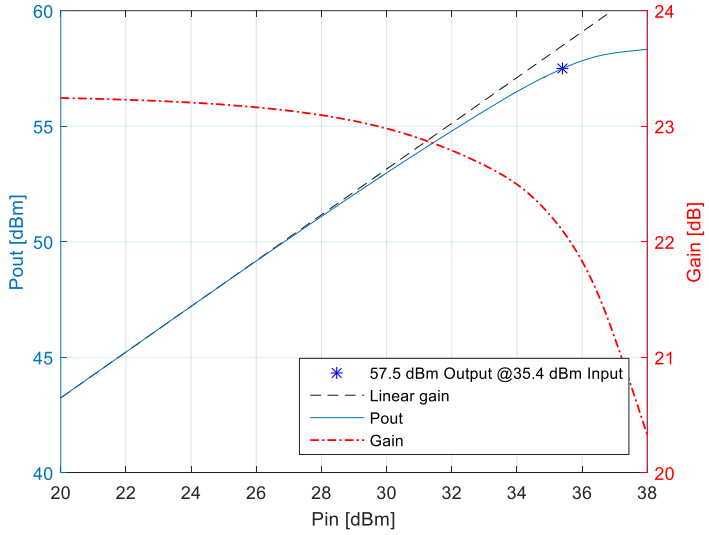

Figure 3.8 Large signal gain and output power of a single PA at frequency 1030MHz. On the left is the power output from the amplifier, plotted in blue, and the linear gain in black lines is extrapolated from the two lowest output powers. Represented as a blue star is the 1dB compression point. On the right hand side axis is the large signal gain together with the gain plotted with a dotted line in red.

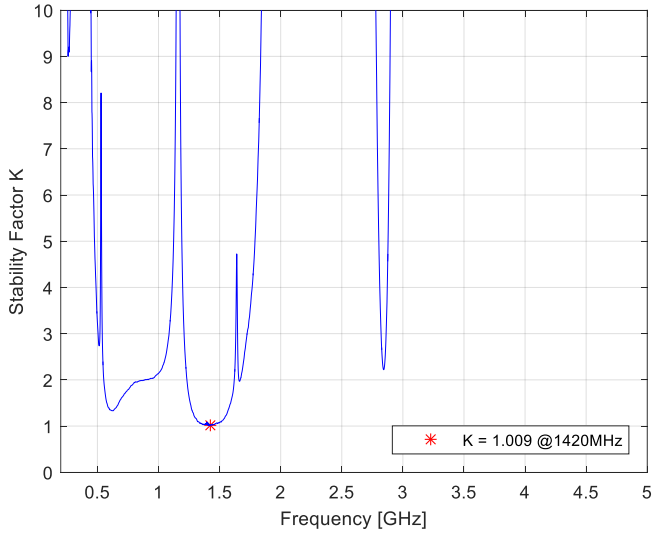

Figure 3.9 Stability factor for a single PA plotted over a small frequency span for the critical area. Represented as a star is the lowest point were k=1.009 at 1420MHz.

For the power output, the double amplifiers are of interest as well as the linearity of the gain. Seen in Figure 3.10 the gain drops off early, but do not go under 1dB until 60.6dBm of output power, equal to 1143W.

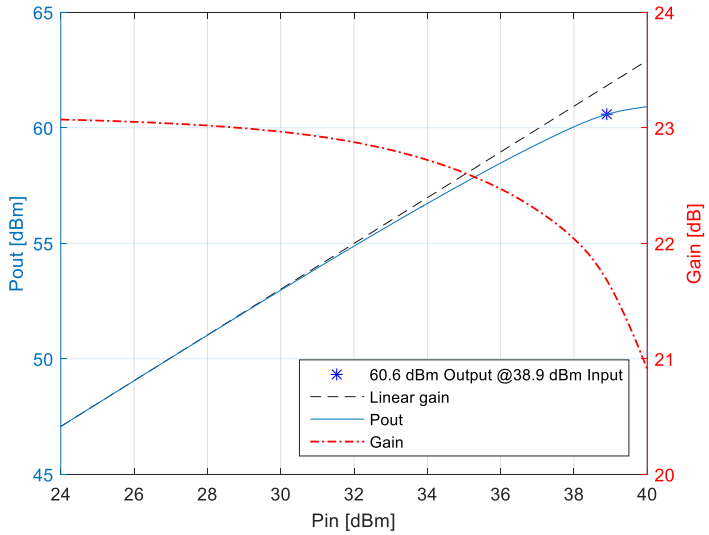

Figure 3.10 Large signal gain and output power of double PA at frequency 1030MHz. On the left is the power output from the amplifier, plotted in blue, and the linear gain in black lines is extrapolated from the two lowest output powers. Represented as a blue star is the 1dB compression point. On the right hand side axis is the large signal gain together with the gain plotted with a dotted line in red.

3.6 Driver

For reaching the 42dBm needed in the simulations for the power amplifier, the NPT1004 from Macom was selected for its high output power of 45dBm. This meant that we could drive the amplifier in a relaxed manner or add a 3dB attenuator after it for added stability. For the simulations, the chip lacked a proper data sheet for the frequencies under 2.5GHz but did provide plots down to 900MHz, ensuring us the gain and 1dB compression point was sufficient for our purposes. The s-parameters provided to us by Macom on request stated that the amplifier would be suitable for us. Unfortunately, the large signal parameters were not complete as the parameters for the capsule were not populated due to being lost. The design had to be done on suggested source and load impedance found in the data sheet and stability using Rollet's condition [21] [11].

3.6.1 Matching driver

The amplifiers data sheet did not include a test circuit, meaning that we had to design our own matching circuit. We used a simple step in TL width and a capacitor to ground, making it easy to tune the device by changing the position of the capacitor or its value.

Matching the amplifier was done by looking at the impedances for source and load at the stated 900 and 1500MHz impedances in the smith chart and by tuning the width and length of the transmission lines and the value and position of the capacitors. The final matching impedances can be seen in Figure 3.11 and Figure 3.12.

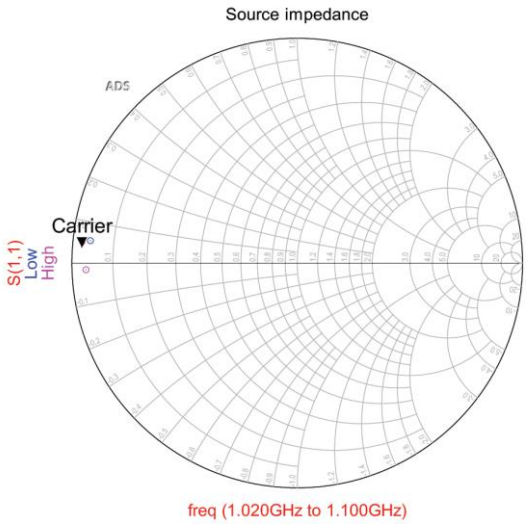

Figure 3.11 Source impedance of the driver network with the recommended impedance for Low=900MHz and High=1500MHz.

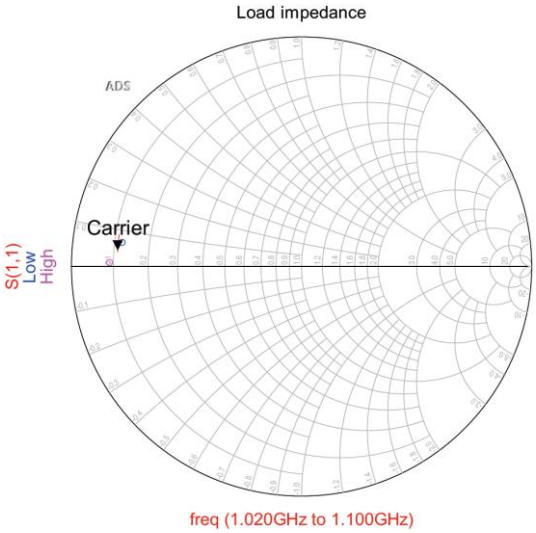

Figure 3.12 Load impedance of the driver network with the recommended impedance for Low=900MHz and High=1500MHz.

The drain and gate bias transmission line were selected to be a quarter wavelength to the decoupling capacitor in order to reduce the leakage and interference of the voltage source on the matching for the driver. Stabilizing was done with a resistor on the source side, coupled to ground. The layout of the test circuit can be seen in Figure 3.13

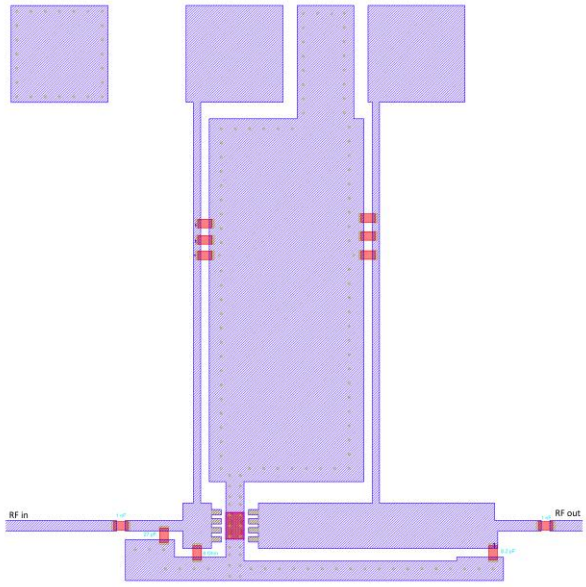

Figure 3.13 Layout of the driver. In each end, coupled to ground there are two capacitors used for matching and a resistor closest to the gate for stabilizing the circuit. On top of the figure are ground, bias and drain voltage supply pads.

3.6.2 **Driver performance**

Due to the matching being done with consideration of the optimal load and source, the performance using small signal simulations with the s-parameters are somewhat off as these changes with power output. This does not give a fair representation of the amplifier design and the performance is hard to evaluate. As mentioned, the design was done so stability can be achieved simply by increasing the resistor at the gate. This meant that if the amplifier differs from the s-parameters, the resistor can be tuned to reach stability. The simulated stability can be seen in Figure 3.14.

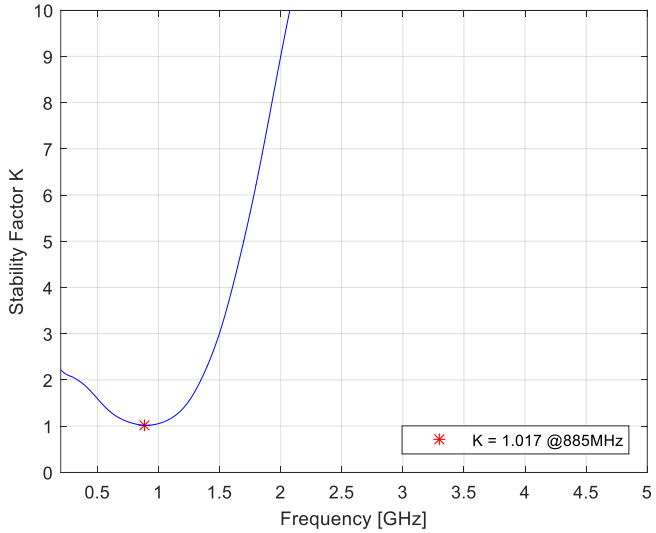

Figure 3.14 Stability factor of the driver over a small frequency span for the critical area. Represented as a star is the lowest point were k is 1.017 at 885MHz.

Due to the matching was done using the optimal load and source, the simulated scattering parameters S_{11} and S_{22} are poor. This also affects the gain as lots of power get reflected at the ports, resulting in lower gain than the 22dB stated in the data sheet. The simulated S_{11} and S_{22} can be seen in Figure 3.15 and the small signal gain (S_{21}) can be found in Figure 3.16.

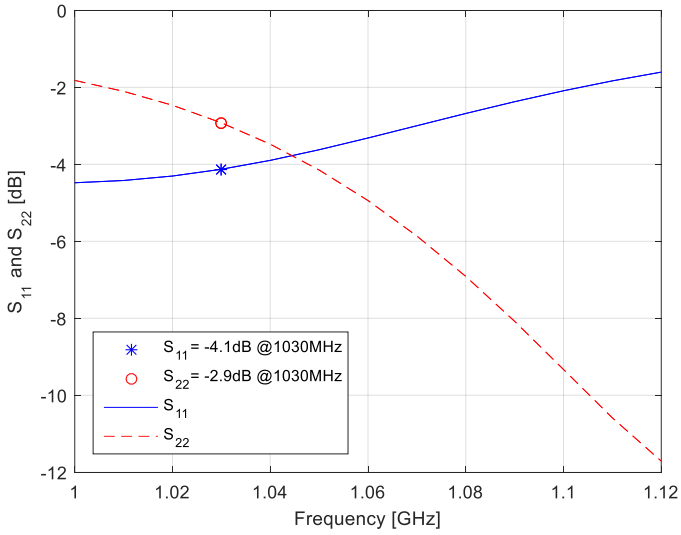

Figure 3.15 S_{11} and S_{22} for the driver circuit. In blue full line is S_{11} and in red lines are S_{22}. Represented as a blue star and a red circle are the values for S_{11} and S_{22} at 1030MHz respectively.

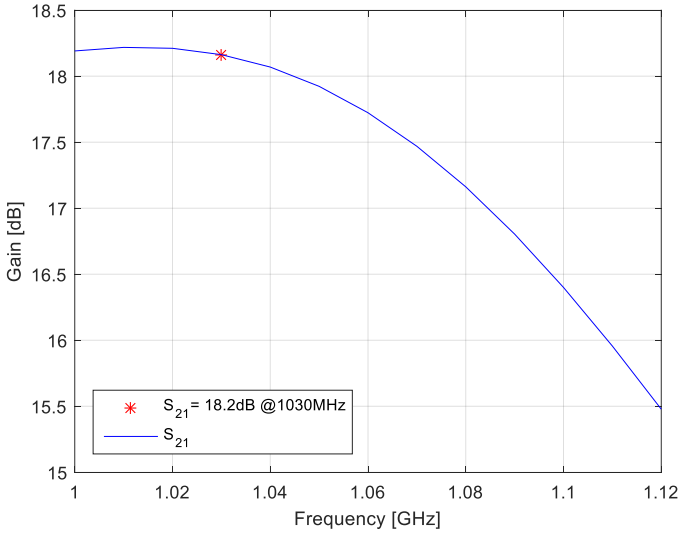

Figure 3.16 The small signal gain (S_{21}) with a marker at 1030MHz reading a gain of 18.2dB.

3.7 Pre-amplifier

The simulated driver needs around 24dBm input in order to deliver enough power to the PA, and 29dBm in order to go into compression. The MMG3006NT1 from NXP was selected due to its price in comparison to gain and its frequency span is well suited for the project. It has a 1 dB compression point at 33dBm output power and a gain of 17.5dB. This gain meant that we will be low under the desired 10dBm input desired from SAAB.

3.7.1 Matching pre-amplifier

Matching was done using the suggested layout provided in the datasheet. Due to being a different substrate, a 14 mil thick FR408, hand tuning in ADS was done in order to reach good matching and gain with the Rogers 4350B substrate. The capacitors used in matching were tuned as well as the width and length of the transmission lines. An overall desire to keep it small and compact was of interest as well. Because the biasing uses a resistor of 100 ohm and the drain has an inductor in series as a RF block, the transmission lines could be kept under quarter wavelength and made compact while not depending on the voltage source. This layout can be seen in Figure 3.17

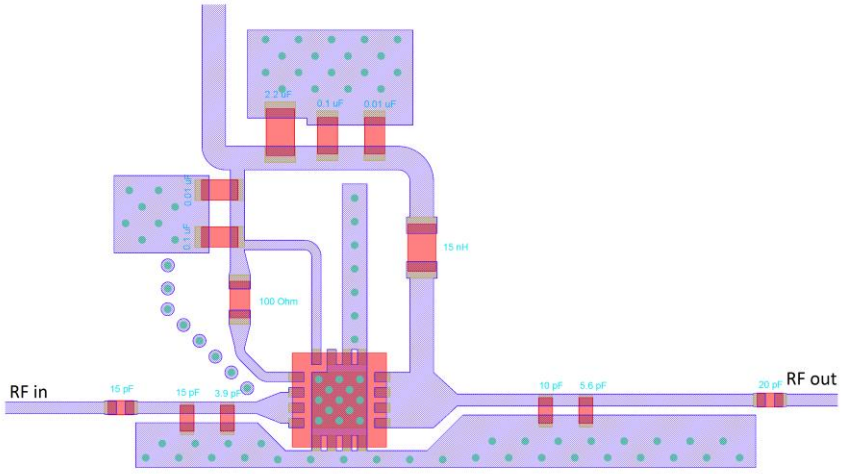

Figure 3.17 Layout of the pre-amplifier with RF in on the left and RF out on the right hand side. In each end, coupled to ground, there are four capacitors used for tuning the circuit. On top of the figure we have a TL going to the biasing of the amplifier.

3.7.2 Simulated pre-amplifier performance

The matching of the amplifier gave a low reflection for a slightly higher frequency. This difference is neglected as the components have a low accuracy in value that will shift it some in the real circuit. These simulation results of the scattering parameters can be seen in Figure 3.18. The simulated gain resulted in a peak at the transmitting frequency of 1030MHz, yielding a high gain for the intended bandwidth and frequency, seen in Figure 3.19.

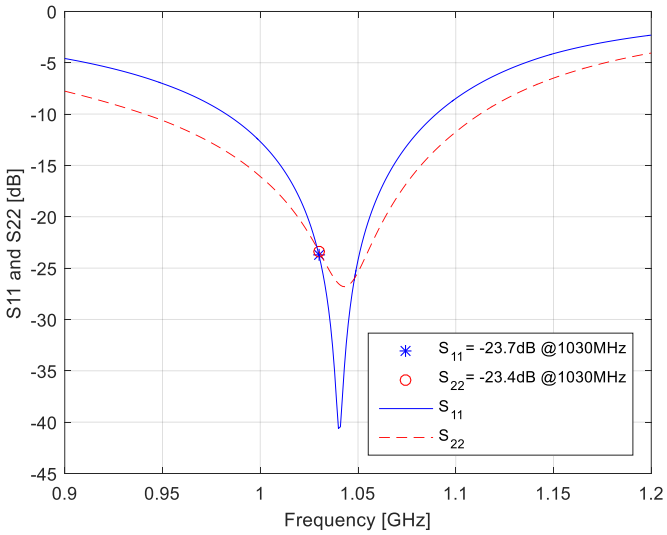

Figure 3.18 S_{11} and S_{22} for the pre-amplifier. In blue full line is S_{11} and in red lines are S_{22}. Represented as a blue star and a red circle are the values for S_{11} and S_{22} respectively at 1030MHz.

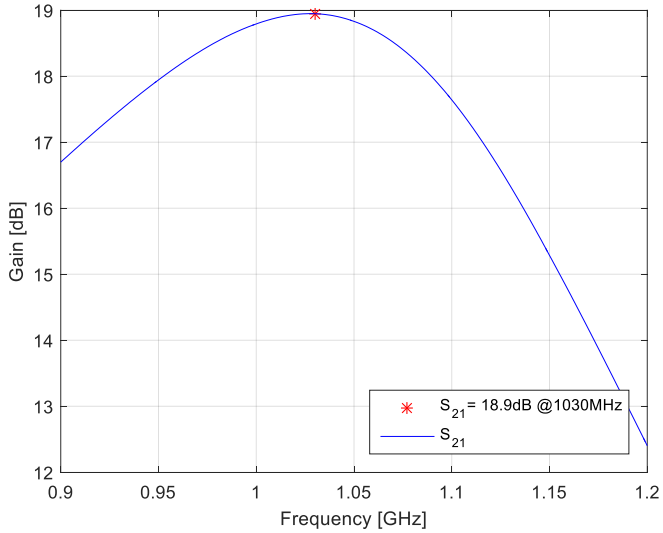

Figure 3.19 The small signal gain (S_{21}) with a marker at 1030MHz reading a gain of 18.9dB.

3.8 Filter

The IFF regulations set by NATO have criteria to follow regarding the harmonic powers in perspective to the carrier, these can be found in Table 3.5 [2]. The simulated PA harmonics can give us estimates of the performance needed by the filter, seen in Table 3.4. The difficult part is suppressing the modes with a prime multiple as the even harmonics are supressed by the baluns and stubs at the PA. In simulations of the amplifier, we found that the 11th harmonic and up already had such a high dBc so natural loss in the system and added reflection from filter at higher frequencies are assumed to be enough to reach the IFF standard. This leaves the filter to only filter out the harmonics of the 3rd, 5th, 7th and 9th order. As for the 9th order being already low and a multiple of the 3rd order, filter characteristics will filter this one out to some extent meant it could be left out in the optimization. The electromagnetic (EM) simulation and optimizations tool in ADS were used for this.

Table 3.4 Harmonics from two power amplifiers coupled via hybrids using s-parameters. The input power and harmonics are stated in dBm and dBc, and carrier power is stated in watts. In bold/colour are the worst case that are to be compensated for by the filter in order to reach the specifications.

Input dBm	2nd	3rd	4th	5th	7th	9th	11th	Carrier[W]
30	78,23	58,53	129,98	97,31	124,14	161,25	187,3	184,72
31	77,33	56,4	127,16	93,44	118,07	153,32	178,03	230,46
32	76,46	54,19	124,43	89,74	111,71	145,72	168,69	286,72
33	75,65	51,92	121,88	86,37	105,14	138,68	159,35	355,44
34	74,89	49,71	119,71	83,61	98,83	132,38	150,44	438,64
35	74,08	47,82	118,38	82,06	93,66	126,99	142,1	538,34
36	72,92	46,73	118,25	83,81	91,62	123,92	142,42	656,16
37	71,18	46,74	118,1	90,73	93,21	128,18	133,24	791,97
38	69,07	47,35	115,04	74,13	81,24	123,87	123,34	941,86
39	67,34	48,16	113,06	67,58	71,36	97,57	110,84	1078,97
40	66,97	50,41	115,13	**67,16**	67,89	91,89	101,24	1152,01
41	67,09	49,15	110,57	70,31	**66,87**	**91,55**	**97,54**	1191,66
42	67,26	**45,94**	107,96	74,87	67	92,16	98,59	1220,04

These numbers are however only for the PA. The circulator that is to be used as the output switch tends to generate harmonics with high power throughput [22]. By looking at the data in Table 3.4 we can calculate the filter needed in order to reach the specifications. The filtering needed is stated in Table 3.5.

Table 3.5 Restriction regarding the power difference between carrier and its harmonics and the filtering needed to reach these [2].

Harmonic	Suppression	Filter needed
2	60 dBc	0 dB
3	80 dBc	34.06 dB
4	100 dBc	0 dB
5	100 dBc	34.84 dB
7	100 dBc	33.13 dB
9	100 dBc	8.76 dB
11	100 dBc	2.46 dB

As for the design it is hard to eliminate specific frequencies with notch filters due to uncertainty of the dielectric constant in the substrate [23]. This made us do three different designs for different dielectric constants, 3.66, 3.76, 3.80 and during measurement determine which one had the best performance and if some changes were to be implemented. In the optimization three double stubs were set up and connecting them is 50 Ω TL, seen in Figure 3.20.

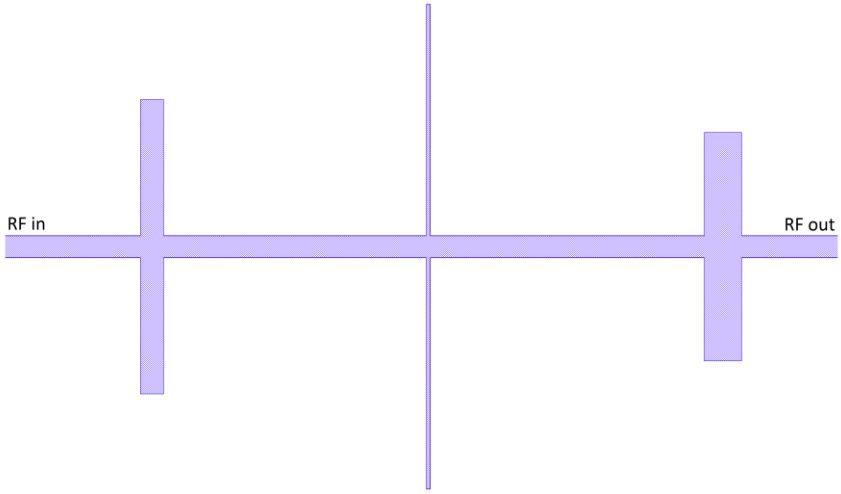

Figure 3.20 The filter layout for ε_r=3.66. The filters for ε_r=3.76 and ε_r=3.80 looks very similar to this one. The signal path is from left to right or the other way around due to being reciprocal. From the left stub to the most right handed side stub it measures 40.6mm. The height measures 32.7mm.

The criteria in the optimization were low loss at the carrier frequency and high reflection in the harmonics with a general high frequency suppression to give the filter a low pass characteristic. This is meant to add some additional filtering to the even harmonics as well as the higher order harmonics if they would be stronger than simulated. The filter was EM simulated, showing a large mismatch between the model used for optimization and the EM simulated one. The notches had been shifted in frequency, not eliminating the harmonics. The difference in frequency was measured and compensated

for in the optimization leaving a filter with the desired characteristics in the EM simulation. The final EM simulated scattering parameters can be seen in Figure 3.21,Figure 3.22,Figure 3.23.

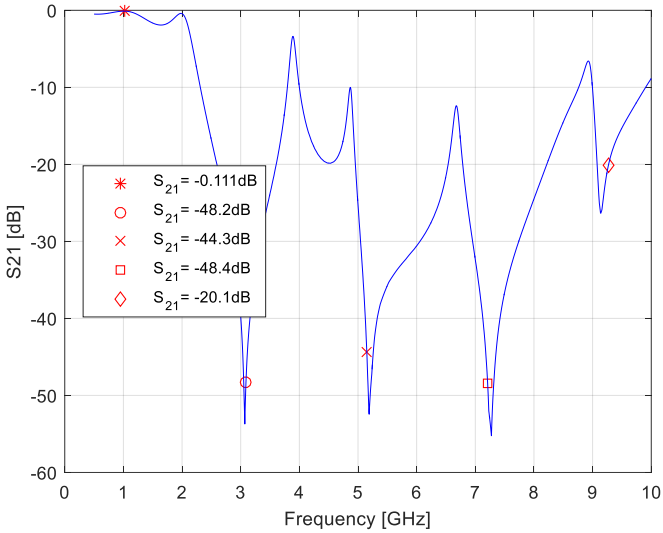

Figure 3.21 Filter with ε_r=3.66 with the attenuation on the y-axis. The markers are at the carrier 1030 MHz and its 3rd, 5th, 7th and 9th harmonic.

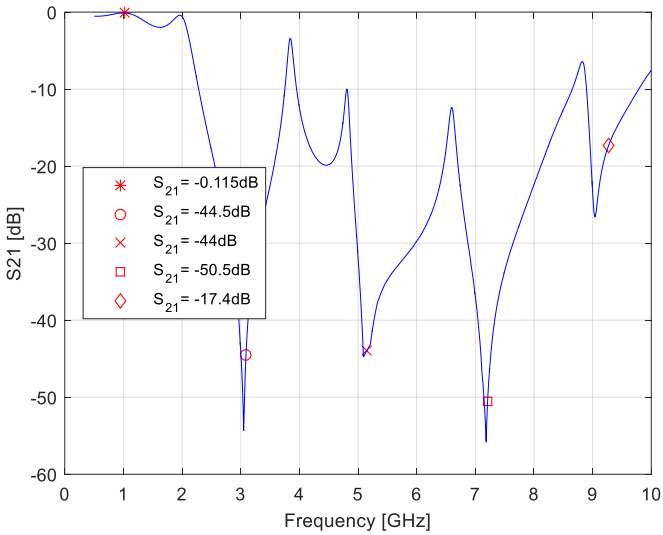

Figure 3.22 Filter with ε_r=3.76 with the attenuation on the y-axis. The markers are at the carrier 1030 MHz and its 3rd, 5th, 7th and 9th harmonic.

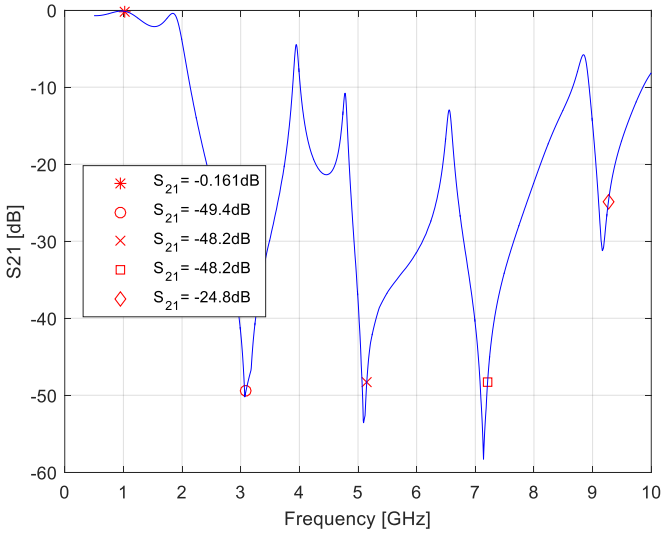

Figure 3.23 Filter with ε_r=3.80 with the attenuation on the y-axis. The markers are at the carrier 1030 MHz and its 3rd, 5th, 7th and 9th harmonic.

Saving these as .s2p files enables us to simulate them together with the amplifier in ADS. In the final design the filter is to be placed after the circulator to supress its potential harmonics as well, so the simulations are not an accurate representation of the layout to be used. The s-parameters for the hybrids connecting the PA´s are only populated up to 6 GHz. This adds uncertainty as ADS extrapolates the s-parameters up to the 11th harmonic. The simulations seen in Figure 3.24 are using the filter with ε_r= 3.76.

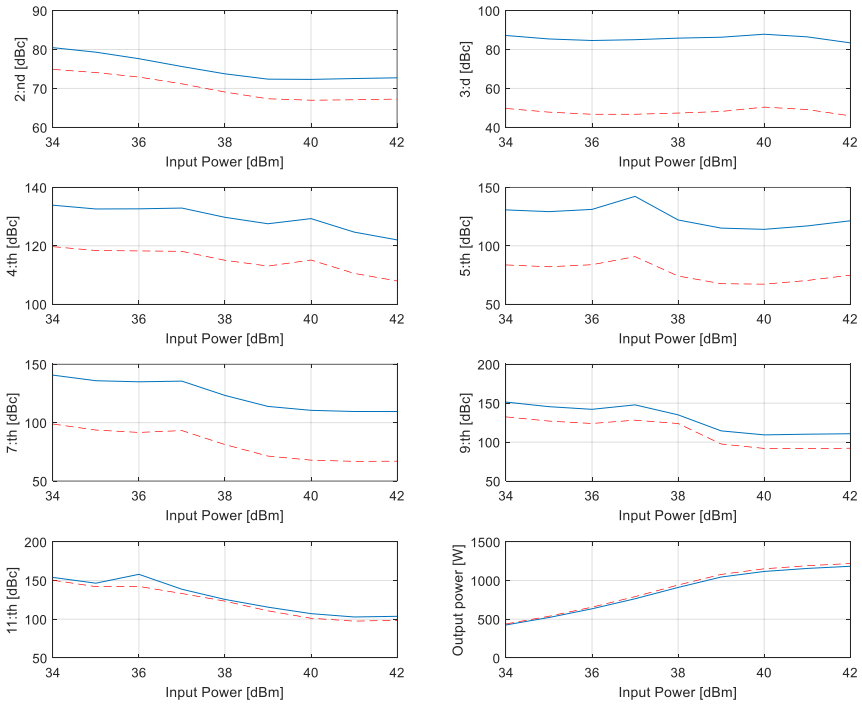

Figure 3.24 Harmonics from two amplifiers in parallel without filter in red lines and with filter in blue solid line. X-axis is input power into the hybrid in dBm and y-axis is power out from the hybrid connecting the amplifiers or out from the filter. Bottom right plot states the output power from the system in watts.

3.9 Limiter

The limiter consists of two PIN diodes, inductor, DC-blocking capacitors and a quarter wavelength transmission line. The diode located at RF out in Figure 3.25 is called the clean-up diode and as the name states limits the signal that goes through the coarse diode. The clean-up diode switches faster than the coarse diode which means that it will start to reflect the signal first. The coarse diode is meant to reflect most of the incoming large signal, but is slower to open due to the thicker I-layer. The clean-up diode will generate a standing wave when it start to reflect and therefore generates a higher potential if done right at the coarse diode, opening it faster. To get the maximum standing wave at the coarse diode a quarter wave transmission line is needed between the diodes.

Figure 3.25 The layout for the limiter. Seen from the left there are a dc block realised with a capacitor, the coarse PIN diode, quarter wavelength TL, clean-up PIN diode, an inductor in parallel and finally a DC blocking capacitor.

The length was EM simulated to get the best performance. The result of the EM simulation can be seen in Figure 3.27. The insertion loss for the limiter when not active (low power) can be seen in Figure 3.26. This value was optimized with help of the two DC-blocking capacitors and the inductor.

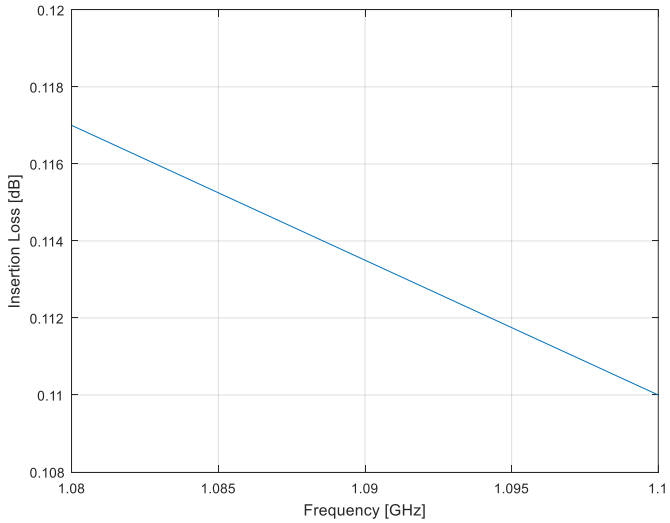

Figure 3.26 The insertion loss of the limiter with a small input signal. As seen the insertion loss is low for the Rx frequency of 1090MHz.

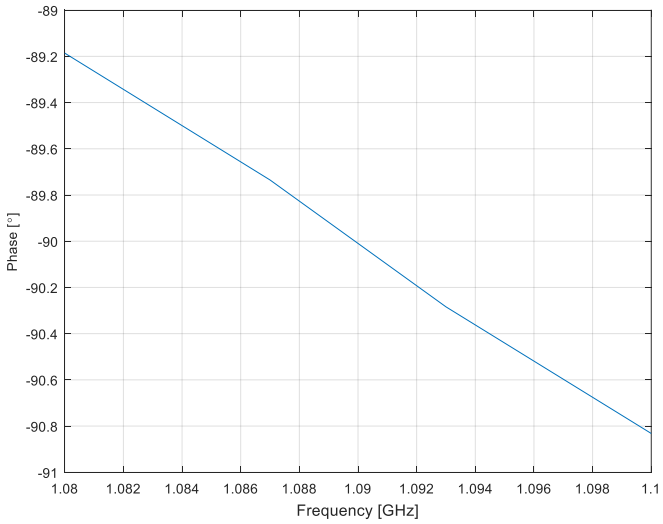

Figure 3.27 The EM simulated phase shift of the quarter wave transmission line between the clean-up diode and the coarse diode. The transmission line is exactly a quarter wave long for the Rx frequency of 1090MHz.

3.10 Isolation Switch

The LNA has a limiter in front of it, protecting it from high powers that can potentially destroy it. If the system is transmitting, then the circulator directing the signal to the antenna are leaking some power to the isolated port to the LNA. In contribution to this, if the antenna is badly matched, the reflections from it are being directed back to the circulator and in to the LNA port. These two signals, if phase matched will sum up and enter the limiter. The circulator MAFR-000613-000001 used in this project and has an isolation of 18dB. This means that the leaked power is around 42 dBm if the PA is outputting 60dBm. The limiter will let some initial power through due to the PIN diodes have a delay. This spike can potentially destroy the LNA and therefore more protection is needed.

The switch is intended to isolate the LNA and direct the incoming power down into a load, leaving little reflection coming back to the PA trough the circulator. In transmission mode, the switch will terminate the signal to 50 Ohm, effectively making the circulator an isolator for signals from the antenna to the PA. The problem is added loss from the switch in receiving mode results in added noise in front of the LNA.

The switch selected is Skyworks SKY12215-478LF for its high power handling of 760W pulsed power and fast switching time of 250ns. If the antenna is connected, the switch will be able to handle the leaked power from the circulator.

In the data sheet is a layout of a test circuit, but as it is very large and unpractical due to not connect leads with the same voltage together, a re-design was made and a more compact and easily steerable circuit was produced. All the components value recommendation were used in the design, but added a resistor for the common voltage supply and a terminating resistor for one port of the switch. The layout can be seen in Figure 3.28.

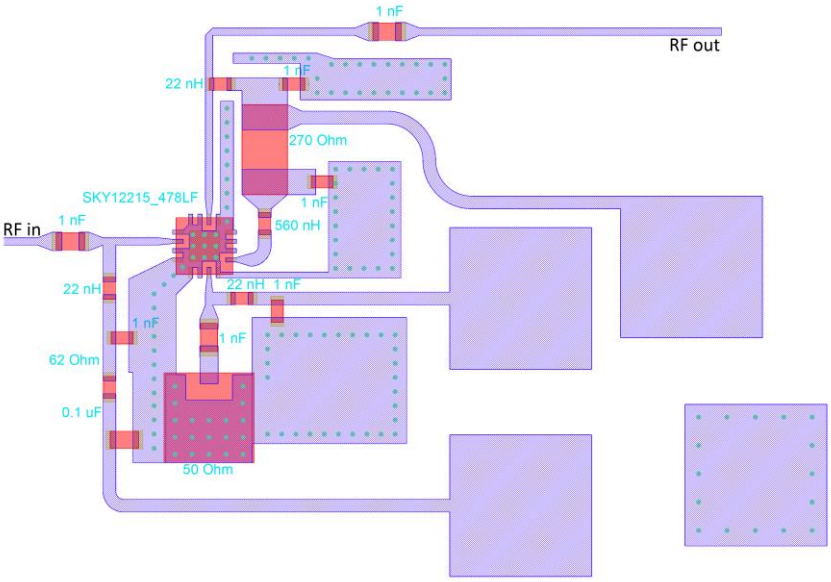

Figure 3.28 Isolation switch terminating the signal coming from the left down into a resistor (large and red 50 Ohm under the switch named SKY12215_478LF). If open, the signal will exit in the TL to the upper right hand side corner. The pads are for switching it on and off, biasing it and a ground pad.

3.10.1 Isolations switch performance

The interesting data are the Insertion loss to see the loss/noise that the switch generates in Rx mode and the isolation and reflection to calculate the power that the LNA receives in Tx mode and the power terminated by the resistor. This was simulated using ADS and the schematic representation of the layout seen in Figure 3.28. Both insertion loss and isolation can be seen in Figure 3.29.

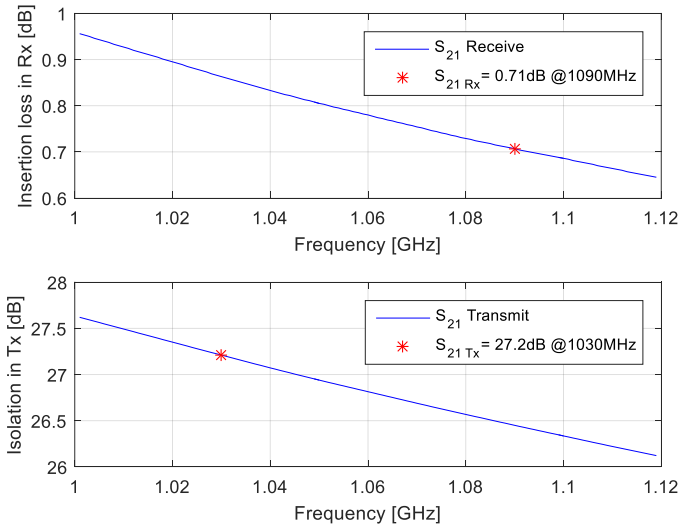

Figure 3.29 In the top graph the insertion loss is plotted as seen from the circulator through the switch. This switch is attenuating the signal 0.71dB at the Rx frequency of 1090MHz. In the bottom graph the switch is set to direct the input signal into a load instead for going to the LNA. At Tx frequency of 1030MHz it has an isolation of 27.2dB.

When the switch is set to terminate to a 50 Ohm load, we want all the power to reach the load. This can be measured with S_{11} from the antenna. If perfectly terminated to 50 Ohm and no leakage to the LNA, the reflection should be zero. The simulated reflection for the schematic representation of the layout in Figure 3.28 using s-parameters for the terminating resistor can be seen in Figure 3.30.

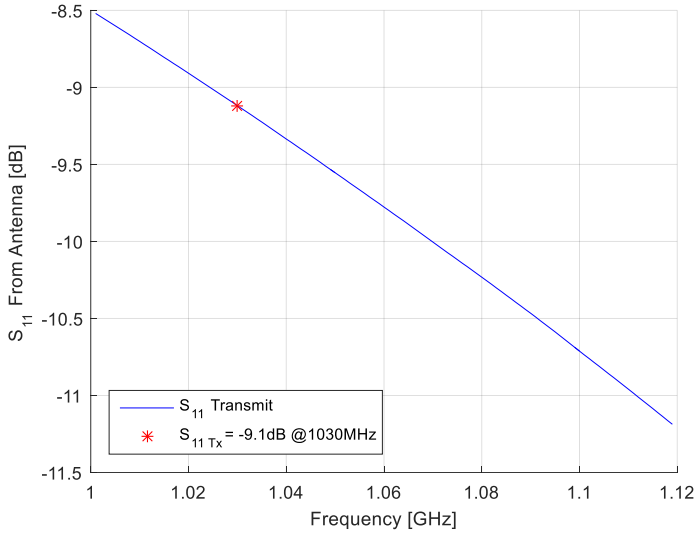

Figure 3.30 The plot is of S_{11} as seen from the circulator. The switch is set to transmission mode and shows that the switch terminates the signal in a load and results in little reflections that can come back to the circulator. At the transmitting frequency of 1030MHz, S_{11} is -9.1dB.

3.11 LNA

The specifications state a noise figure of 1dB for our frequency but is not a specification that are of high importance according to SAAB. It is difficult to keep the noise down due to the components in front of the LNA as it needs the circulator, as well as the limiter, filter and isolation switch to protect it. It is however of interest to design a good LNA to keep the noise down, despite there being components in front of it with greater implication.

The chip used for the LNA are Mini-Circuits PMA2-33LN+. The datasheet states a noise figure of 0.38dBm for our frequencies and a gain around 18dB. The data sheet has a resistor Rb that after the user's desire can control the current draw of the devise in exchange for disadvantages in other areas. For this project, the power consumption is not a major concern, so the resistor is set fairly low in favour of performance rather than efficiency.

3.11.1 Matching LNA

This amplifier has a good match to 50 Ohm on the input assuring a low noise, as $\Gamma_{opt} = 0.108\angle 102.9°$. This meant that using the existing recommended test circuit with just a DC block and 50 Ohm TL is good enough for matching and keeping the circuit simple. The IC was unconditionally stable so no stabilization is needed.

Using the test circuit design the noise was good, but the input and output reflections were not acceptable. Adding an open stub to the output improved the matching on both the input and output while the noise was hardly affected in the simulations. The final layout can be seen in Figure 3.31.

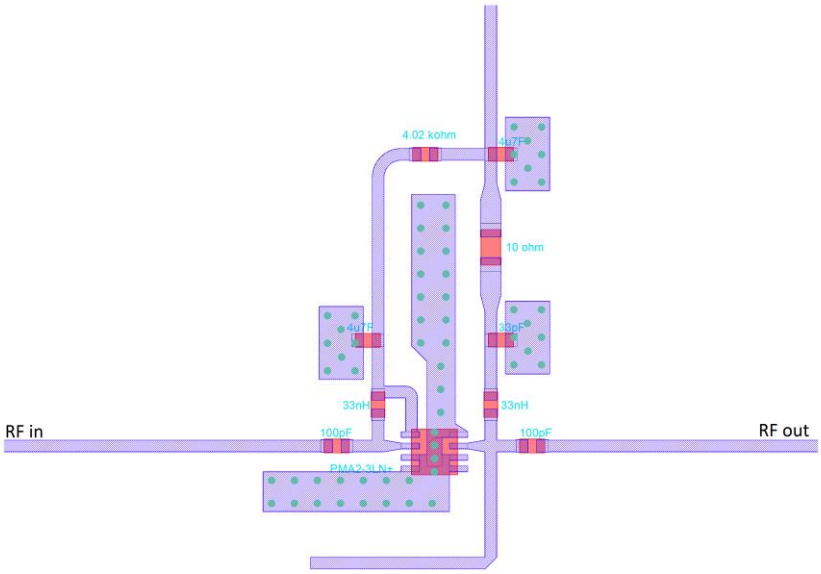

Figure 3.31 The LNA circuit using the PMA2-33LN+ from MINI-Circuits. On the left is the RF in and on the right hand side is the RF out. From the top is the voltage supply, splitting the signal to the left for the gate and straight down for drain. In biasing the gate resistor is Rb=4.02kOhm, controlling the current draw.

3.11.2 LNA performance

With the suggested matching circuit, the LNA managed to get a broad band match for both input and output, seen in Figure 3.32.

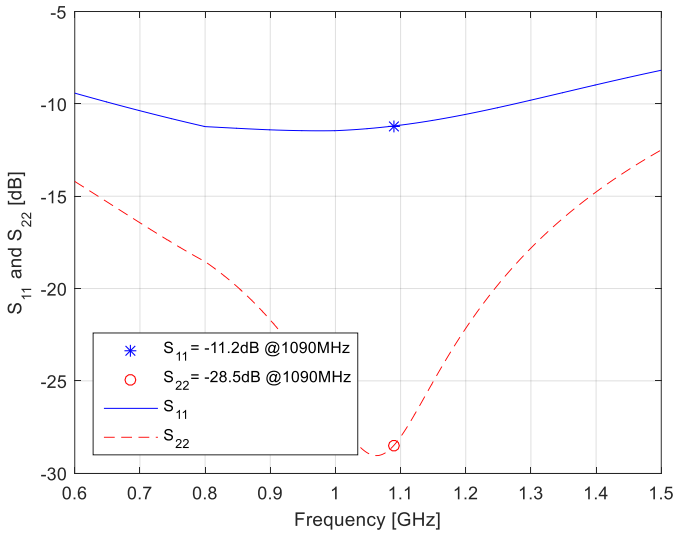

Figure 3.32 S_{11} and S_{22} for the LNA. In blue full line is S_{11} and in red lines are S_{22}. Represented as a blue star and a red circle are the values for S_{11} and S_{22} at 1030MHz respectively. S_{11} is -11.2dB and S_{22} is -28.5dB at 1090MHz.

The gain plot shown in the data sheet is highly dependent on the frequency at the lower spectra, dropping off as the frequency increases. This can be seen in our simulations as well, presented in Figure 3.33.

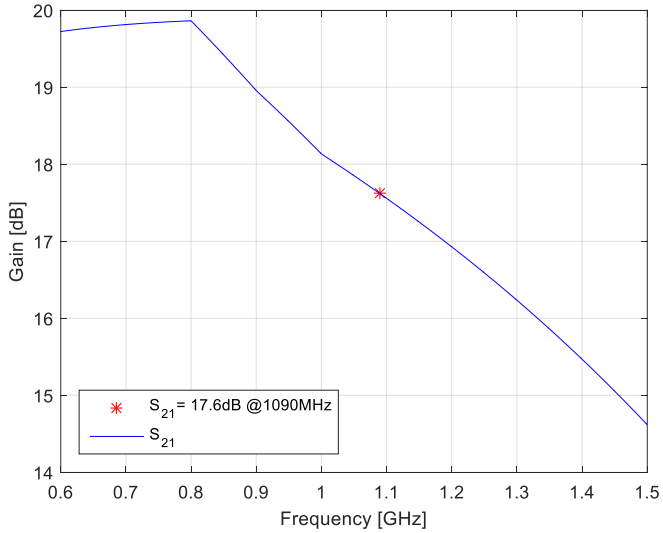

Figure 3.33 The small signal gain (S_{21}) with a marker at 1090MHz reading a gain of 17.6dB.

The noise figure was simulated and found to be lower than the one presented in the data sheet were they display a noise figure of around 0.35dB. This could be due to our simulations not being physically accurate. The noise figure simulation plot can be seen in Figure 3.34.

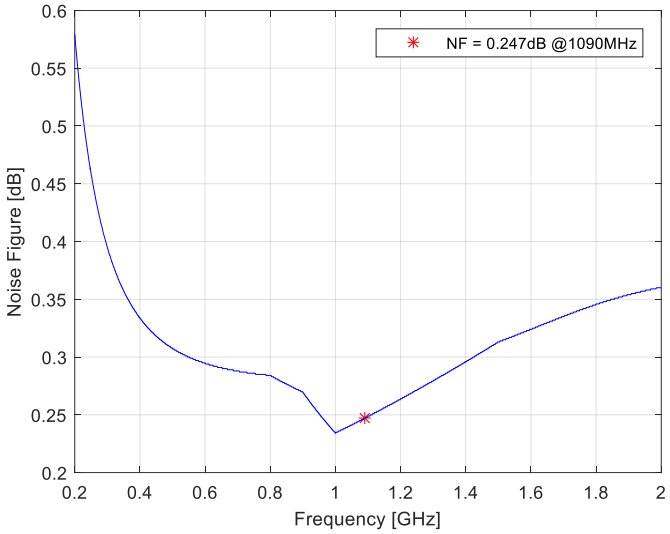

Figure 3.34 Noise figure for the LNA. Represented as a star is the noise figure of 0.247dB at 1090MHz.

4. Test circuit measurements and adjustments

4.1 Phase shifter

4.1.1 Own design

The phase shifter was initially soldered using the oven and later some ICs were exchanged using a hot plate and hot gun. The pull down resistors were not populated in this measurement. The pads were marked with the voltages for 0° phase shift. To activate a switch, the poles are switched. A black ground wire was added to the ground plane, all seen in Figure 4.1.

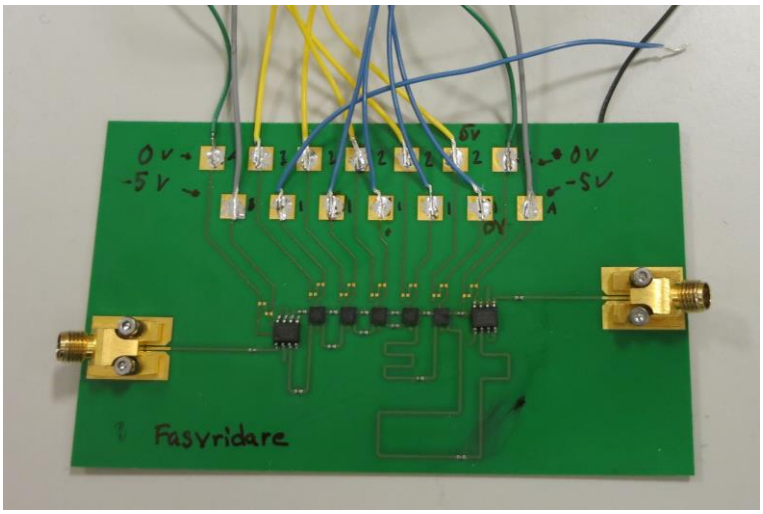

Figure 4.1 An image of the phase shifter using switches and different length of transmission lines. The cables are connected to each switch and were connected to appropriate voltage level to phase shift.

The measurements were done using Rohde & Schwarz ZVA24 and documenting the phase shift and loss for 1030MHz and 1090MHz was done. The reference phase shift of 0° were subtracted from each bit measured to get the difference in phase shift. The results can be seen in Table 4.1.

Table 4.1 Measured phase shift and loss for each bit in the phase shifter and all shifters enabled for a 354.375° phase shift.

Ideal Phase Shift	Measured phase difference and loss			
	1030 MHz		1090 MHz	
0°	0°	-4.06dB	0°	-4.11dB
5.625°	7.32°	-4.203dB	7.4°	-4.246 dB
11.25°	13.19°	-4.256 dB	13.6°	-4.295 dB
22.5°	25°	-4.287 dB	26.19°	-4.335 dB
45°	45.41°	-4.23 dB	48.05°	-4.248 dB
90°	93.85°	-4.242 dB	99.27°	-4.201 dB
180°	190.7°	-4.428 dB	200.94°	-4.47 dB
354.375°	367.14°	-5.046 dB	388.21°	-4.92 dB

4.1.2 IC Phase shifter

The IC phase shifter were soldered using the soldering oven and then added cables afterwards for easy connection to ±5V, ground and for connecting the bits. In the measurements of the phase shifter, loss for 1030MHz and 1090MHz for every individual bit, 0° and all bits activated were made.

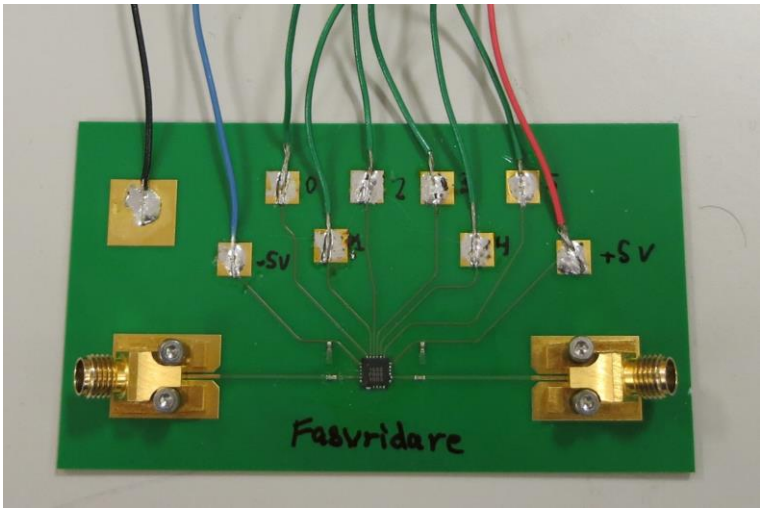

Figure 4.2 The bought phase shifter with ground, voltage supply and control bits connected to wires.

Same as for our own designed phase shifter, the bought phase shifter was measured using the Rohde & Schwarz ZVA24 network analyser. The phase shifts were established by subtracting the reference of 0° off each bit. The result can be seen in Table 4.2.

Table 4.2 Measured phase shift and loss for each bit in the phase shifter and all shifters enabled for a 354.375° phase shift.

Ideal Phase Shift	Measured phase difference and loss			
	1030 MHz		1090 MHz	
0° (Ref)	38.81°	4.06 dB	55.78°	3.8 dB
5.625°	7.994°	3.91 dB	7.74°	3.74 dB
11.25°	13.29°	4.05 dB	12.93°	3.79 dB
22.5°	26.44°	3.863 dB	25.41°	3.792 dB
45°	49.79°	3.732 dB	48.92°	3.648 dB
90°	95.23°	3.604 dB	94.02°	3.655 dB
180°	166.49°	5.39 dB	172.32°	4.55 dB
354.375°	353.24°	5.03 dB	355°	4.53 dB

4.2 Attenuator

The attenuator, HMC624a, was soldered using the oven and afterwards wires were connected to easily connect the voltages. The LE pin and voltage source pin were both set to 5 volts.

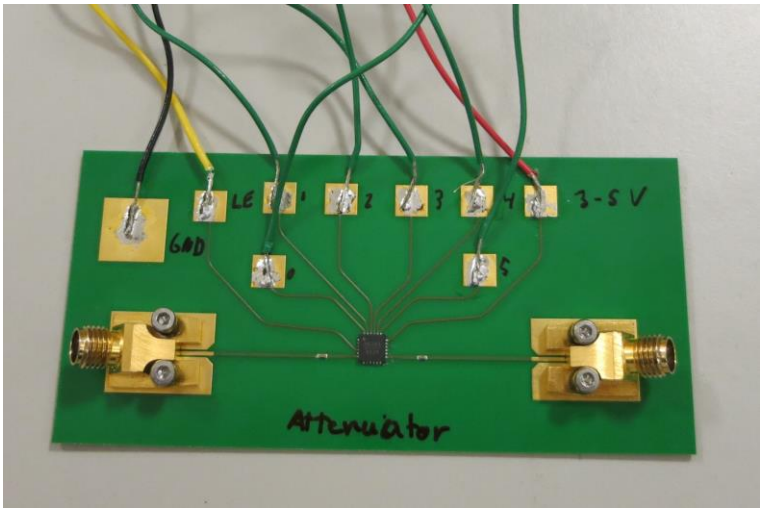

Figure 4.3 The attenuator with ground, voltage supply, LE and bits to set the attenuations, all connected to wires.

In the measurement the bits were set to measure the specified attenuation span and resolution for 1030MHz and 1090MHz. Due to the IC having a resolution of 0.5dB and the specification asked for 1dB resolution, the 0.5dB was used to minimise the error. This was only necessary for the 8, 9 and 10dB attenuation as these were low enough for the additional 0.5dB to minimise the error. The results can be seen in Table 4.3.

Table 4.3 The measured attenuation. The 8, 9 and 10dB attenuator are compensated using the 0.5dB resolution in the IC for less difference to the intended attenuation.

Ideal attenuation	Measured [1030 MHz]	Measured [1090 MHz]
0dB (ref)	1.613 dB	1.612 dB
1 dB	1.012 dB	1.017 dB
2 dB	1.992 dB	1.998 dB
3 dB	3.001 dB	3.005 dB
4 dB	3.774 dB	3.791 dB
5 dB	4.869 dB	4.875 dB
6 dB	5.876 dB	5.88 dB
7 dB	6.866 dB	6.875 dB
8 dB	8.218 dB	8.225 dB
9 dB	9.225 dB	9.23 dB
10 dB	10.215 dB	10.217 dB

4.3 Power Amplifier

4.3.1 Tuning, testing and troubleshooting

All the surface mounted parts were done in the oven except for the transistor and electrolytic capacitors. To make sure the amplifier was acting as simulated we used the same technique as for the driver and connected the coaxial cable over the transistor ports in order to measure the reflection using a VNA, see Chapter 4.4. We then set up a simulation of the same setup in ADS with a 50ohm load termination on the input and output, measuring the reflection from the transistor ports. These results were then compared with the VNA measurements, and from this, tuning was made to achieve the same reflection in the real amplifier as the simulated one. The results of this were an apparent problem in the calibration as the reflection was outside of the smith chart. In addition to this, when shorting the port with a wire close to the soldered coaxial cable, the result was as well outside of the smith chart and several degrees of the low impedance point.

Proceeding to solder the transistor and voltage cables to the amplifier and connecting the gate and drain voltages. For the amplifier not to get too warm, the gate voltage was pulsed only when the RF signal was on the input, minimizing the average drain current. The decupling capacitors on the gate was too large for the pulse to be switched on and off fast enough. This was solved by removing all the caps except the smallest valued on the rail. This enables the pulse to have a fast-enough rise and fall time for turning the transistor on and off.

When driving the gate peak voltage up for an average of 100mA on the drain, the simulated voltage of 4.5V was not possible to achieve due to the current being extremely high. The simulations were then redone with a more realistic gate voltage of 2.6V and found the amplifier to be very stable and losing some power. After some success with tuning the component values the simulated power were able to reach a healthy 550W. This meant that with some hand tuning of the amplifier, the power specification would easily be reached and a loss of only a couple of tens of watts would be made by changing the voltage, according to the simulations.

4.3.2 Measuring and troubleshooting

When first turning the amplifier on, the P1dB was only around 20W but with a reasonable gain. After some tuning, P1dB only increased to 40W. Checking the currents in each cable to the two drains, there were some off balance in them. This suggests that the two transistors in the single amplifier case were not working in symbiosis. The current seemed to become negative on one side as the RF signal entered the amplifiers. This indicated that ether one side of the amplifier was not preforming as well as the other or that the capacitor banks were uneven on the both sides. After changing the transistor to a new one the results were unchanged, indicating the capacitors were at fault for this.

The fact that the gain was there but not the power indicates the matching on the output must be off. If the input would be badly matched the power would have decreased as it reaches the input, but a higher input power would have compensated for this to some degree and with a lower gain still reached a high output power. Therefore, it is most probable a matching error at the output that is causing the lacking power.

4.3.3 Trying different tuning techniques

Desoldering the transistor were then done in order to test a new tuning strategy. The plan is to measure the reflection from the input and output into the matching circuit without the amplifier attached. This reflection can then be compared to the simulation of the same set up, and from there tune the matching components to give the circuit the same global reflection as the simulations. When trying this the gain increased up by a small amount but not near the results expected.

Finally trying the same tuning technique of measuring the reflection from the input and output but with the transistor mounted and no voltages on the gate and drain, i.e. switched off. Doing the same in the simulations, setting the voltages to 0, the reflections were off by a quarter turn anti clockwise in the smith chart on the output. Once tuned to have the same reflection as the simulation, the amplifier was up several hundred watts.

A very effective way of tuning was to have a piece of foil encapsulated by kapton tape, to preventing shorting the circuit when used. This piece was later held around spots on the board while driving the amplifier to see if the power increased in compression. When a good spot was found, measurements were taken on the reflection in the VNA with the amplifier turned off. These measurements were later matched using components at the point. Doing this, the capacitance between the transistors was removed and a small capacitance were added closest to the gate. Capacitance was added on top of both baluns to ground and on the output of the balun on the amplifier input to ground. The stub on the output was tuned looking at the 2nd harmonic in hard compression and with foil placing it at the best position to minimize the power at that frequency. The final design can be seen in Figure 4.4.

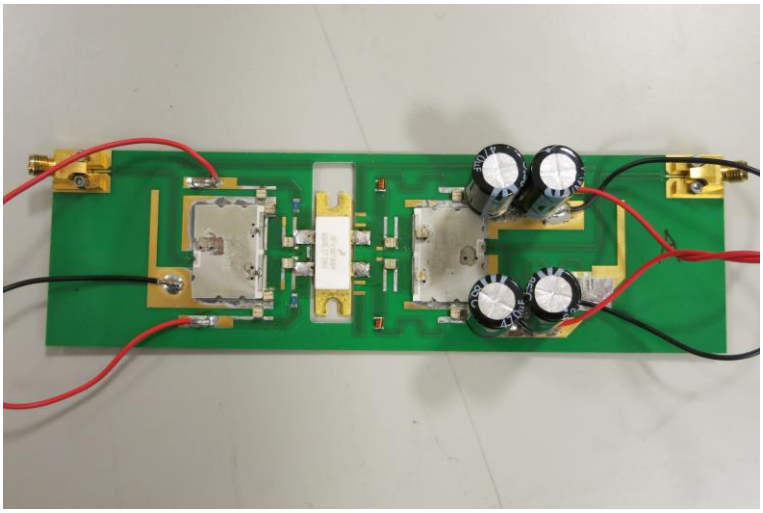

Figure 4.4 The finished tuned single PA with wires connected to the gates and drains. Visible on the baluns are tuning caps soldered on top of them.

When sufficient power was reached for the single amplifier, another one was produced identical to that. They were then connected using identical hybrids and ridged cables of similar pared length, seen in Figure 4.4 and Figure 4.5.

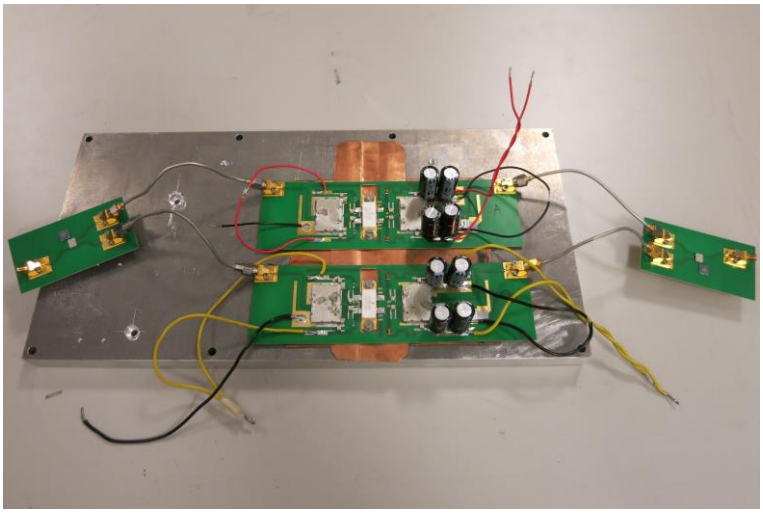

Figure 4.5 Two PA connected with hybrids on the input and output. Separate voltage supplies showed if the amplifiers were equal. The large metal plate is for cooling the amplifiers and the copper plates are for chiming the PCB to accommodate the drop down transistor. The copper foil under the transistors are for establishing a well-grounded connection of the transistor and the PCB.

4.3.4 **Measurements**

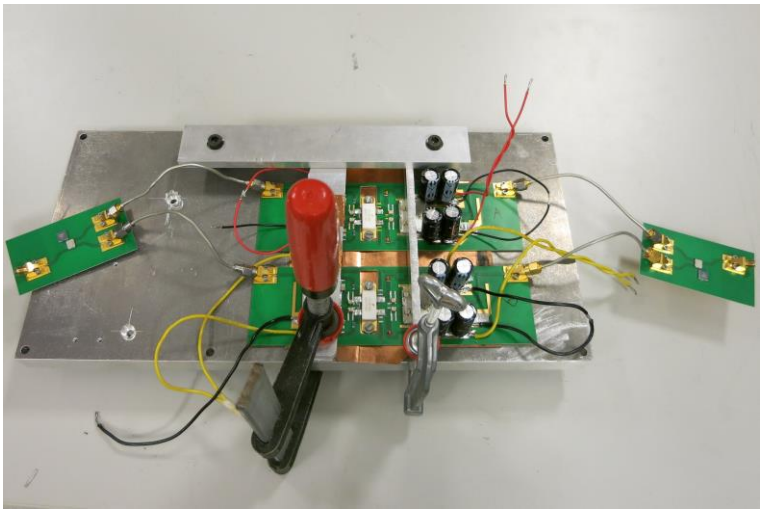

Figure 4.6 The setup used during measurements. The clamps are clamping down on bars going across the grounded baluns to keep the PCB grounded to the copper cheats.

The measurements were done using a two-channel signal generator producing a pulsed square wave. One signal was supplying the gate voltage, other signal, controlling the RF signals length and timing. The pulse was placed at the end of the longer pulse opening the gate. This is due to the capacity of the gate line discussed in 4.3. The RF control pulse was connected to a fast switch connected between the RF generator and RF amplifier shaping the RF to a short pulse with fast rise and fall time. The pulse was then amplified again using our driver before measuring the power in front of the hybrid using a directional coupler. The output power was then put through attenuators and into the power meter. The full setup for both the single and double amplifier is seen in Figure 4.7 and Figure 4.8.

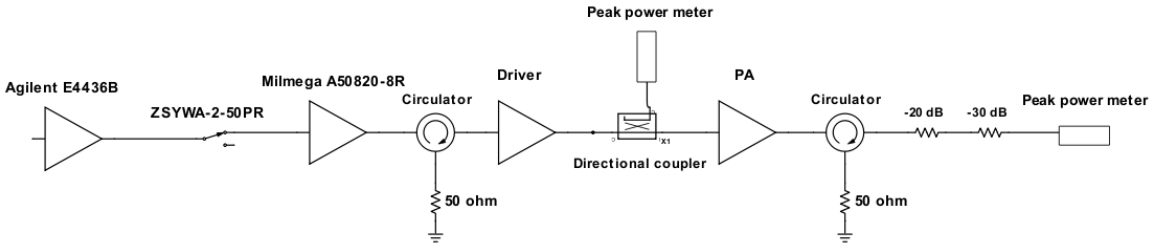

Figure 4.7 The measurement setup for a single PA stage when performing a peak power measurement.

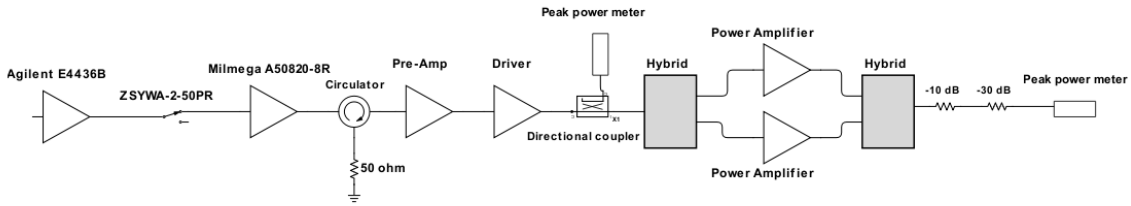

Figure 4.8 The measurement setup for a double PA stage when performing a peak power measurement.

Ideally the rise and fall-time of the pulsed signal would be around 50 to 100ns and 50 to 200ns as the specification demands [1] [3]. This was hard to achieve due to its demand in a very specific filter or a slower switch, neither of which were available. The input signal can be seen in yellow together with the output in blue in Figure 4.9. The rise time of the power specified on the power meters were 55ns for the input and 50ns for the output. This means that the pulse put into the amplifier is probably steeper than displayed in Figure 4.9. To keep in mind is the rise and fall time of the IFF system is of the voltage and the measurements seen in Figure 4.9 are of the power.

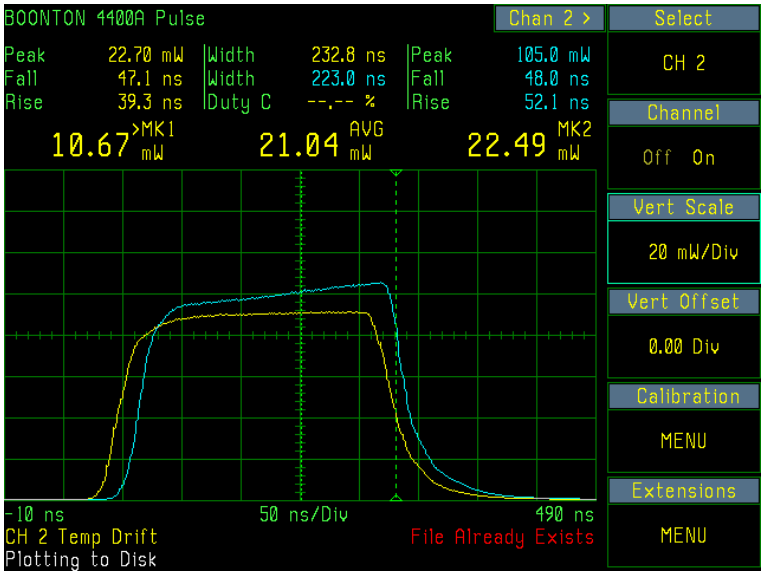

Figure 4.9 Displayed in yellow is the envelope of the input signal and blue is output from the double PA at 1dB compression point. These signals do not include the attenuations on the output nor the loss in the decoupling of the input signal. In the top left and right corners are rise and fall-time displayed from 10% - 90% of the power.

The power measurement was done using the peak value for the input and output displayed on the power meter in watts and using averaging. The power output from the driver with the directional coupler after it, provided just enough power to put the PA into compression before itself going into hard compression. Due to this the gain does not drop extensively and a 1.32dB gain loss is just reached in this measurement. The efficiency was simultaneously registered for both amplifier sides. The power and gain can be seen in Figure 4.10 where P1dB of 60.35dBm or 1084W was reached. The efficiency and power are displayed in Figure 4.11, where the efficiency of A (top amplifier in Figure 4.5) is slightly lower than that of B.

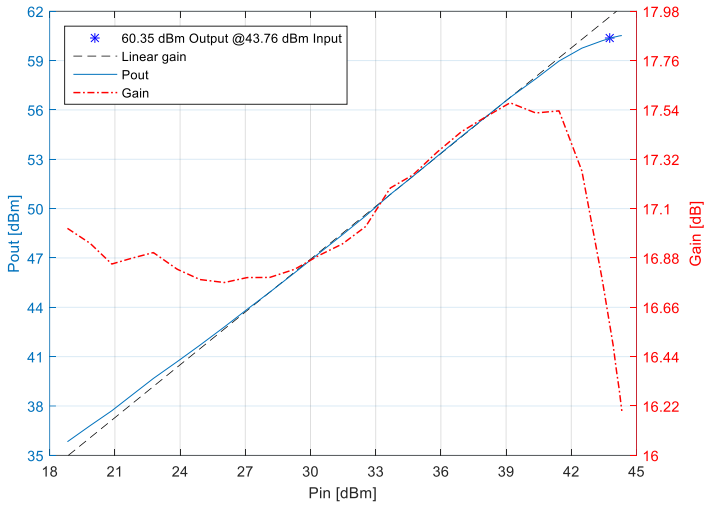

Figure 4.10 Large signal gain and output power for the double PA stages at frequency 1030MHz. On the left is power output from the amplifiers, plotted in blue, and linear gain in black lines is extrapolated from two points located a linear part of the output power line. Represented as a blue star is the 1dB compression point. On the right-hand side axis is the large signal gain together with the gain plotted with a red dotted line.

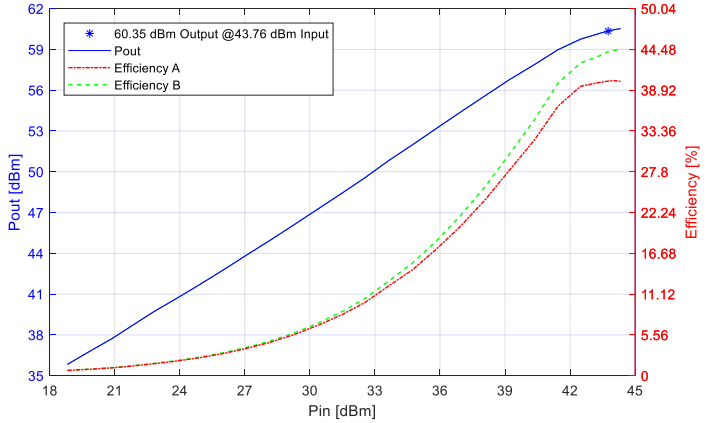

Figure 4.11 Large signal gain and output power for the double PA stages at frequency 1030MHz. On the left is the power output from the amplifiers, plotted in blue. Represented as a blue star is the 1dB compression point. On the right-hand side axis is the efficiency of the amplifiers A and B plotted in percent.

The efficiency could be improved by switching the gate on and off using a MOSFET located after the capacitors in the gate line. This would enable the gate pulse to become smaller, eliminating drain current when no RF is applied, decreasing the average current draw while sustaining the same power output.

4.4 Driver

The Driver was constructed using a coaxial cable soldered onto one of the pads on the input and output of the matching network while the input and output of the driver were terminated using 50ohm load. This enables the VNA to be connected where the chip would be placed and from there measure the reflection and compare it to the suggested one in the data sheet. The calibration was done using a TSOL then connecting the open coaxial. To accommodate for the extra length and split end, offsets were put in the VNA, placing the reflection at the open end of the smith chart. The setup of the coaxial cable mounted on the output can be seen in Figure 4.12.

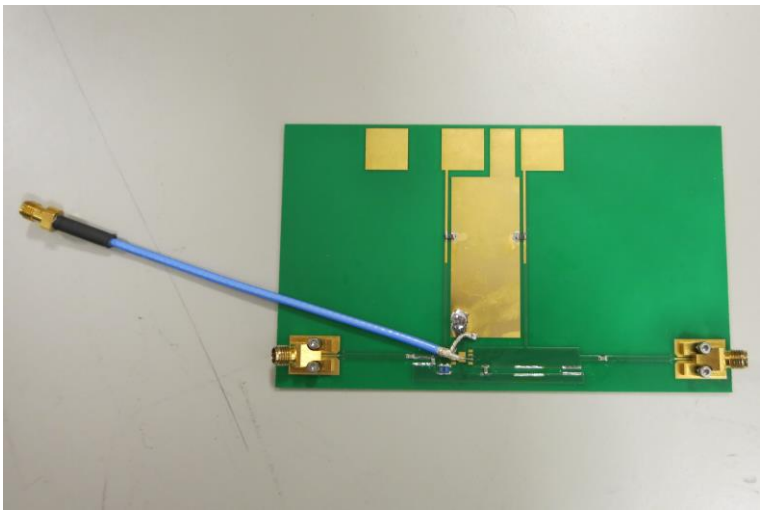

Figure 4.12 The setup used to tune the driver. The ground of the coaxial is connected to the large ground plane and the centre line connects to a single pad on the drain/gate pad.

After doing the measurement of the reflection, the tuning capacitor on the output was moved close to the output of the drain. The resistors were measured to 9 ohms combined and this resulted in a stable amplifier. The decoupling capacitors were placed where the tuning said it would be good and the cooling pad/ground under the transistor was soldered to the via holes connecting it to the ground plane. The final design can be seen in Figure 4.13 and the measurement setup can be seen in Figure 4.14 where a clap was used for good heat transfer to the bras block. The measurement setup is displayed as a block diagram, seen in Figure 4.15

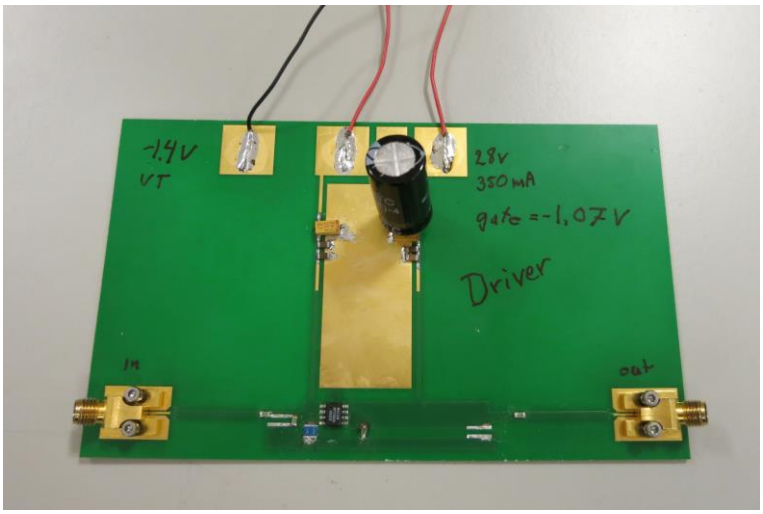

Figure 4.13 The finished driver circuit. On the gate to ground two 17.5 resistors were used for handling the high current going through. From top left is ground, gate and drain voltage pads.

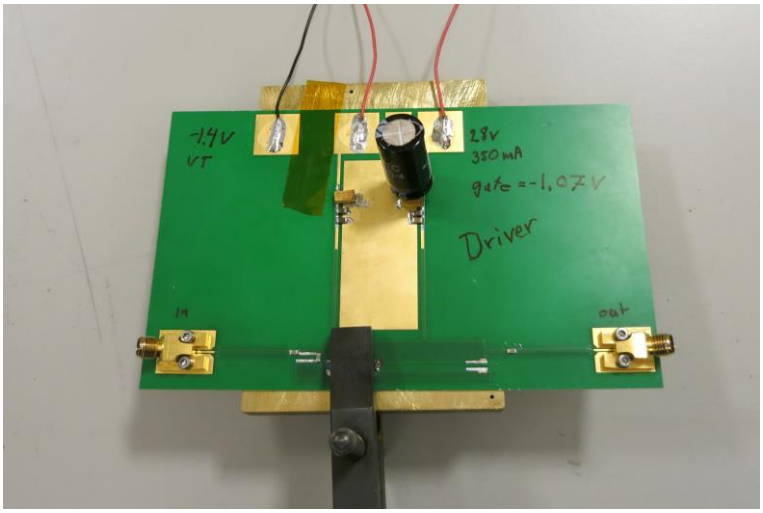

Figure 4.14 The measurement setup used. The brass plate is for cooling and the clamp at the bottom of the picture are clamping on the transistor making a good heat transfer from the ground-plane to the brass.

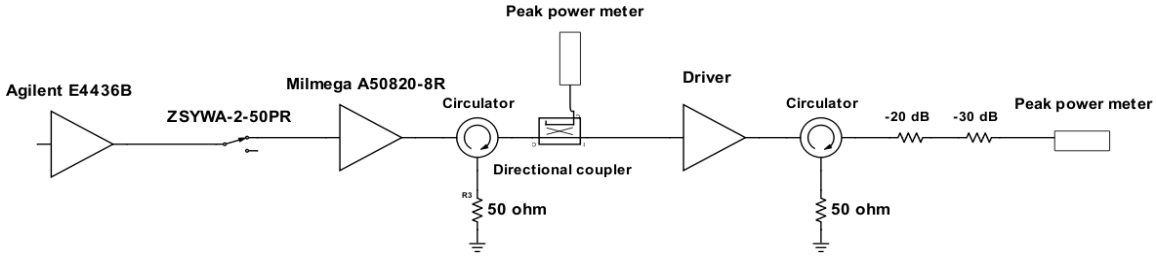

Figure 4.15 The measurement setup for the driver when performing a peak power measurement.

The rise time and fall time are seen in Figure 4.16 and are produced with the same setup as for the PA in 4.3.4. As for the PA, the rise and fall-time that is close to what the instruments can measure and therefore the values displayed on the measurement are unreliable.

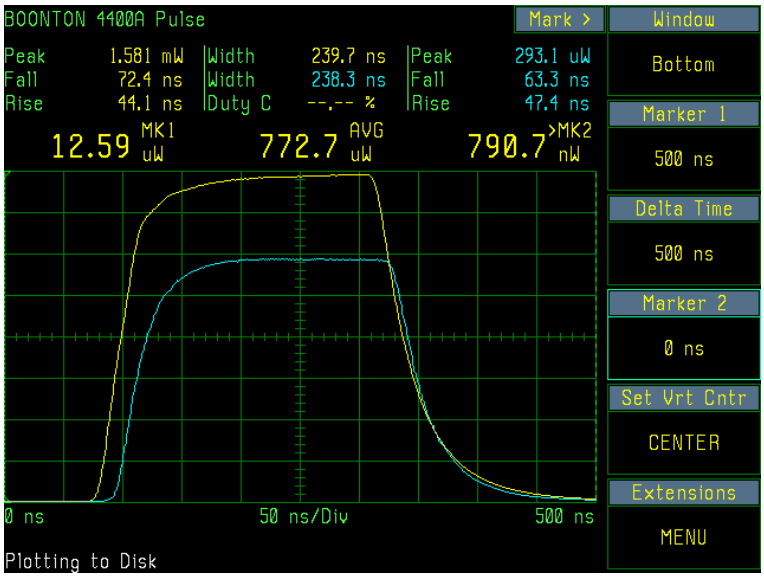

Figure 4.16 Displayed in yellow is the envelope of the input signal and blue is output from the driver at P1dB. These signals do not include the attenuations on the output nor the loss of the decoupling of the input signal. In the top left and right corners are rise and fall-time displayed from 10% - 90% of the power.

When measuring power delivered, the peak-power reading was used in combination with some small averaging to get a stable reading. This resulted in a P1dB of 45dBm or 31.6W seen in Figure 4.17.

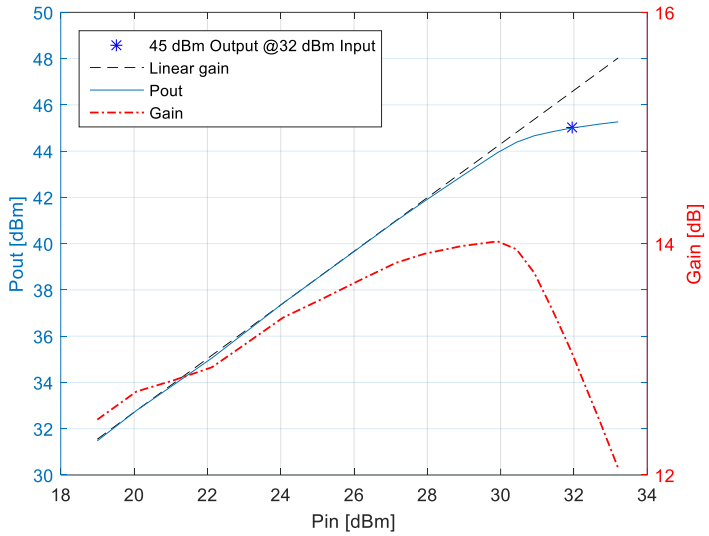

Figure 4.17 Large signal gain and output power for the driver at frequency 1030MHz. On the left is power output from the amplifier, plotted in blue, and the linear gain in black lines is extrapolated from the linear part of the output power line. Represented as a blue star is the 1dB compression point. On the right-hand side axis is the large signal gain together with the gain plotted with a dotted line in red.

Same as the PA, the gain increases with the power up to 28dBm input power and from that it tapers off to 30dBm to then dropping off. When measuring the drain current, it dropped as the power increased and therefore the efficiency increased up to 12%. The efficiency value is however not of interest due to the gate always being on, resulting in a horrible efficiency. In the future, the gate is also to be pulsed, same as for the PA.

4.5 Pre-amplifier

The measurements started off with a low gain and a slightly higher power output at a lower frequency. Looking at the recommended circuits for the pre-amp moving the matching capacitors closer to the IC matches for a higher frequency and moving those further away matches for lower frequencies. Based on the higher gain for a lower frequency we moved the capacitors closer to the IC. This made it a bit better in terms of gain and power output. After trying with a bit of foil and a stick, applying capacitance to the TL laying the foil flat on the PCB, capacitive connecting it to the ground through the dielectric material, the amplifier burned up and we had to manufacture a new one.

We later preformed the measurement on this layout. But when preforming the full amplifier chain, we found the lacking power from the pre-amp not sufficient for the project and the amplification was not linear up to the compression of the PA's.

Using the knowledge gained from matching the PA, we measured the output of the pre-amp in the VNA and by applying a capacitor close to the DC blocking capacitor we managed to move close to the same point in the smith diagram as for the foil tape. This however did not improve the performance and only with the tape foil on the output, high power is achieved. Before individual measurement could be done in the amplifier without being in the amplifier chain in Figure 4.8, the taped circuit burned up for the fourth time. A decision to abandon the pre-amp as made despite having the potential to deliver the power. The reason being it ran very hot and had

a tendency to break when switched of and back on again, something not desired for SAAB as reliability over several years in high temperatures is a requirement. The circuit used in measurements of the PA can be seen in Figure 4.18.

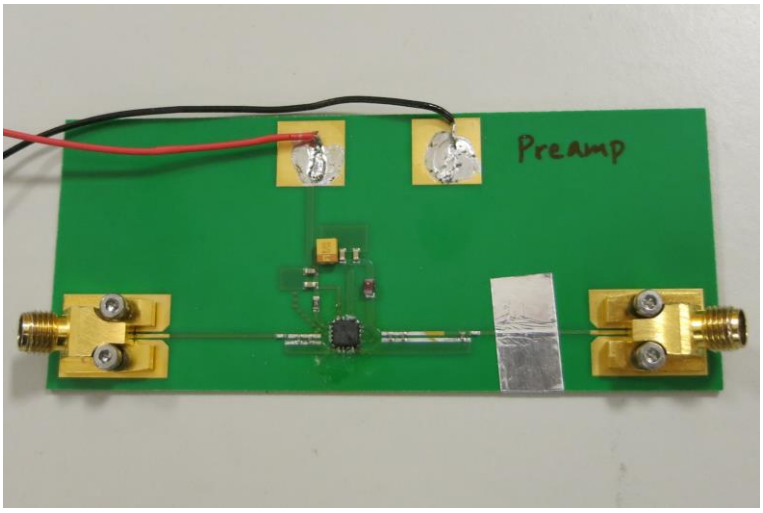

Figure 4.18 Pre-amplifier used for the final measurement in the full amplifier chain with the foil added on the output. The red cable is for a common power supply for gate and drain and the black cable is for ground.

One measurement was performed without the tape on the output and there the P1dB was at 28.4dBm with a gain of 14.8dB. This can be seen in Figure 4.19 where the large signal gain and power output are plotted.

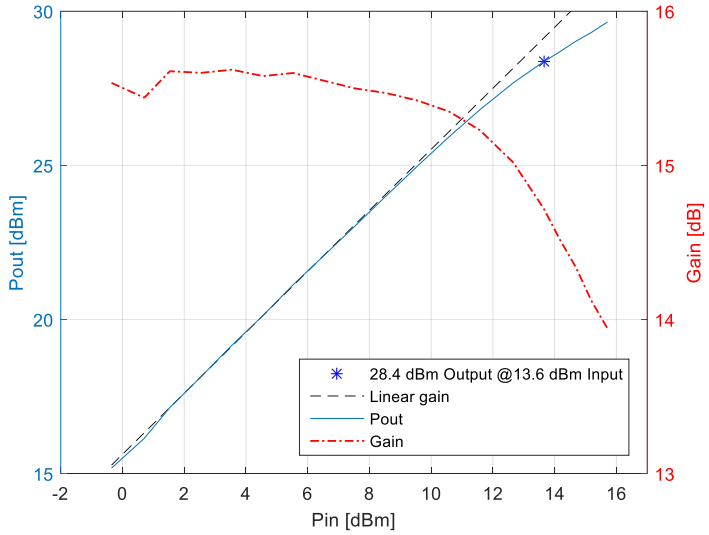

Figure 4.19 Large signal gain and output power for the pre-amp before tape foil was added at frequency 1030 MHz. On the left is the power output from the amplifier, plotted in blue, and the linear gain in black lines is extrapolated from two points located at the linear part of the output power line. Represented as a blue star is the 1dB compression point. On the right-hand side axis is the large signal gain together with the gain plotted with a dotted line in red.

The Measurements were carried out using a constant power delivered to the amplifier while pulsing the RF at a rate of 2% duty cycle, same as the driver. Due to the gate being switched on even without the RF applied, the efficiency was below 0.4% as it draws a continuous 860mA at 5V. The setup used in the measurement can be seen in Figure 4.20.

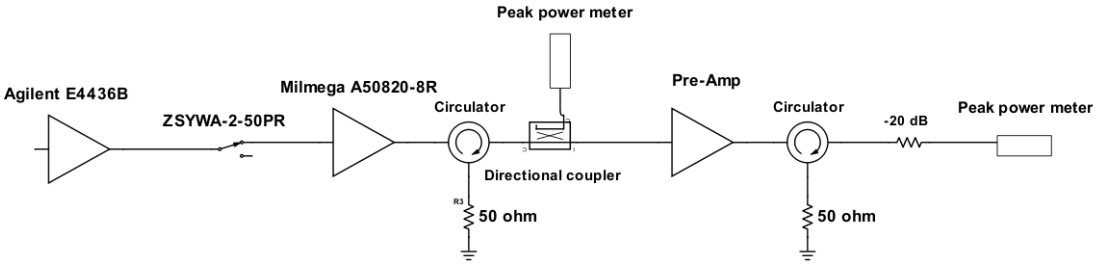

Figure 4.20 The measurement setup for the pre-amp when performing a peak power measurement.

4.6 **Filter**

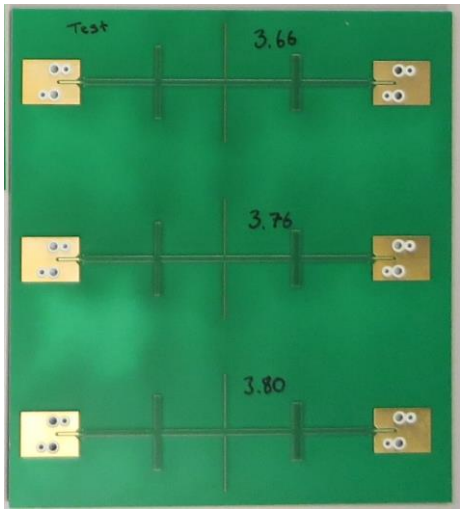

Figure 4.21 The filter without connectors. From top to bottom is the filters for ε_r=3.66, 3.76 and 3.80. The lighter green parts are inconsistency in the protective coating.

The measurements done on the filters were performed using a TSOL calibration to account for the cables. This is due to the high frequency span needed for measuring the filter was not compatible with our calibration, accounting for the connectors. The disadvantage of this is the loss of the connectors is included in the measurements of the filter, hence the large loss. The measured performance can be seen in Figure 4.22Figure 4.23, Figure 4.24. A measurement was done on the carrier frequency, where the calibration kit accounting for the connecters could be used, seen in Figure 4.25.

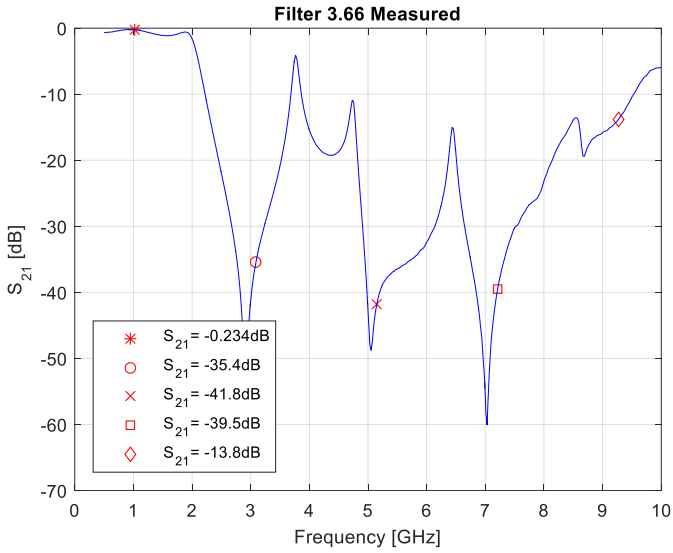

Figure 4.22 The measured filter with ε_r=3.66 with the attenuation on the y-axis. The markers are at the carrier 1030MHz and its 3rd, 5th, 7th and 9th harmonic.

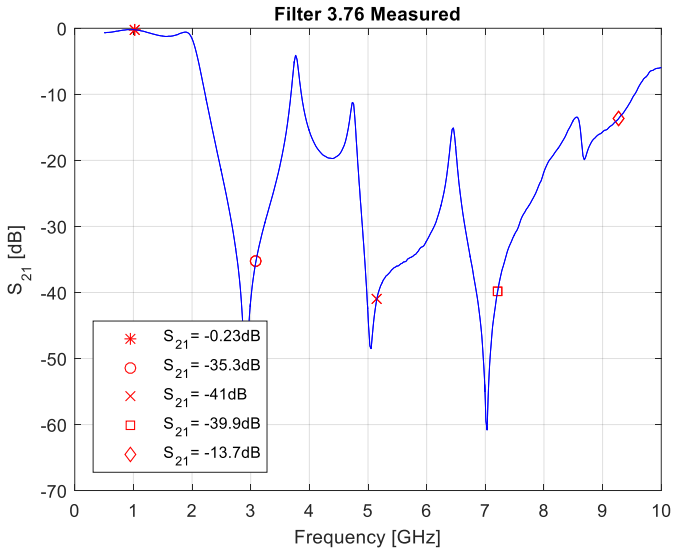

Figure 4.23 The measured filter with ε_r=3.76 with the attenuation on the y-axis. The markers are at the carrier 1030MHz and its 3rd, 5th, 7th and 9th harmonic.

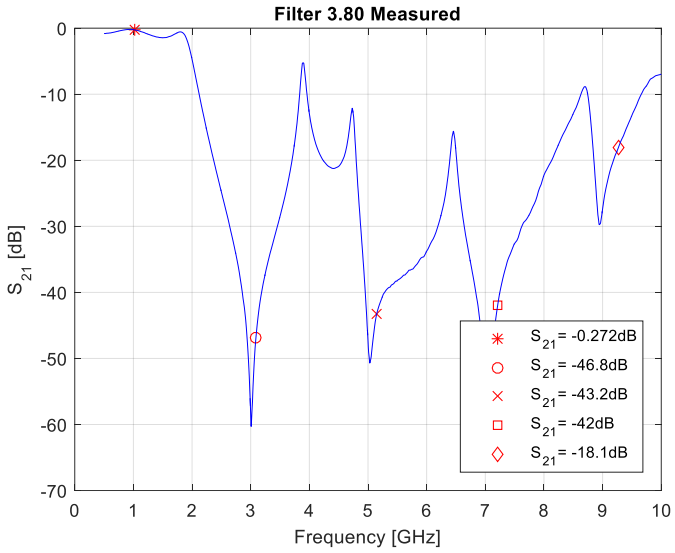

Figure 4.24 The measured filter with ε_r=3.80 with the attenuation on the y-axis. The markers are at the carrier 1030MHz and its 3rd, 5th, 7th and 9th harmonic.

The simulation using ε_r=3.80 is the one with best performance in filtering out the harmonics. As the notches are shifted down in frequency with higher ε_r. Ideally, a filter with an even higher dielectric constant should have been constructed seeing the results. When doing measurement on the 1030MHz and 1090MHz frequencies the filter is right at 1030MHz as designed, seen for ε_r=3.80 in Figure 4.25.

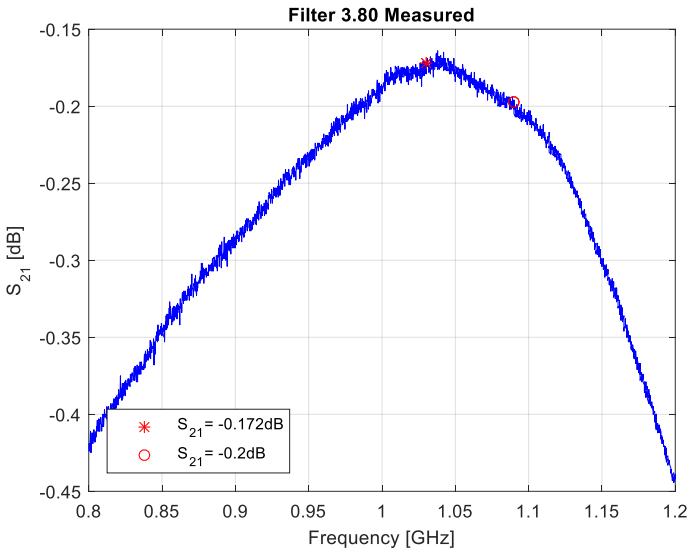

Figure 4.25 The measured filter with ε_r=3.80 with the attenuation on the y-axis. The markers are at the carrier 1030MHz and 1090MHz represented as a star and a circle respectively. The attenuation reeds 0.172dB for 1030MHz and 0.2dB for 1090MHz.

4.7 Limiter

The limiter was constructed in the lab with two PIN diodes CLA4608-085LF and CLA4609-086LF as clean-up diode and coarse diode. In Figure 4.26 you can see the two diodes, the inductor to ground for dc currents and the two capacitors to minimize insertion loss. All of the components were soldered using an oven. The measured insertion loss for the limiter was measured with a VNA to 0.34 dB for both Tx and Rx. The plot for this can be seen in Figure 4.27.

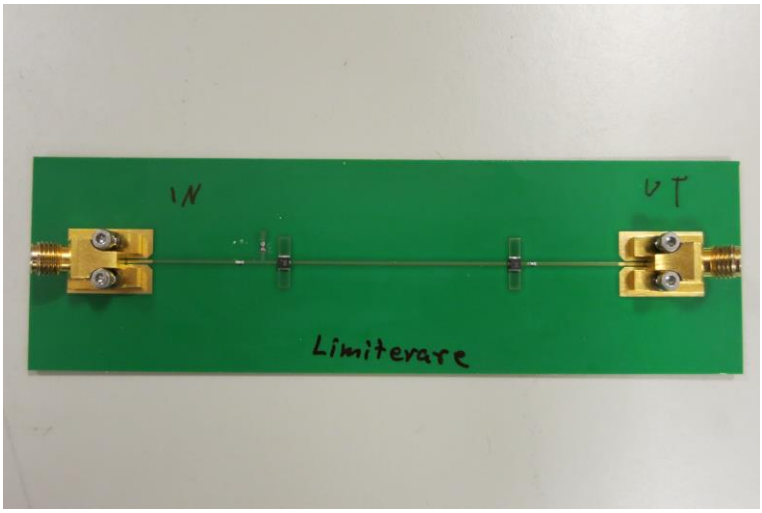

Figure 4.26 The limiter with the two diodes in the middle connected with a quarter wavelength of TL. On the input, the inductor going to a via hole connecting it to the ground-plane.

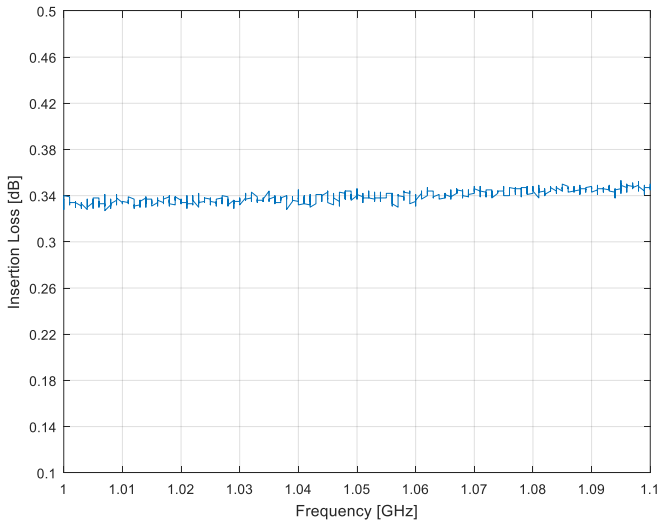

Figure 4.27 The insertion loss when small signals are applied to the limiter. It reads around 0.34dB loss for the 1090MHz.

Measurement with high power signal can be observed in the Figure 4.28. The spike leakage before the limiter starts to fully reflect is at its highest 21 dBm. The limiter limits the power to below 20 dBm from 32 dBm to 43 dBm of input power. The spike leakage can be observed in Figure 4.29 from the peak power meter measurement. Furthermore, a measurement when the limiter is in full limiting mode can be seen in Figure 4.30.

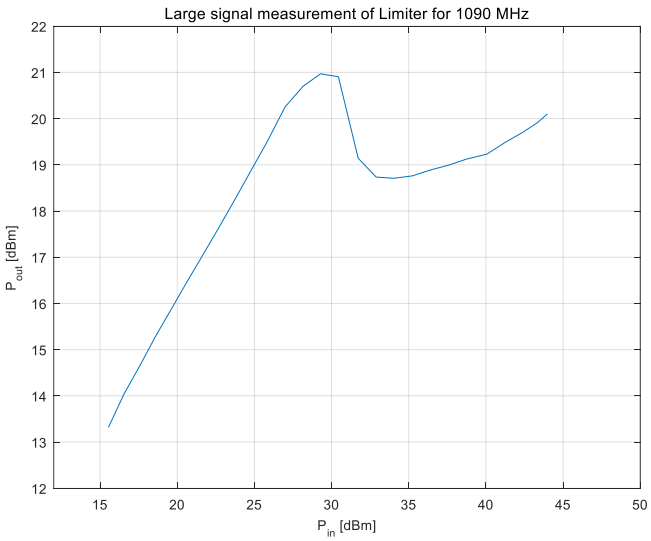

Figure 4.28 The large signal output power for the limiter up to 44 dBm of input power. The spike visible at 30dBm input power corresponds to Figure 4.29.

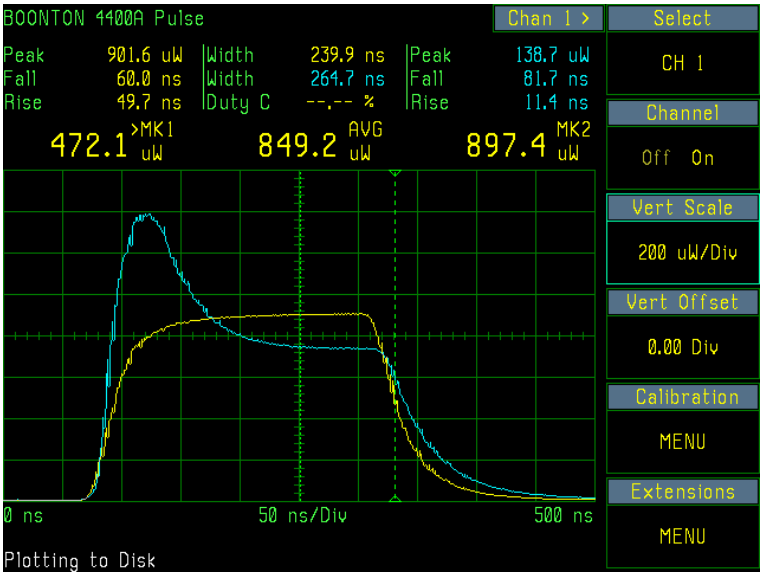

Figure 4.29 The input pulse in yellow and the output pulse from the limiter in blue. The spike leakage seen before the limiters diodes are fully open and reflecting the power. When the circuit starts to limit, the wave is lowered at the end first, moving forward and limiting more of the pulse as the input power increases.

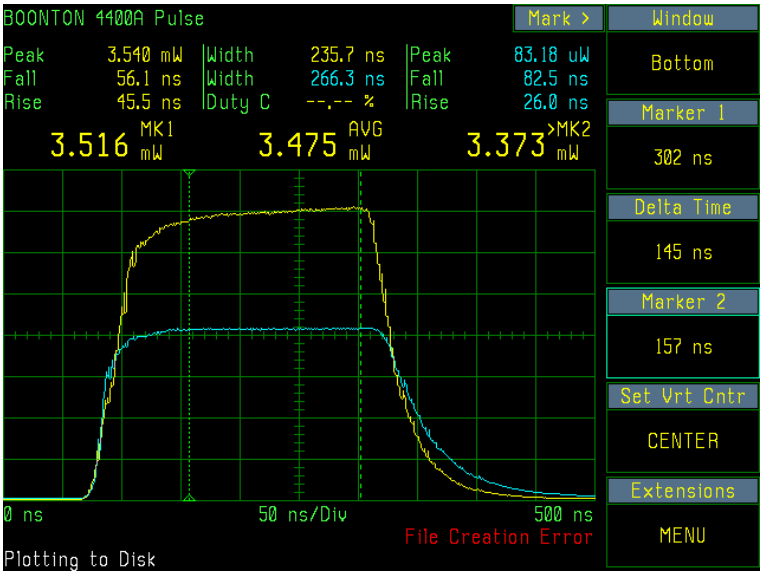

Figure 4.30 The input pulse in yellow and the output pulse from the limiter in blue. When the limiter is in full limiting mode and both diodes is reflecting the power away from the receiver circuit of the TRM.

4.8 Isolation switch

The Isolation switch was soldered using the oven and the cables were connected afterwards. The measurements were carried out using the VNA. The isolations switch can be seen in Figure 4.31 and the measured isolation and insertion loss are plotted in Figure 4.32. The circuit was driven by applying 5V to antenna and 28V/0V or 0V/28V at Rx /Tx to open and close the switch. Due to the circulator transferring the reflected power to the PA, the reflection is of interest as well, seen in Figure 4.33. The reflection also gives an indication of how well terminated the signal is in the 50 ohm load.

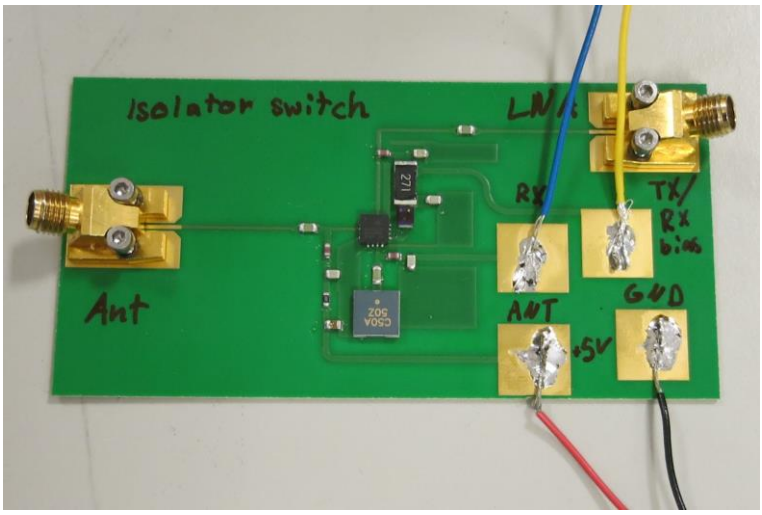

Figure 4.31 To the left is the antenna port that are connected to the circulator in our design. To the left is the LNA port connected to the limiter. The red cable is for biasing the antenna port with continuous 5 volts. The Rx and Tx / Rx bias are shifted between 0 and 28v for opening and closing the switch. The GND is a common ground.

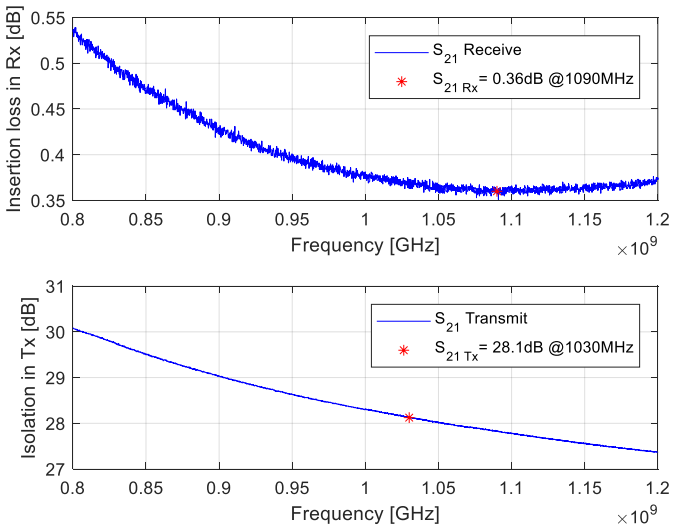

Figure 4.32 In the top graph the insertion loss is plotted as seen from the circulator through the switch. This switch is attenuating the signal 0.36dB at the Rx frequency of 1090MHz. In the bottom graph, the switch is set to direct the input signal into a load instead of going to the LNA. At Tx frequency of 1030MHz it has an isolation of 28.1dB.

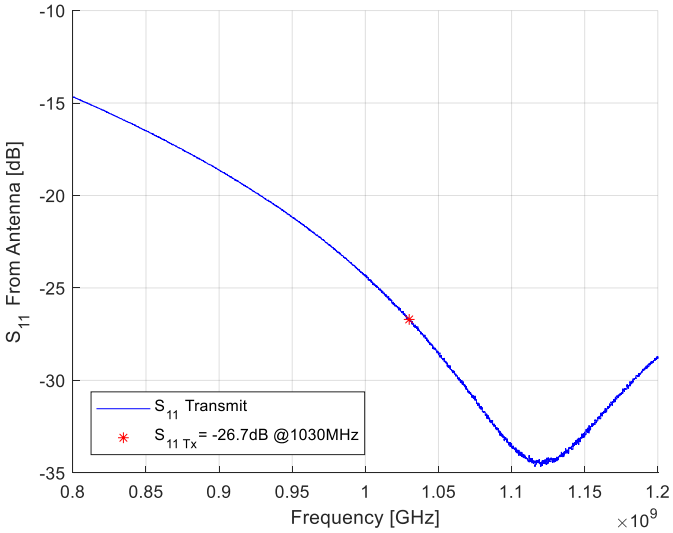

Figure 4.33 The plot is of S_{11} as seen from the circulator. The switch is set to transmission mode and shows that the switch terminates the signal in a 50ohm load, resulting in little reflections that comes back to the circulator. At the transmitting frequency of 1030MHz, S_{11} is -26.7dB

4.9 LNA

The LNA was soldered using the oven and the cables were connected afterwards. The measurements were carried out using the VNA and a noise spectrum meter. No tuning was performed, and the design can be seen in Figure 4.34. The measurement of its noise is highly sensitive to disturbance, therefore encapsulating it was an effort to shield it from the environment. This setup is seen in Figure 4.35.

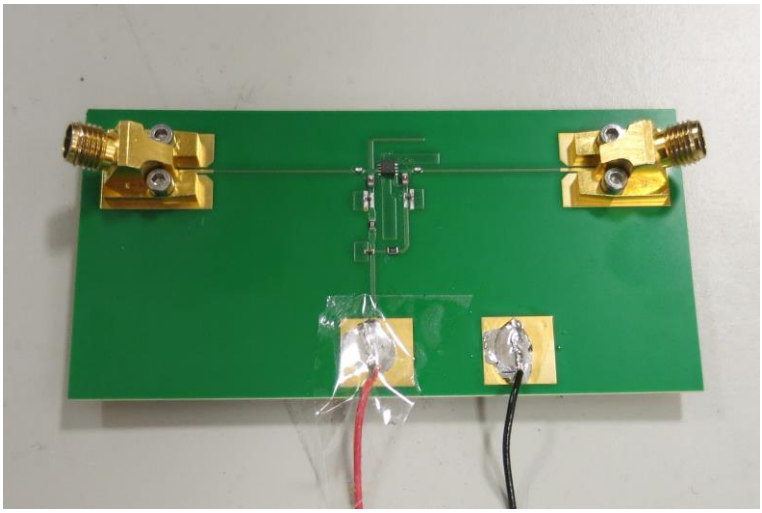

Figure 4.34 The LNA with the in input on the right-hand side, and output of the left-hand side. The red cable is for a common power supply for both gate and drain voltage. The tape on the positive voltage pad is to prevent it from shorting out in the container.

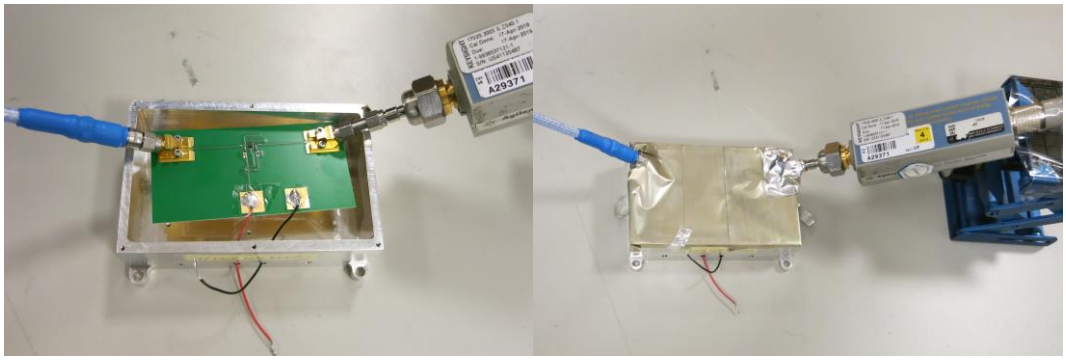

Figure 4.35 On left is the open shielding container with the LAN inside. Connected to the left is the noise generating input signal for the noise measurement and on the left is a SMA connected to the instrument. The right image is the sealed container using foil tape. An additional ground cable was connected to the mounting holes on the container, grounding it further.

In the VNA the measurements for gain and reflections were taken. The reflections for the LNA can be seen in Figure 4.36 and the gain is displayed in Figure 4.37 where a gain of 16.4dB was reached for the frequency 1090MHz.

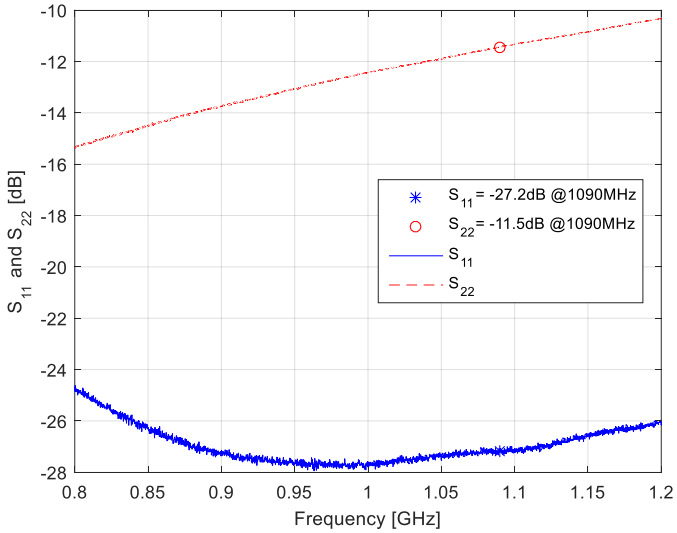

Figure 4.36 S_{11} and S_{22} for the LNA. In blue full line is S_{11} and in red lines are S_{22}. Represented as a blue star and a red circle are the values for S_{11} and S_{22} at 1030MHz respectively. S_{11} is -27.2dB and S_{22} is -11.5dB.

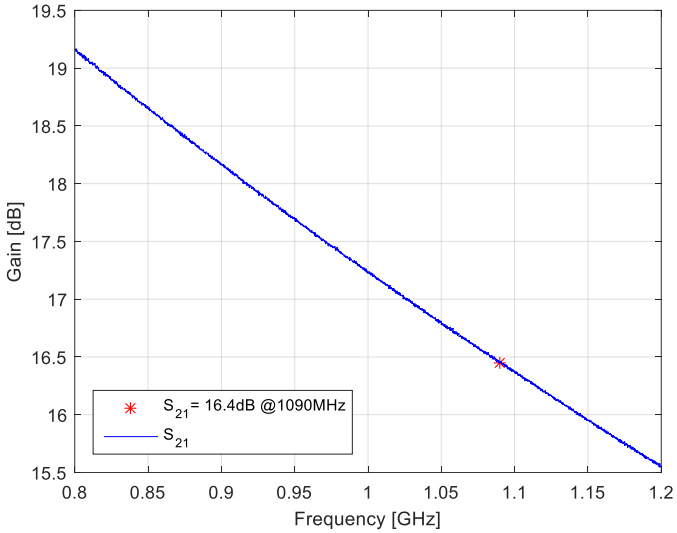

Figure 4.37 The small signal gain (S_{21}) with a marker at 1090MHz reading a gain of 16.4dB.

The noise measurement was conducted using Agilent N8975A noise figure meter and subtracting the loss of 0.035dB for the input contact from the noise level. The noise level is plotted in Figure 4.38. The measurement are conducted using an average of 20 passes to minimize system noise. Due to this measurement being so sensitive, a contaminating signal can be seen at 1030MHz (IFF interrogator frequency) is introduced from an unknown source.

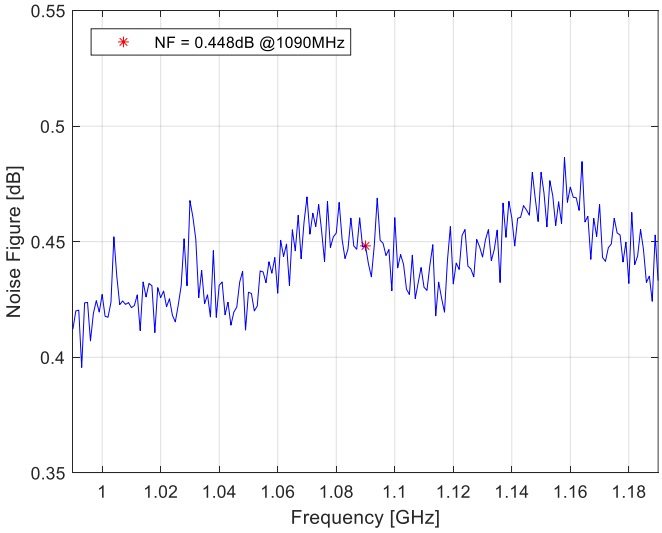

Figure 4.38 Noise figure for the LNA. Represented as a star is the noise figure of 0.448dB at 1090MHz. Present in the plot is a peak at 1030MHz from an external unknown signal source.

5. Design of antenna

Two types of elements were evaluated for the antenna in the design stage, a notch element and a dipole element. The first setup of the antennas was of an infinite array of identical elements. This makes it simpler to optimize for several steering angles since only one unit cell of the array needs to be modelled and analysed. The infinite array antenna was optimized for the three steering angles ±0°, ±30° and ±60°. The optimization goals for these three angels were the reflection coefficient of the infinite array antenna, using HFSS optimization tool. To give a more accurate design and simulations of the array the next step was to design a finite array antenna design with 15 elements.

The 15-element antenna was divided into two sections according to this patent [24]. The main antenna consisted of 10 elements and the control antenna consisted of 4 elements. The two antennas were separated by a ground plane and a dummy element was placed at the far end of the antenna beside the main antenna. This helps with the reflection of the last active element. The optimization was once again performed but this time on the finite array. Both type elements are fed at the bottom of the element which gives a convenient feed and allows for all-metal elements [25]. The optimization was performed for the 10 element main antenna when excited with uniform amplitude.

When satisfied with the optimization the key measurements were extracted from HFSS i.e. the electrical field and the S-parameters for the finite array antenna. The data were imported to MATLAB to get the result for the embedded element, from the electrical field, and the active reflection coefficient from the S-parameters. The advantage of using MATLAB for this is that the steering angle can be easily changed in MATLAB to simulate the active reflection coefficient and the embedded element pattern with different steering angles.

5.1 Dipole

The dipole antenna used in the simulations in HFSS is seen in Figure 5.1

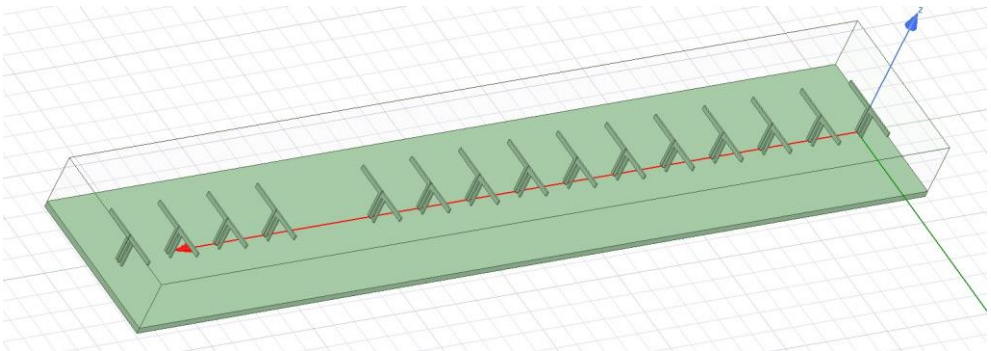

Figure 5.1 the dipole antenna with its 15 elements. On the left is the control antenna and on the most right hand side is the passive element. The remaining 10 elements are the main antenna used in the simulations below.

5.1.1 S active

The measure of return loss i.e. the scatter parameter S_{11} is a valid parameter when designing for a single antenna. However, when designing an array antenna, it will experience coupling between all the elements. The active reflection coefficient has to be used for an accurate evaluation of the reflection for each element, discussed in Chapter 2.4.2. Simulations of this parameter was conducted for the main antenna on the antenna aperture i.e. the 10 elements seen in Figure 5.2Figure 5.3Figure 5.4 Figure 5.5.

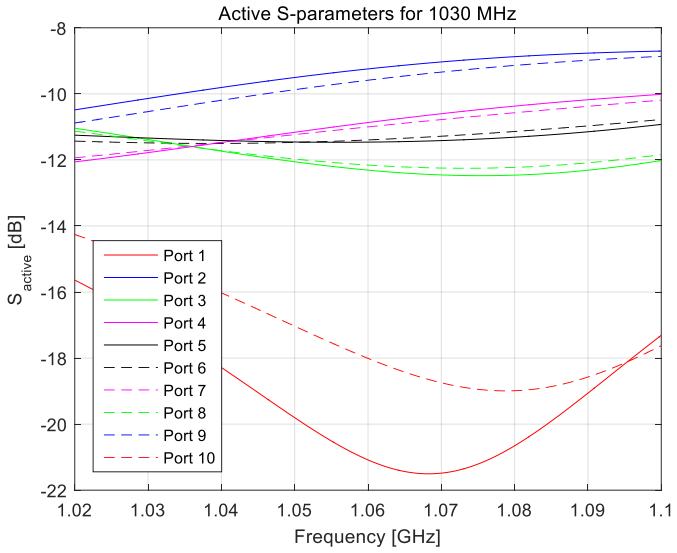

Figure 5.2 T The active S-parameters for the main antenna with 10 active antenna elements. The steering angle for the linear array is set to 0°. Here it is clear the outer most elements have the lowest reflection and then every other element inwards has a high/low reflection, same as for the Notch.

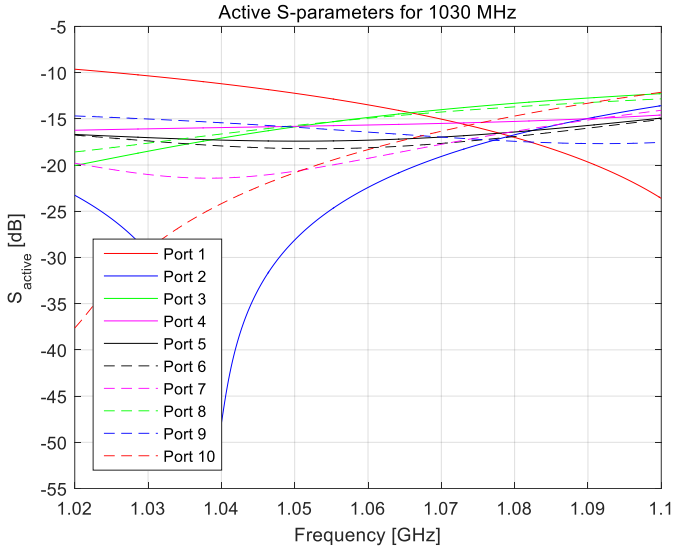

Figure 5.3 The active S-parameters for the main antenna with 10 active antenna elements. The steering angle for the linear array is set to 30°.

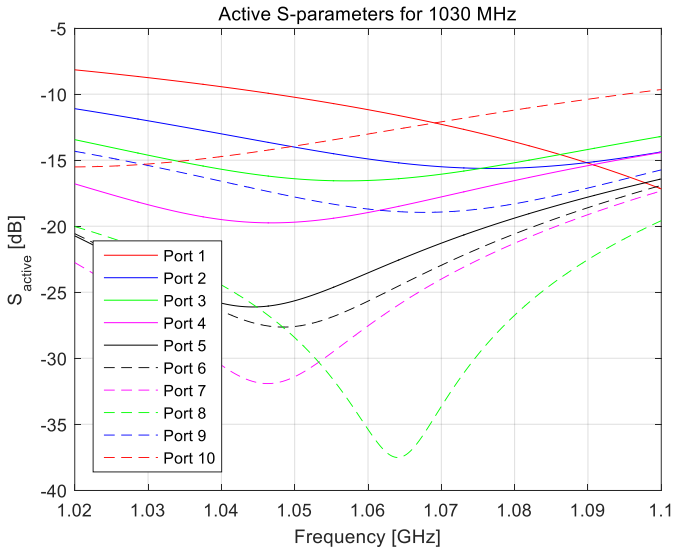

Figure 5.4 The active S-parameters for the main antenna with 10 active antenna elements. The steering angle for the linear array is set to 45°.

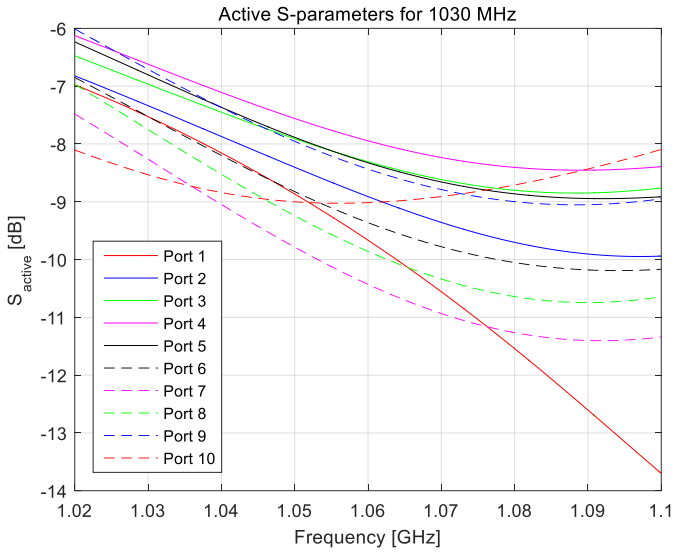

Figure 5.5 The active S-parameters for the main antenna with 10 active antenna elements. The steering angle for the linear array is set to 60°.

5.1.2 **Main antenna radiation pattern**

The main antenna radiation pattern in both H-plane and E-plane can be seen in the figures below with different steps in steering angle for the array. The data was extracted from the program HFSS and then imported to MATLAB to modulate different steering angles for the array. Uniform amplitude excitation has been used.

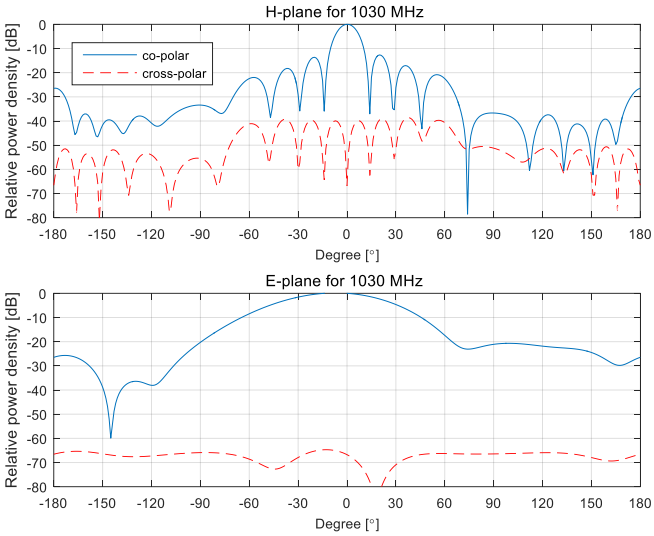

Figure 5.6 The normalized main antenna radiation pattern for a steering angle of 0 ° for the array. The co-polar radiation pattern for the H- and E-plane is the blue line and the corresponding cross-polar radiation pattern is the dashed red line in the figure.

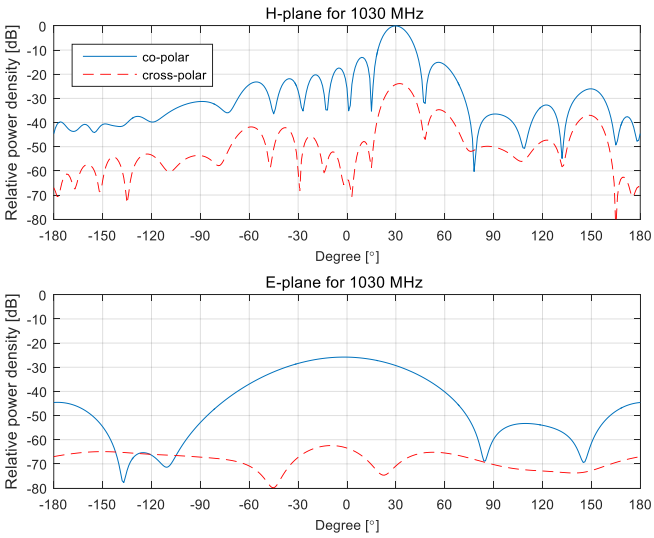

Figure 5.7 The normalized embedded element pattern for a steering angle of 30 ° for the array. The co-polar radiation pattern for the H- and E-plane is the blue line and the corresponding cross-polar radiation pattern is the dashed red line in the figure.

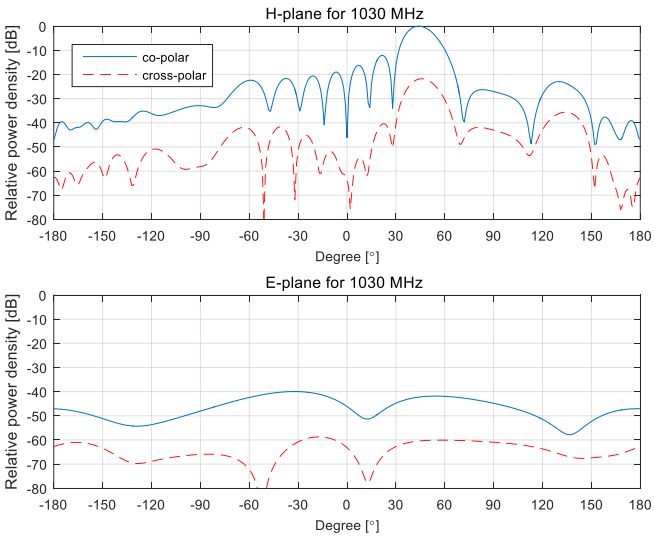

Figure 5.8 The normalized embedded element pattern for a steering angle of 45 ° for the array. The co-polar radiation pattern for the H- and E-plane is the blue line and the corresponding cross-polar radiation pattern is the dashed red line in the figure.

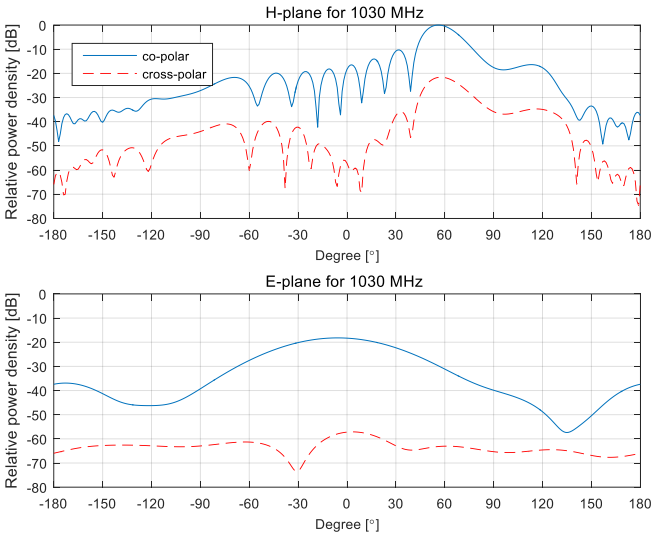

Figure 5.9 The normalized main antenna radiation pattern for a steering angle of 60 ° for the array. The co-polar radiation pattern for the H- and E-plane is the blue line and the corresponding cross-polar radiation pattern is the dashed red line in the figure.

5.2 Notch

The 15 elements notch antenna is visible in Figure 5.10. This antenna, different from the dipole, have not had its control antenna separated. However, this will not increase its performance in the simulations but increase it as it is closer to the infinite antenna, used for optimization.

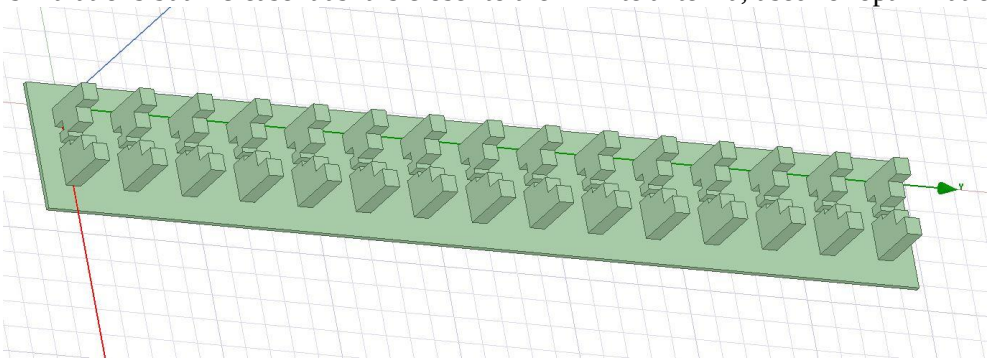

Figure 5.10 The 15 element notch antenna. Different from the dipole antenna, this antenna had not had its control antenna separated from the main antenna. This however will not increase its performance during the simulations.

5.2.1 S active

This result is measured in the same way as is described in Chapter 5.1.1.

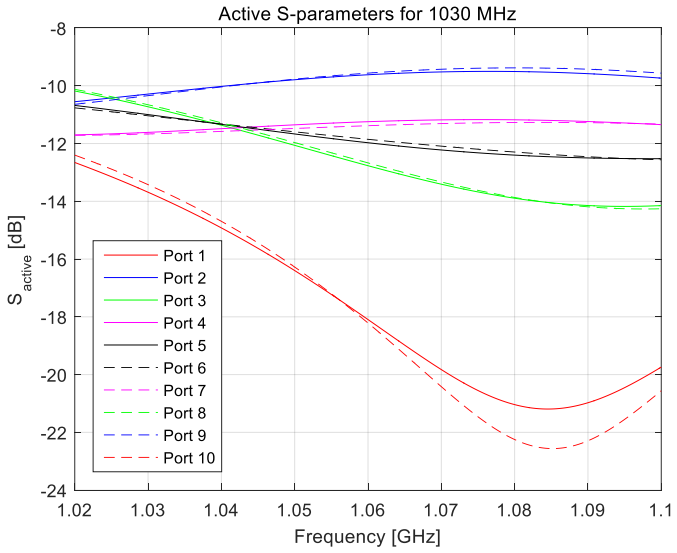

Figure 5.11 The active S-parameters for the main antenna with 10 active antenna elements. The steering angle for the linear array is set to 0°. Here it is clear the outer most elements have the lowest reflection and then every other element inwards has a high/low reflection.

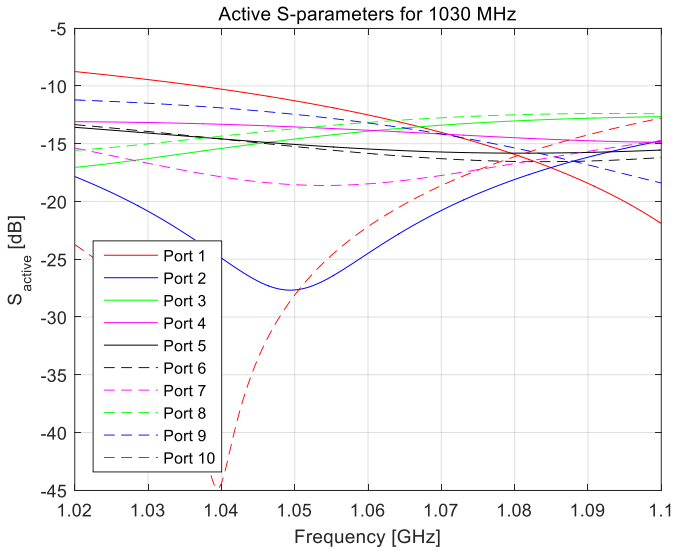

Figure 5.12 The active S-parameters for the main antenna with 10 active antenna elements. The steering angle for the linear array is set to 30°.

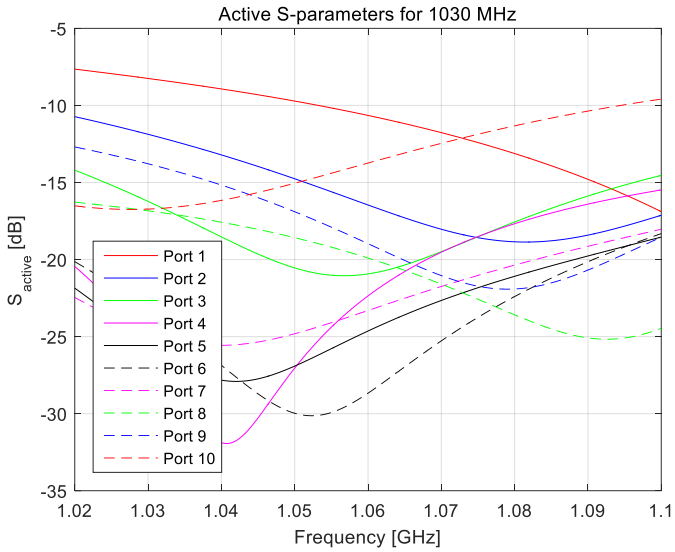

Figure 5.13 The active S-parameters for the main antenna with 10 active antenna elements. The steering angle for the linear array is set to 45°.

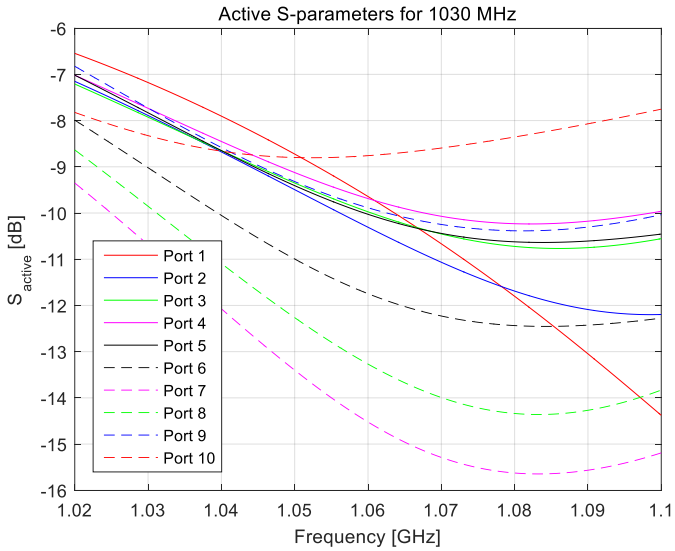

Figure 5.14 The active S-parameters for the main antenna with 10 active antenna elements. The steering angle for the linear array is set to 60°.

5.2.2 Main antenna radiation pattern

These results are measured in the same way as is described in chapter 5.1.2.

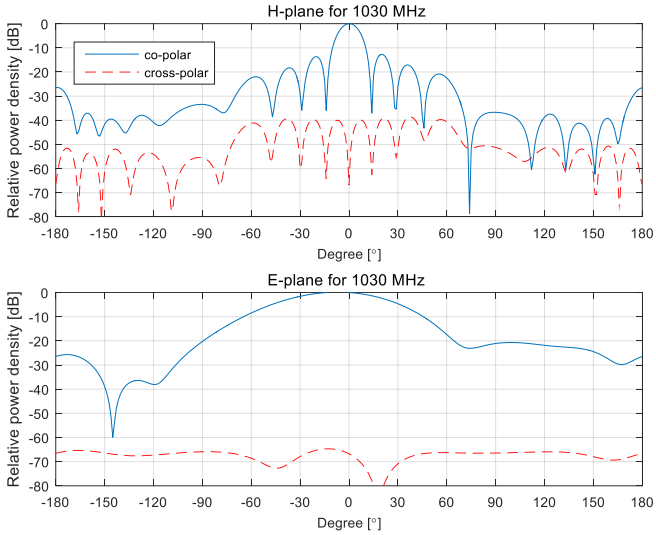

Figure 5.15 The normalized main antenna radiation pattern for a steering angle of 0 ° for the array. The co-polar radiation pattern for the H- and E-plane is the blue line and the corresponding cross-polar radiation pattern is the dashed red line in the figure.

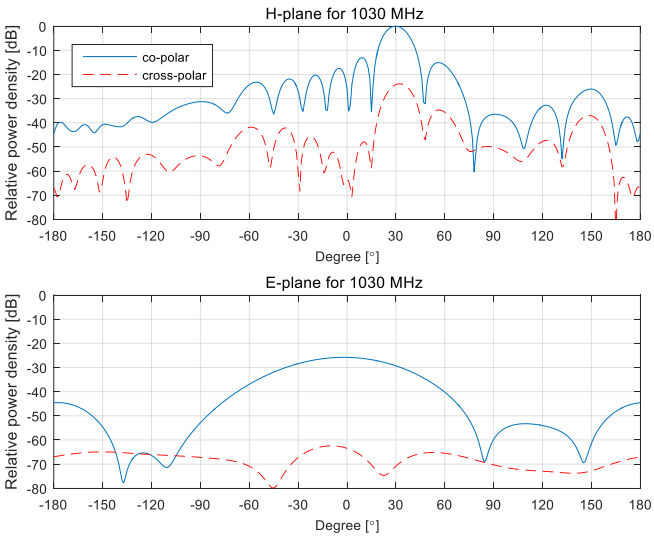

Figure 5.16 The normalized main antenna radiation pattern for a steering angle of 30 ° for the array. The co-polar radiation pattern for the H- and E-plane is the blue line and the corresponding cross-polar radiation pattern is the dashed red line in the figure.

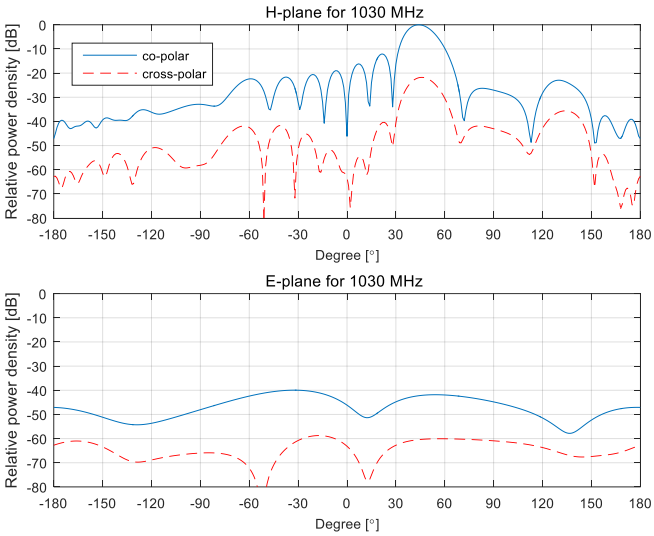

Figure 5.17 The normalized main antenna radiation pattern for a steering angle of 45 ° for the array. The co-polar radiation pattern for the H- and E-plane is the blue line and the corresponding cross-polar radiation pattern is the dashed red line in the figure.

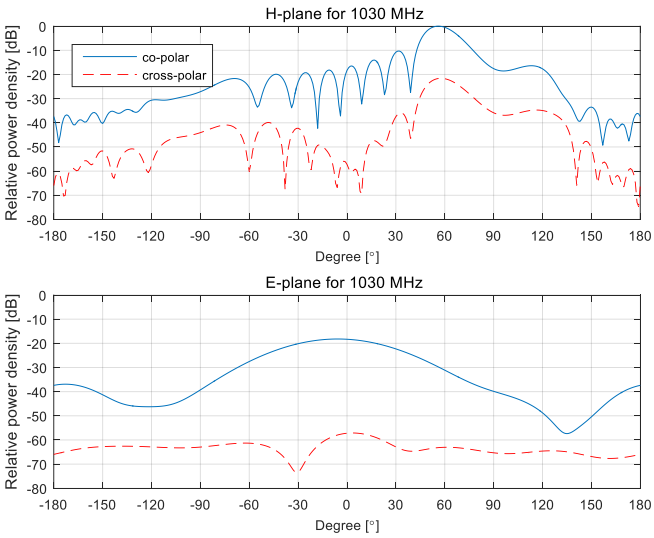

Figure 5.18 The normalized main antenna radiation pattern for a steering angle of 60 ° for the array. The co-polar radiation pattern for the H- and E-plane is the blue line and the corresponding cross-polar radiation pattern is the dashed red line in the figure.

6. Calculated performance

6.1 TRM

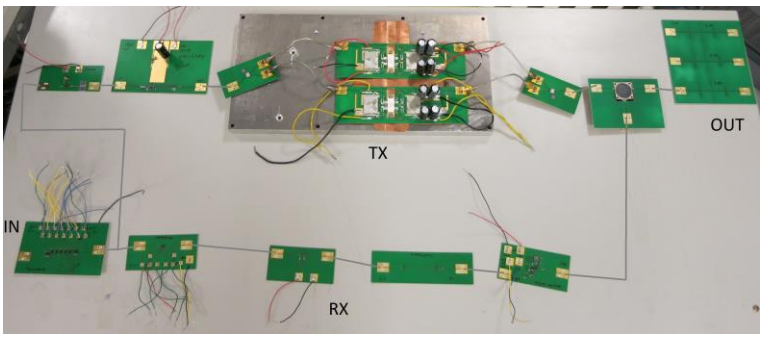

Figure 6.1 A view of every test circuit that would be a part of the future TRM, at the input you have the phase shifter and then at the lower part of the picture you can observe the Rx chain. Furthermore, you have the Tx chain at the upper part of the picture and lastly the circulator and the filter at the output.

To evaluate the performance of the full design, measurements were carried out on the full amplifier chain consisting of pre-amp, driver and two parallel PA, connected with the hybrids. The harmonics and powers were read using a spectrum analyser and the IFF pulses used in previous tests. The filter was later added on top of this due the equipment not having the dynamic range to measure 100dBc necessarily. The phase shifters, switches and attenuator were also later added to the calculations to get the full system performance. The receiver side is constructed using the individual measurements and adding them together, extracting gain and noise.

6.1.1 Output power from Tx

The measurements of the full chain were performed the same way as the other amplifiers, using IFF pulses and pulsing the PA. The output power was captured using a spectrum analyser, taking the max value over a few averages.

The data displayed in Figure 6.2 are the large signal and gain measurement, where a strange bump in gain is present and two sequential drops in power are visible, one earlier and one later.

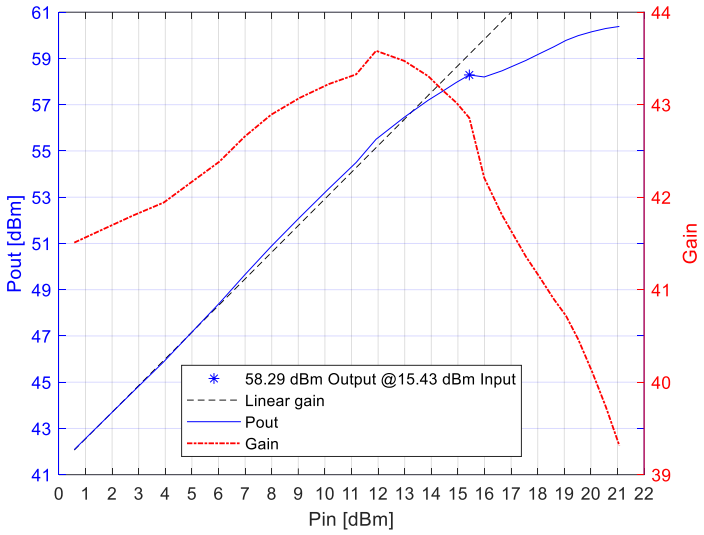

Figure 6.2 Large signal gain and output power for the full amplifier chain without tuning the pre-amp. On the left is the power output from the chain, plotted in blue, and the linear gain in black lines is extrapolated from the linear part of the output power line. Represented as a blue star is roughly the 1dB compression point. On the right-hand side axis is the large signal gain together with the gain plotted with a dotted line in red.

This is due to the pre-amp, as measurements in chapter 4.5 shows, having a P1dB at 13.6dBm input. After the gain drops of the second time is due to the PA hitting compression. The lacking in power from the pre-amp was fixed using a piece of foil raped in kapton tape and probing around. This revelled a spot at the output of the pre-amp where a large piece of foil tape was added, seen in Figure 4.18. This resulted in improvement of both gain and compression point. The measurements were done again, resulting in a greater gain and P1dB, displayed in Figure 6.3 and the waveform in compression in Figure 6.4 Figure 6.5.

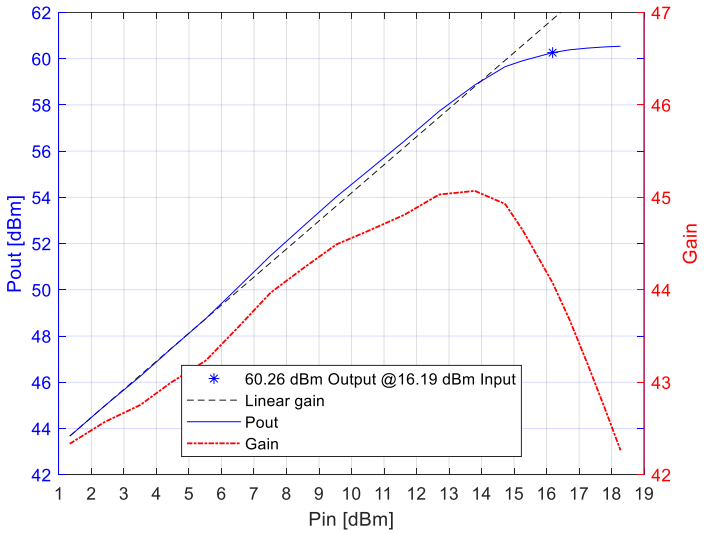

Figure 6.3 Large signal gain and output power for the full amplifier chain with a tuned pre-amp. On the left axis is the power output from the chain, plotted in blue, and the linear gain in black lines is extrapolated from the linear part of the output power line. Represented as a blue star is the 1dB compression point. On the right-hand side axis is the large signal gain together with the gain plotted with a dotted line in red.

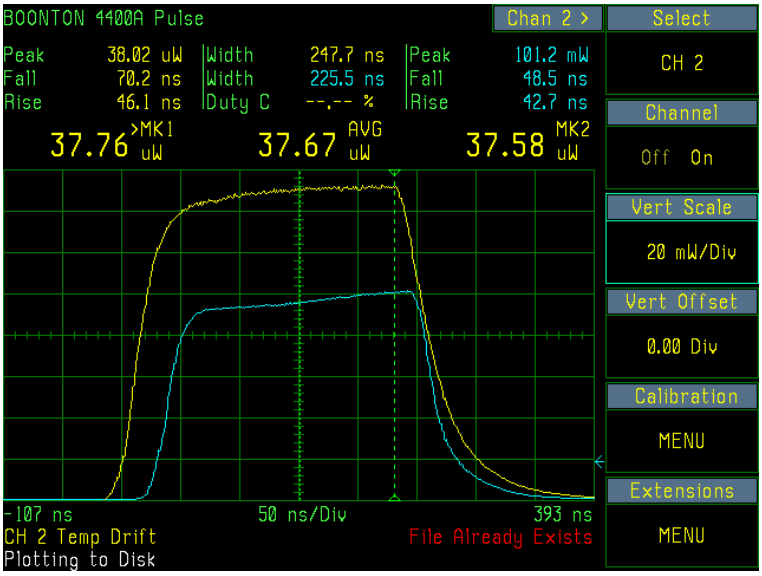

Figure 6.4 P1dB (60.26dBm or 1062W) where the input pulse is presented as yellow and the output is displayed in blue. These signals do not include the attenuations on the output nor the loss in the decoupling of the input signal. In the top left and right corners are rise and fall-time displayed from 10% - 90% of the power.

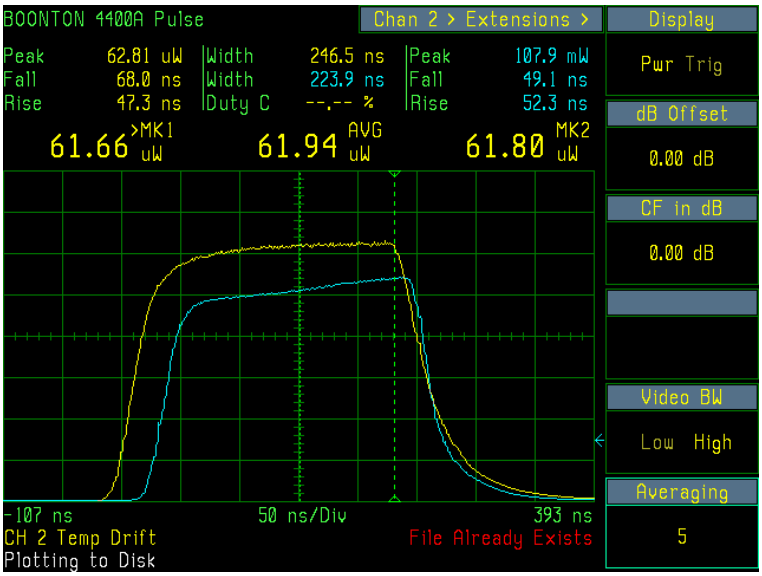

Figure 6.5 last measured point with an output power of 60.54dBm or 1132W where the input pulse is presented as yellow and the output is displayed in blue. These signals do not include the attenuations on the output nor the loss in the decoupling of the input signal. In the top left and right corners are rise and fall-time displayed from 10% - 90% of the power.

In front of the amplifier chain are the phase shifter, a SPDF switch and the attenuator. A decision was made to use the phase shifter designed using TL. This is due to its phase shift for 180° is better and has a more even loss and lower max loss. The phase shifter has a loss from 4.06dB to 5.046dB and the attenuator has a minimum loss of 1.613dB. The SPDF switch had no measurements preformed on it but the data sheet states a loss of typical 0.5dB. Using these values results in a loss of around 6.173 to 7.159dB for min and max loss in the phase shifter.

At the end of the chain are the circulator and the filter. The circulator did not arrive in time and therefore no measurements were possible. For the following calculations, an assumed insertion loss of 0.3dB is used, stated in the datasheet. The filter located after the circulator has a loss of

0.172dB at Tx frequency.

All these gives a final power and gain plot in Figure 6.6 representing how the system should behave, assuming the passive components behave linear and using the maximum loss for the phase shifter.

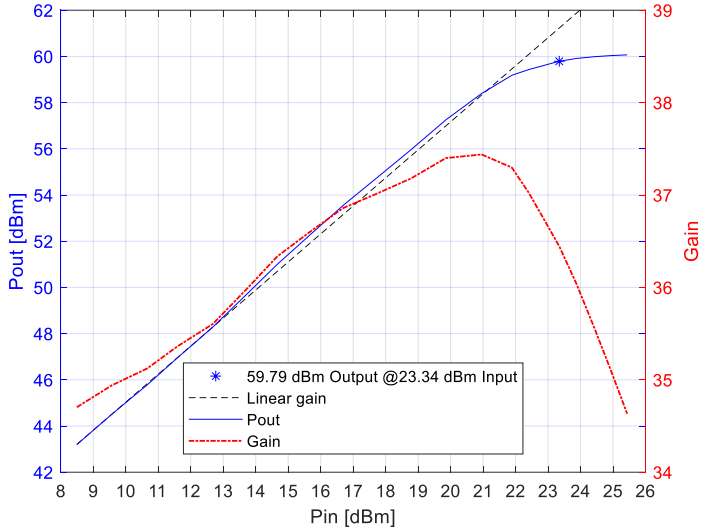

Figure 6.6 Large signal gain and output power for the full Tx chain with a tuned pre-amp (with tape). On the left is the power output from the filter, plotted in blue, and the linear gain in black lines is extrapolated from the start of the curve. Represented as a blue star is the 1dB compression point. On the right-hand side axis is the large signal gain together with the gain plotted with a dotted line in red.

To reach P1dB, the TRM would need 23.34dBm of input power to deliver 953W, assuming the worst phase shift in the data sheets.

6.1.2 Harmonics

When preforming harmonic measurements with a spectrum analyser, there is a risk of the instrument itself creating harmonics from your carrier frequency. This is solved by having an adaptive filter in the spectrum analyser. This only takes in the frequency band that you select and therefore it can eliminate the carrier from entering the instrument, not creating additional harmonics in the frequency you are measuring. The measurements in Table 6.1 and Table 6.2 were preformed using a spectrum analyser with an adaptive filter active between 2.9 and 6.5GHz. This means that the 2nd harmonic measurement has these additional harmonics added to them, however, it is hard to know how profound they are.

The harmonic measurements were preformed in two steps, one with the faulty, not tape tuned pre-amp in Table 6.1 and one with the tape tuned good preforming pre-amp in Table 6.2.

Table 6.1 The harmonics and output powers without the filter and circulator. The amplifier chain consists of the driver and the double PA stage.

Input [dBm]	2nd [dBc]	3rd [dBc]	5th [dBc]	Carrier[W]
18.10	-80.10			282.00
18.85	-73.28			355.39
19.91	-72.23	-74.83		442.40
20.81	-71.96	-72.39		524.17
21.35	-69.99	-71.95		573.44
21.87	-68.89	-69.99	-76.46	625.86
22.35	-67.39	-67.16	-75.62	674.08
22.91	-65.63	-64.40	-74.20	660.45
23.58	-63.90	-61.50	-71.47	702.38
23.96	-62.09	-58.36	-70.49	733.83
24.48	-60.84	-55.61	-68.41	778.91
24.97	-58.12	-53.56	-61.86	830.28
25.53	-57.93	-52.70	-59.33	892.13
25.99	-58.05	-52.31	-58.45	950.84
26.45	-58.09	-52.02	-57.32	996.97
26.96	-58.26	-52.03	-56.99	1036.80
27.48	-58.23	-52.00	-56.63	1070.35
27.99	-58.15	-51.91	-56.21	1092.36

Table 6.2 The harmonics and output power with the filter attached and without circulator. The chain consists of the driver and the double PA stage ends.

Input dBm	2nd [dBc]	3rd [dBc]	5th [dBc]	Carrier[W]
18.10	-87.25			271.05
18.85	-80.43			341.59
19.91	-79.38	-121.46		425.22
20.81	-79.12	-119.02		503.81
21.35	-77.15	-118.58		551.17
21.87	-76.05	-116.62	-119.49	601.55
22.35	-74.54	-113.79	-118.65	647.90
22.91	-72.78	-111.03	-117.23	634.81
23.58	-71.05	-108.12	-114.49	675.11
23.96	-69.24	-104.98	-113.51	705.34
24.48	-68.00	-102.24	-111.44	748.67
24.97	-65.27	-100.19	-104.89	798.04
25.53	-65.09	-99.33	-102.36	857.49
25.99	-65.20	-98.94	-101.48	913.92
26.45	-65.24	-98.64	-100.34	958.25
26.96	-65.41	-98.65	-100.01	996.54
27.48	-65.38	-98.62	-99.65	1028.79
27.99	-65.30	-98.54	-99.24	1049.95

Later switching to a different spectrum analyser with an adaptive filter eliminated the possibility for the analysers own harmonics being present and only measured the amplifiers. In the new spectrum analyser, the frequency bandwidth limits it to the 2nd and 3rd harmonics. The noise-floor was also larger and the measured harmonics lower. These changes made the measurement difficult and only a small set of data points were taken. This measurement was only preformed using the tuned pre-amp. As the pre-amp broke for the 4th time afterwards, measurements using an analyser with wider frequency span were not possible. As seen in Table 6.3, the filter fulfils the criteria of the of 60dBc in 2nd harmonics and 80dBc at 3rd harmonic with 60.11dBc at 1021W output and 86.99dBc at 1068W output respectively.

Table 6.3 The output powers and harmonics of the full amplifier chain with the tape foil on the pre-amp using the filter and no circulator. Marked in red is the 1dB compression point.

Input dBm	2nd [dBc]	3rd [dBc]	Carrier[W]
9.53		-101.05	242.84
10.54		-99.20	316.50
11.63		-97.47	423.20
12.69		-95.75	569.31
13.80		-92.89	740.10
14.73		-91.68	887.72
15.25		-89.93	940.12
15.81	-61.97	-89.15	987.47
16.19	-60.11	-88.29	1020.73
16.71	-60.23	-87.41	1049.95
17.27	-60.31	-86.99	1068.09
17.77	-60.36	-87.03	1080.18
18.27	-60.39	-87.07	1088.24

6.1.3 **Rx performance**

The Rx chain consists firstly of the filter, then the circulator and last the LNA. For the calculations, only a single LNA amplifier is used instead of two in parallel as shown in the block diagram in Figure 3.1. This will make the noise lower as the noise power from the amplifier will be half of that from two and the hybrid also introduces loss in front of the amplifiers.

Calculating the noise from the system, the loss of the circulator was taken from the data sheet and is 0.3dB. The filter has a loss of 0.2dB in the Rx frequency. The switch has a loss of 0.36dB and the limiter 0.34dB. Adding all of this results in a noise figure of F_{chain}=1.648dB assuming a T_0=T_{filt}=T_{circ}=T_{switch}=T_{lim}=290K and using the equations below.

$$F_{filt} = 1 + \frac{(L_{filt} - 1) * T_{filt}}{T_0}$$
$$F_{circ} = 1 + \frac{(L_{circ} - 1) * T_{circ}}{T_0}$$
$$F_{switch} = 1 + \frac{(L_{switch} - 1) * T_{switch}}{T_0}$$
$$F_{lim} = 1 + \frac{(L_{lim} - 1) * T_{lim}}{T_0}$$
$$F_{amp} = 10^{\frac{0.448dB}{10}}$$

$$F_{chain} = F_{filt} + \frac{(F_{circ} - 1)}{G_{filt}} + \frac{(F_{switch} - 1)}{G_{filt}G_{circ}} + \frac{(F_{lim} - 1)}{G_{filt}G_{circ}G_{switch}} + \frac{(F_{amp} - 1)}{G_{filt}G_{circ}G_{switch}G_{lim}}$$

The gain in the LNA is 16.4dB, adding the loss on the input and the loss on the output, the full Rx gain is then $G_{chain} = -0.2 - 0.3 - 0.36 - 0.34 + 16.4 - 7.332 = 7.868\text{dB}$

6.2 Antenna

The result for the antenna array in terms of Active reflection coefficient and main antenna radiation patterns will be presented in the Chapters 6.2.1 and 6.2.2. In Table 6.4 the side lobe levels are compared to the main beam of the antenna. In the table is a clear decrement of the difference of power between the main lobe and the first side lobe as an increased steering angle in applied.

Table 6.4 The side lobes presented for the 4 different steering angles using 10 active elements

Side lobes [dBc]	Theta [θ°]
-13	0
-12.3	30
-11.7	45
-10.3	60

6.2.1 Active reflection coefficient

A measurement was done on all the scattering parameters for all the 15 elements using a two port VNA at SAABs antenna facility A15. During this measurement the antenna was directed into absorbing material to simulate a free space environment, seen in Figure 6.7 .

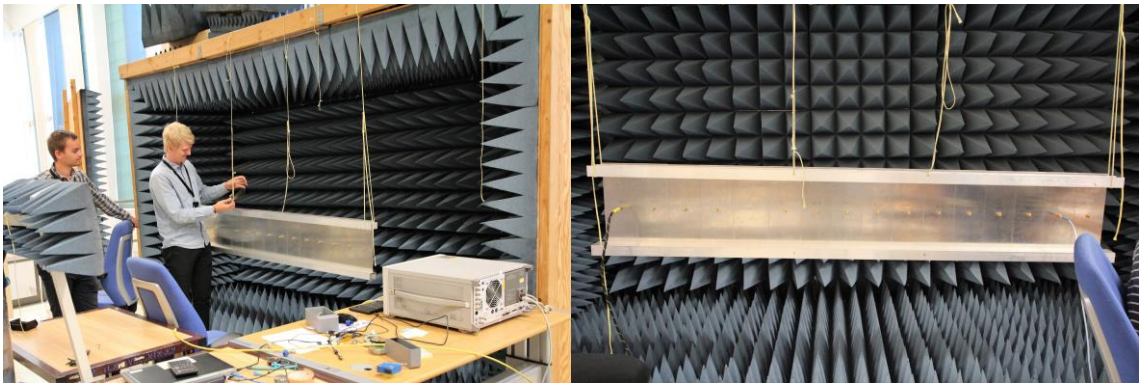

Figure 6.7 The setup for measuring s-parameters. The antenna is suspended in mid-air using ropes. On the image to the right, the coaxial cables are connected to port 2 and 15.

In MATLAB these measurements were later imported and the active reflection coefficient for the main antenna i.e. the 10 elements, was plotted for 0°, 30°, 45° and 60° steering angle. These plots are seen in the Figures Figure 6.8 to Figure 6.11 below.

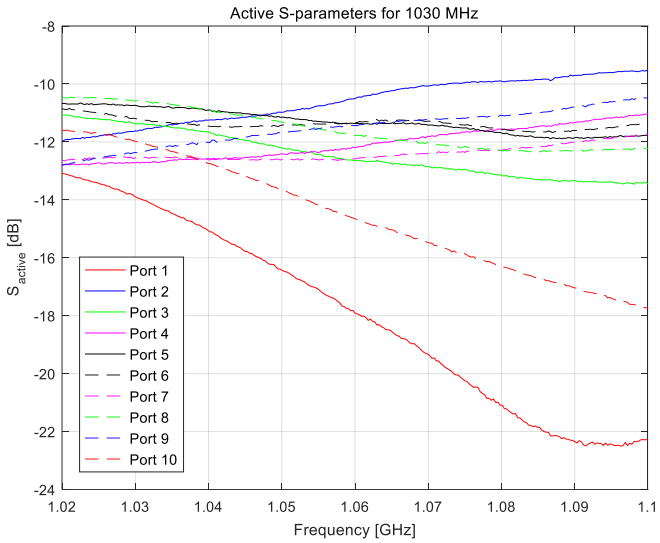

Figure 6.8 The active S-parameters for the main antenna with 10 active antenna elements. The steering angle for the linear array is set to 0°. Same as for the simulated antenna, the outer most elements have the lowest reflection and then every other element inwards has a high/low reflection.

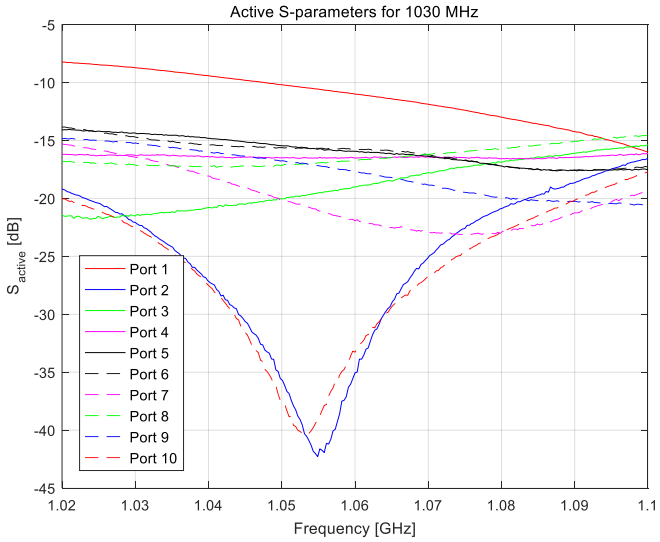

Figure 6.9 The active S-parameters for the main antenna with 10 active antenna elements. The steering angle for the linear array is set to 30°.

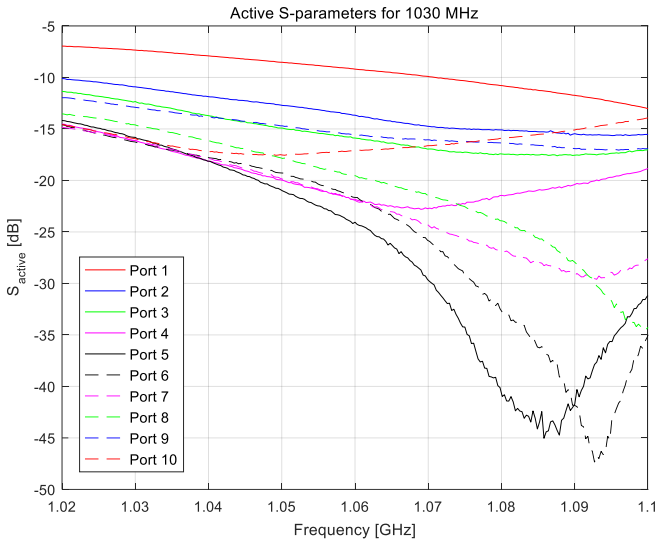

Figure 6.10 The active S-parameters for the main antenna with 10 active antenna elements. The steering angle for the linear array is set to 45°.

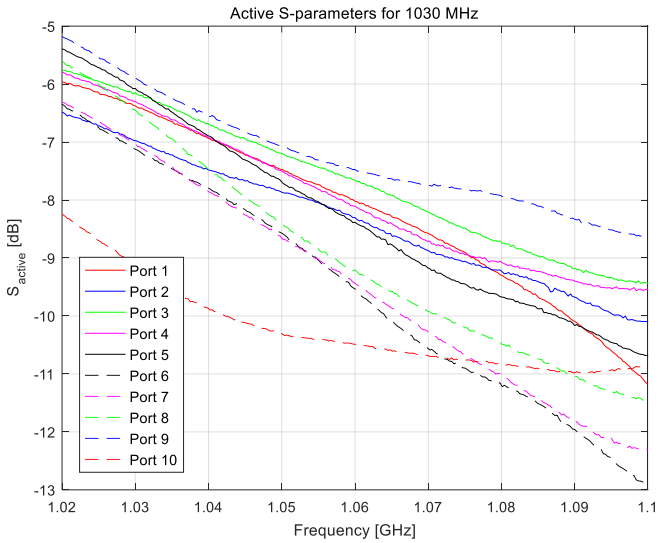

Figure 6.11 The active S-parameters for the main antenna with 10 active antenna elements. The steering angle for the linear array is set to 60°.

6.2.2 Main antenna radiation pattern

The embedded element pattern of all 15 elements was measured at the Saab A15 antenna test facility. A±110° sweep was performed for both the H and E-planes in steps of 0.5°. The test range can be seen in Figure 6.12.

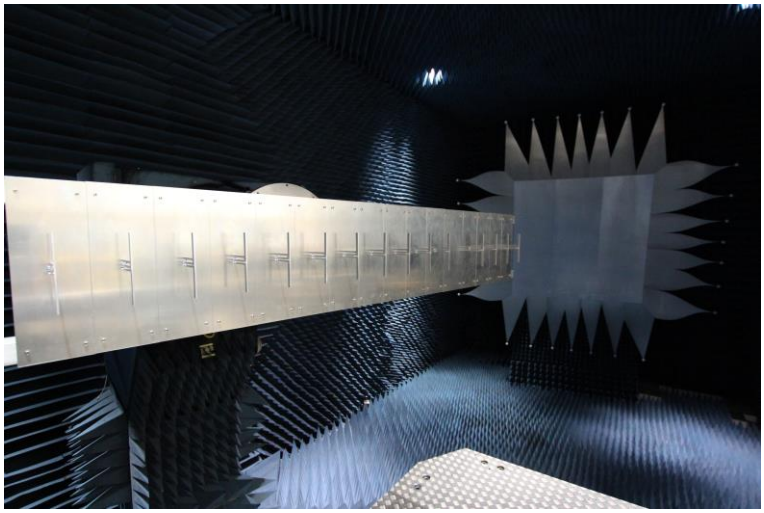

Figure 6.12 The dipole antenna array mounted on an arm in the measurement facility. In the further end on the room is a reflector, and the transmitting antenna is located under the camera at floor level.

The data were then imported into MATLAB to superpose to full main antenna radiation pattern for different steering angles for the array and plot the fields. The main antenna (10 elements) radiation pattern in both H-plane and E-plane can be seen in Figures Figure 6.13 to Figure 6.16 for steering angles 0°, 30°, 45° and 60°. The gains of the antenna is 20.13dB for 0° and 18dB for 60°.

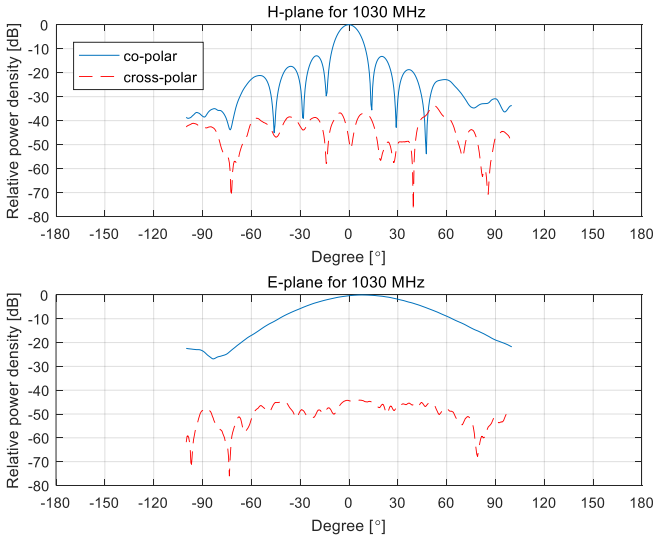

Figure 6.13 The main antenna radiation pattern for a steering angle of 0 °. The co-polar radiation pattern for the H- and E-plane is the blue line and the corresponding cross-polar radiation pattern is the dashed red line in the figure.

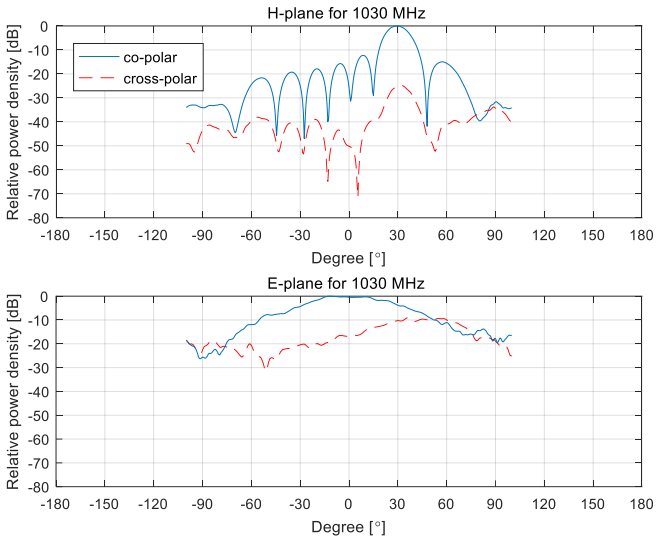

Figure 6.14 The main antenna radiation pattern for a steering angle of 30 °. The co-polar radiation pattern for the H- and E-plane is the blue line and the corresponding cross-polar radiation pattern is the dashed red line in the figure.

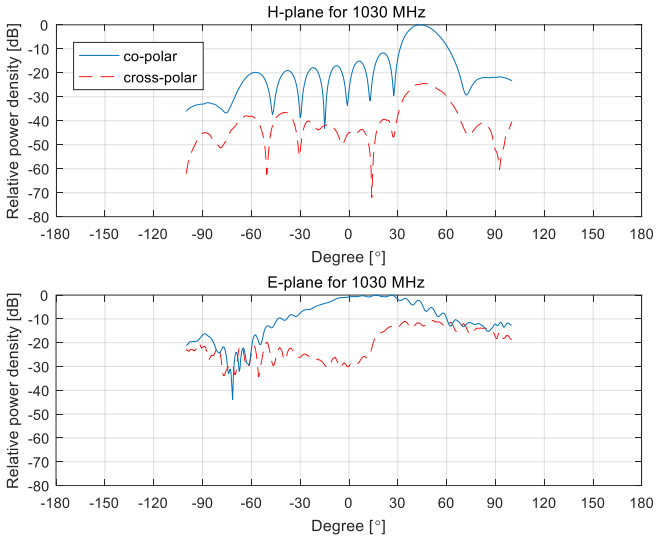

Figure 6.15 The main antenna radiation pattern for a steering angle of 45 °. The co-polar radiation pattern for the H- and E-plane is the blue line and the corresponding cross-polar radiation pattern is the dashed red line in the figure.

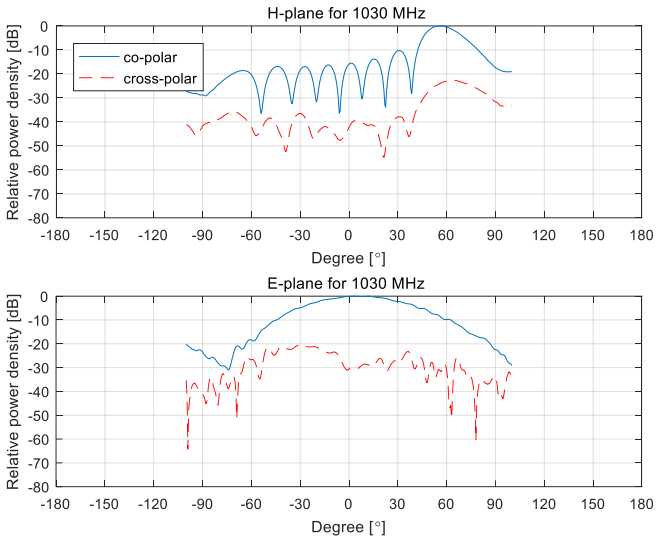

Figure 6.16 The main antenna radiation pattern for a steering angle of 60 °. The co-polar radiation pattern for the H- and E-plane is the blue line and the corresponding cross-polar radiation pattern is the dashed red line in the figure.

7. Discussion and future work

7.1 Discussion of challenges in the project

7.1.1 Pre-amp

The pre-amplifier is manufactured by NXP USA Inc and bought from Digi-key. Problem matching it resulted in a low gain and power. This amplifier also ran hot for some reason and on one occasion suddenly didn't work after turning it off and then back on again, without moving it. This chip stopped working and had to be replaced a total of 4 times during the project.

A design choice that was explored during the design phase was to replace this amplifier with a variable gain amplifier and by that, making an attenuator for the Tx chain obsoletely. One for our high power however was hard to find and a fixed gain amplifier had to be used. The measurements have shown that an additional amplifier stage is needed in the early stage. A variable amplifier can be used followed with a high power output pre-amplifier, solving the gain, high power output and eliminating the use of an attenuator.

7.1.2 PA

The design of the power amplifier took a considerable time to design, simulate and measure. This was due to the challenges of keeping the PA stable when designing it. It became apparent that the stability wasn't the biggest challenge when manufacturing the circuit in the lab. There the matching of the PA was a problem and a power of 20 watts was the first result without tuning. Firstly, we tried to measure the reflection from the transistor ports with a VNA and coaxial cable connected to the transistor. The calibration did not succeed and strange result from the VNA made us give up on this idea. Secondly, some tuning without a proper method yielded a power of 40 watt, which was still a long way from the 560W simulated. Lastly, the model for the transistor was included when measure the reflections. Then the input and output reflections for the matching networks from simulations were compared to the same reflection from the circuit with the transistor included as well. The result from this indicated that the matching for both the input and output were wrong. From this result the input and output were tuned to have the same reflections as the simulated ones. This gave us a satisfactory result and after additional tuning, the power of using two of these power amplifiers reached P1dB of 1084W

7.1.3 Phase shifter

The phase shifter with transmission lines took some time to get fully functional due to some mis-alignment of one of the DPDT. The switch was resoldered by hand to get proper connection to the footprint of the PCB. Two of the SPDT switches broke down during the troubleshooting of the phase shifter, they were replaced, and the measurement of the phase shifter could continue.

This design, however being marginally better, uses more components and takes up a larger area on the board. In a world where this would become an actual product, the phase shifter is recommended to be exchanged against a MMIC substitution. At the time of this project we only found one MMIC chip available to order for a 0.9 to 1.2GHz frequency band. The data was however a little too good to feel reliable and the company where a small one originated from India, moved to Singapore and made a name change in a small timeframe. This was something we weren't dedicated to take upon, even if we had a price offered to us from them.

7.1.4 **LNA**

The noise level stated by SAAB was 1dB, however, upon asking this requirement was taken from thin air it seemed and the requirement of a low noise didn't seem to be that great. If looking back at the master thesis done back in 2009 [19], they interpreted it as the noise level the LNA was to have, not the front end. In this case, F_{LNA}= 0.433dB is much lower than 1dB and achieves the goal.

If a lower noise level for the front end is desired, the filter can be moved in front of the circulator, reducing the noise by 0.2dB down to 1.448dB. In order to do this, measurements need to be done with the circulator, to see if it reduces the harmonics with its limited bandwidth or amplifies them by going into compression.

For the case of using two LNA:s connected in parallel, it improves the robustness of the system and the power capability. The LNA is singly capable of handling 27dBm for 5 minutes and 14dBm up to 1.5GHz and +22dBm up to 3GHz continuously. With the limiter, limiting the signal to 21dBm at the peak of the pulse, a single amplifier should be sufficient. This is however a discussion that needs to be taken with people, more experienced in designing rugged military equipment.

A total gain of 8dB was achieved on the frontend. This seems small, and due to more room is available, a second amplifier after the LNA would be preferable. As for the case for the pre-amp, a variable gain amplifier could be appropriate here as well, as the attenuator is removed by implementing a variable gain amplifier in the Tx chain. As the Tx and Rx frequencies are almost the same, a common chip set could be used in both the pre-amp and the LNA stage.

7.2 Recommended future works

- For future work, in terms of filtering, could be to design a band-pass filter instead of a notch filter to supress the harmonics generated by the amplifiers in the circuit. This way you have more control over the desired bandwidth you want to send and receive in.

- In this project we only simulated and designed a TRM. Future work is to finish the design of the TRM and send it to be manufactured with the improvements made on them. This would give a more accurate result since you would see the effect that each different circuit have on each other in the TRM. Furthermore, you can thoroughly test the switching between the Tx and Rx branch. The circuits would be integrated together in the TRM which would lead to more coupling, this coupling could then be mitigated and tested for in the lab. To efficiently pulse the gate of the PA, driver and pre-amplifier, minimizing heat and power consumption for the whole system, usage of MOSFET switches to control the gates are to be added.

- The pulse distortion when amplifying the signal in the Tx chain should not exceed the restriction set by the IFF standards. It would be of interest to do further measurements of this with proper pulse shapes and to do it on a complete TRM. This would yield a more exact result when considering a final product.

- Since the TRM will be a compact design, it will generate some heat even if all the gates in the Tx chain are pulsed. This applies a cooling system is needed to be engineered into the system.

- Further investigation could be done for the receiver in terms of link budget, then it can be decided if there should be an amplifier after LNA to further amplify the incoming signal. There could also be an investigation if there should be two LNAs connected via hybrids to make the LNA stage withstand more power. This would make up a more redundant receiver circuit.

- The pre-amp needs to be re-designed and/or replaced with a variable gain amplifier for convenience, replacing the variable attenuator.

- For future works it could be beneficial to design an IC phase shifter for the IFF frequency band. This would help to minimize space for the TRM and would probably could yield lower loss and a more accurate phase shift.

- The TRM would need a power circuit and a digital circuit to have a fully functional product. This means that optimization of space would become more important to keep the space constraints, further pushing for a MMIC phase shifter. This digital part would also need to communicate with the interrogator as this decides the power level needed as for when to transmit and receive signals.

- In the measurements of the antenna the active reflection factor had shifted up in frequency from the simulated results. This can be solved by tuning the antenna with the Teflon pieces between the two arms of the antenna. This could lead to a better active reflection factor and be closer to the simulated result.

8. Conclusion

The design of test circuit for a TRM was done for an IFF system and tested as such. There were a few key requirements that were aimed for in this project. The power requirement of 700 watt was set and a result of 1084W for the 1 dB compression point from the amplifiers. After filtering and isolation, the power output is 953W. The Phase shifter designed with TL's is chosen for the TRM, enabling a phase shift of 360° to be made. The LNA has a noise figure of 0.448dB and together with all the filtering and isolating, a total noise figure of 1.648dB was realized.

There was a size requirement for the TRM module and when designing the TRM with test circuit it was concluded that this size requirement could be kept intact. There was also room to extend the size to make room for digital circuits and power circuits. The size requirement was 120x250x50 mm and the length 250mm could be extended to 350mm. A concept layout of a 250x117mm area can be seen in APPENDIX B.

One requirement was keeping the switching time for all circuits below 0.5μs. The circuit that had the slowest switch time was the isolation switch (SKY12215-478LF) with a switch time of 0.25μs, therefore fulfilling the requirement.

One of the main requirements was to assure that the pulse should propagate through the system with low distortion. This is due to a special requirement for the rise and fall time of the pulse in the IFF standard as well as the frequency spectra. The pulse shape is therefore desired not to be distorted in the TRM. Due to lacking capabilities of generating the necessary pulse required for this test, no conclusive result can be taken is it distorts it too much. Furthermore, the result for the harmonics also indicated that with the filter attached after the circulator should fulfil the requirement of the IFF standard for the harmonics assuming a low harmonic increment from the circulator.

The antenna module chosen for the antenna array was the dipole, this resulted in a good return loss for the array and a small and light antenna array. However, it didn't reach a 10 dB return loss for all steering angles as stated in the requirements. The result showed that when the steering angle was 60° you got an active reflection coefficient of 5 dB for some of the antenna modules. There is not always necessary to have exactly 60° steering angle, as the definition are a 3 dB drop in the steering angle. The report, in definition, steers therefore over 60°. This means that the result for the worst antenna module would be below 6 dB instead.

The full system would operate with a passive antenna followed with 10 active elements driven with our designed TRM. The remaining 4 antenna elements would also be equipped with the TRMs constructed in the report. This would give the 10 elements a steerable EIRP of 60.1dBW with 0° of phase shift and 57.97dBW for 60°. However, there could be a problem with the reflections from the antenna, creating standing waves resulting in dielectric break down in some connectors and components. As a peak EIRP of max 52.5dBW is stated in ICAO annex 10 [2], and is much less than what this system is capable to produce, it is deemed sufficient.

9. **Bibliography**

[1] "BASIC CONCEPTS ON MSSR MODE-S SYSTEMS TRAINING COURSE Surveillance Radar Systems ATM Doc. Nº: 0011810000800MA07 Edition: 4 Revision: 0," 2014.

[2] North Atlantic Treaty Organisation, "STANAG 4193 Part 1 Edition 2," 1990.

[3] North Atlantic Treaty Organisation, "STANAG 4193 Part 4 Edition 2," 1990.

[4] B. Beasley, "Understanding Mode S technology," 2012.

[5] David K. Cheng, Field and Wave Electromagnetic, 2 ed., 2014, p. 703.

[6] W. H. (. H. Hayt and J. E. (. E. Kemmerly, Engineering circuit analysis, 2nd ed., McGraw-Hill, 1971, p. 653.

[7] G. Gonzalez, Microwave transistor amplifiers : analysis and design, Prentice Hall, 1997, p. 506.

[8] Electronics Tutorials, "Class AB Amplifier Design and Class AB Biasing," [Online]. Available: https://www.electronics-tutorials.ws/amplifier/class-ab-amplifier.html.

[9] S. C. Cripps, RF Power Amplifiers for Wireless Communications Second Edition, 2006, p. 456.

[10] G. T. Watkins, "Enhancing Second Harmonic Suppression in an Ultra-Broadband RF Push-Pull Amplifier".

[11] D. M. Pozar, Microwave engineering, 4 ed., Wiley, 2012, p. 756.

[12] Jimb, "Switch Basics - learn.sparkfun.com," [Online]. Available: https://learn.sparkfun.com/tutorials/switch-basics/poles-and-throws-open-and-closed.

[13] "Low Cost Surface Mount Power Limiters," 1999. [Online]. Available: https://literature.cdn.keysight.com/litweb/pdf/5091-4931E.pdf?id=1115273.

[14] "PIN Limiter Diodes in Receiver Protectors," 2006. [Online]. Available: http://www.skyworksinc.com/uploads/documents/200480C.pdf.

[15] R. Cory, "PIN-limiter diodes effectively protect receivers," *EDN*, p. 6, 2004.

[16] S. Kildal, "Foundations of Antenna Engineering: A Unified Approach for Line-of-Sight and Multipath," 2017.

[17] D. F. Kelley, "Embedded element patterns and mutual impedance matrices in the terminated phased array environment," in *IEEE Antennas and Propagation Society, AP-S International Symposium (Digest)*, 2005.

[18] W. K. Kahn, "Active Reflection Coefficient and Element Efficiency in Arbitrary Antenna Arrays," *IEEE Transactions on Antennas and Propagation,* p. 2, 1969.

[19] O. Axelsson and J. Schleeh, "L-Band Antenna Array-LARA," Gothenburg, 2009.

[20] J. Coonrod Rogers Corp, "Selecting Circuit Materials for Microwave Power Amps," vol. 57, no. 11, p. 6, 2014.

[21] J. M. Rollett, "Stability and Power-Gain Invariants of Linear Twoports*," p. 4, 1962.

[22] G. Carchon, "Power and noise limitations of active circulators," *IEEE Transactions on Microwave Theory and Techniques,* pp. 316-319, 2000.

[23] R. Corporation, "RO4000® Series High Frequency Circuit Materials".

[24] L. SUNDELL, P. WALL and B. SVENSSON, "METHOD AND SYSTEM FOR OPERATING AN IFF/SSR ANTENNA (WO2017184042)," 27 10 2017.

[25] B. SVENSSON, "SURFACE MOUNTED BROADBAND ELEMENT(WO2016099367)". 24 6 2016.

[26] D. Wagner, "Using Data Sheet Impedances for RF LDMOS Devices - EB212," p. 7, 2004.

APPENDIX A

2.2 Antennapertur

2.2.1 Spec

- Linjär array med 15 element i sida
- Jordplansstorlek (storlek på bakomliggande mekanisk struktur) ca 1900 x 460 mm
- En SMA-kontakt på varje element
- Elementavstånd 120 mm
- Typ av element TBD (To Be Defined)
- Max -10 dB return loss vid ±60° utstyrning i oändlig array
- Frekvensband: 1030±10 MHz och 1090±10 MHz eller hela bandet 1020-1100 MHz.

2.2.2 Arbetspaket

- Konstruktion av ett element med periodiska randvillkor (motsvarande en oändlig array) i sida. Använd HFSS.
- Använd ovanstående konstruktion och modellera hela den ändliga antennen med en kontakt på varje element i HFSS.
- Beräkna S-matrisen och summera aktiv reflektionsfaktor för olika utstyrningar ±60°, ±45°, ±30°, 0°
- Summera också *embedded element pattern* för alla elementen med olika aperturfördelningar och utstyrningar.
- Gör tillverkningsunderlag (enkla mekaniska skisser och ev mönsterkort) för tillverkning
- Mätning på antennmätsträcka
- Utvärdering av mätdata och jämförelse med HFSS-simuleringar

2.3 TRM (TransmitReceiveModule)

2.3.1 Spec

- Frekvens sändning: 1030±10 MHz
- Frekvens mottagning: 1090±10 MHz
- Brusfaktor LNA < 1 dB TBC
- Uteffekt på antennkontakt: > 700 W peak
- Fasvridare 6 bitar TBC (gemensam Tx/Rx)
- Dämpare 6 bitar inom 10 dB dynamik (gemensam Tx/Rx)
- Omkopplingstid fasvridare: < 0.5 μs
- Arbetsfaktor: max 2.2% (11W) men under "lång tid" 0.5% (2.5 W)
- Storlek: < 250 x 120 x 50 mm
- Filter: TBD
- Fasvridare, dämpare och uteffekt skall kunna styras via gränssnitt TBD
- Mottagarskydd
- Tx/Rx-switch och biasering skall vara styrbar med blockeringssignal (detta är en standardiserad signal som finns ut från alla Interrogatorer)

APPENDIX B

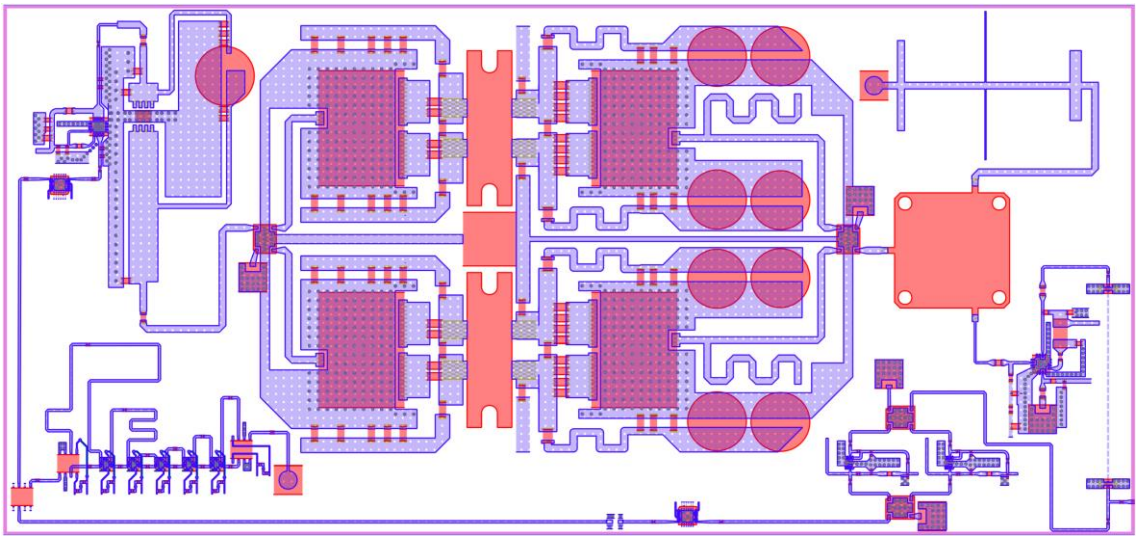

A concept layout of the components without the modifications and improvements found to be necessary in the testing and measurements. The layout fit in a 250x117mm board and most bus lines can be directed down to the corner. In this design there are two attenuators, one at the beginning of the amplifier chain and one after the two LNA's.

APPENDIX C